Chem Soc Rev

Dynamic Article Links

Cite this: *Chem. Soc. Rev.*, 2011, **40**, 1107–1150

www.rsc.org/csr

**CRITICAL REVIEW**

# Multifunctional hybrids by combining ordered mesoporous materials and macromolecular building blocks†

**Galo J. A. A. Soler-Illia*[ab] and Omar Azzaroni[c]**

***Received 13th December 2010***
**DOI: 10.1039/c0cs00208a**



This *critical review* presents and discusses the recent advances in complex hybrid materials that result from the combination of polymers and mesoporous matrices. Ordered mesoporous materials derived from supramolecular templating present high surface area and tailored pore sizes; pore surfaces can be further modified by organic, organometallic or even biologically active functional groups. This permits the creation of hybrid systems with distinct physical properties or chemical functions located in the framework walls, the pore surface, and the pore interior. Bringing polymeric building blocks into the game opens a new dimension: the possibility to create phase separated regions (*functional domains*) within the pores that can behave as "*reactive pockets*" of nanoscale size, with highly controlled chemistry and interactions within restricted volumes. The possibilities of combining "hard" and "soft" building blocks to yield these novel nanocomposite materials with tuneable functional domains ordered in space are potentially infinite. New properties are bound to arise from the synergy of both kinds of components, and their spatial location. The main object of this review is to report on new approaches towards functional polymer–inorganic mesostructured hybrids, as well as to discuss the present challenges in this flourishing research field. Indeed, the powerful concepts resulting from the synergy of sol–gel processing, supramolecular templating and polymer chemistry open new opportunities in the design of advanced functional materials: the tailored production of *complex matter displaying spatially-addressed chemistry* based on the control of chemical topology. Breakthrough applications are expected in the fields of sustainable energy, environment sensing and remediation, biomaterials, pharmaceutical industry and catalysis, among others (221 references).

## 1. Introduction

The field of mesoporous materials has experienced an impressive growth in the last two decades.[1] Supramolecular pore templating, introduced by the seminal works of the Mobil group,[2] and by Yanagisawa *et al.*,[3] was conceived as a breakthrough to solve the size limitations of the classical pore templating methods used in zeolite chemistry. Apart from the creation of controlled cavities, this approach also permits to transcribe potentially any organic space structure into shaped inorganic materials.[4,5] In a similar way, hybrid mesoporous architectures merging the properties of inorganic materials and macromolecular building blocks have found an incredible resonance and attracted widespread interest as a fundamental and technological challenge to chemists, physicists and engineers during the past two decades.[6,7] Part of the appeal of hybrid mesoporous materials is the unique and thorough molecular control of their intrinsic topological and chemical characteristics that self-assembly techniques[8] and nanochemistry[9] are able to provide. With the correct choice of building blocks and self-assembly conditions, it is possible to produce nanostructured materials *via* sol–gel processes with precisely defined and tunable chemical functions incorporated into well-defined ordered mesostructured frameworks; this translates into a corresponding fine control in the way such building blocks define chemistry and topology across different length scales.[10,11] This "biomimetic approach" leads to the possibility to build hierarchical nanosystems with unprecedented control of functional positioning from soft chemistry methods, in a similar way to what nature does.[12,13]

In addition, explorations in the use of polymer chemistry have also significantly expanded our ability to conceive and realize novel hybrid functional mesostructures. A rich toolbox for macromolecular design provides almost unlimited

[a] *Gerencia Química, CNEA, Centro Atómico Constituyentes, Av. Gral. Paz 1499, San Martín, B1650KNA, Argentina. E-mail: gsoler@cnea.gov.ar*
[b] *Departamento de Química Inorgánica, Analítica y Química Física, FCEN, Universidad de Buenos Aires, Ciudad Universitaria Pabellón II, Buenos Aires, C1428EHA, Argentina*
[c] *Instituto de Investigaciones Fisicoquímicas Teóricas y Aplicadas (INIFTA), Departamento de Química, Facultad de Ciencias Exactas, Universidad Nacional de La Plata, CONICET, CC. 16 Suc. 4, La Plata, 1900, Argentina. E-mail: azzaroni@inifta.unlp.edu.ar*

† Part of the themed issue on hybrid materials.

possibilities for further tailoring and diversification by means of intelligent processing technologies. As a matter of fact, design of hybrid mesoporous materials has benefited from the great strides made in macromolecular science and a better fundamental understanding of the key processes that control polymer synthesis in nanoconfined environments. For instance, the blend of concepts from *"sol–gel processes"* and *"soft matter"* has been a definitive success in taming complexity and functionality[14] as they can interact together without disrupting their own function, a concept often referred to as *"integrative chemistry"*.[15–17] The resulting paradigm shift has opened up new horizons in molecular materials science, and has led to exciting new developments in which nanochemistry played a fundamental role. Indeed, understanding the structural organization of materials and controlling their functional features at the molecular scale has been a long-standing challenge of condensed matter physics and chemistry. What is important to realize is that control of composition, size, shape, and morphology of mesostructured materials[18] is an essential cornerstone for the development of highly functional units. It might be worth to add here that all these requirements do not represent a formidably complicated synthetic task. On the contrary, the combination of self-assembly and sol–gel processes is nowadays one of the simplest methods to develop complex but well-defined, nanostructured materials with innovative properties.[19,20]

First and foremost among the motivations for exploring new avenues towards hybrid mesoporous materials is the desire to synthesize new robust, functional and technologically relevant materials by mimicking the dynamic and functional versatility of nature.[21] Much of the inspiration for the design of hybrid mesostructured materials arises from the observation of biological systems. In nature, organization on the nanometre scale is crucial for the remarkable properties and functional capabilities of biological machineries. The highly sophisticated functions found in biological entities originate from their elaborate structures. Rather than consisting of monolithic architectures, these structures are spatially organized assemblies of different specific functions in which the harmony of supramolecular and covalent interactions leads to "smart" and adjustable functions. In particular, this strategy opens the possibility of generating localized *functional domains* with distinct physical properties and chemical environment located in well-defined regions of space (framework walls, pore surface, pore interior, see Fig. 1). On the other hand, the degree of organization and the functional properties that can be obtained for hybrid polymer–inorganic materials certainly depend on the chemical nature of their components, but they are also heavily influenced by the interaction between these counterparts. Thus, a key point for the design of new mesoporous hybrids is the control over the nature, the extent and the accessibility of the inner interfaces.

A second impetus is the desire to design new synthetic mesostructured materials combined with macromolecular building blocks that feature even more useful ensemble properties emanating directly from ordering and confinement at different length scales, in which they may exhibit a significant degree of functionality and complexity through processes occurring within the mesopores—like doing chemistry in an 8 nm test tube.[22] The chemical processes that occur in constrained spaces of mesostructured materials deserve particular attention for they are a fundamental part of many synthetic procedures commonly used in nanoscience and nanotechnology. In a physically constrained environment, interfacial interactions, symmetry breaking, and confinement-induced entropy loss can play dominant roles in determining molecular organization or chemical reactivity.[23,24] Confinement inside a nanoscale pore can significantly change the interaction between molecules and their surroundings.[25] The proximity of any confined chemical species to the mesopore walls inevitably represents a perturbation to the "guest" molecule that could ultimately be harnessed as a "synthetic strategy" to

**Galo J. A. A. Soler-Illia**

*Galo Juan de Avila Arturo Soler-Illia was born in Buenos Aires in 1970. He obtained his degree (1989–93) and his PhD in Chemistry (1994–98) at the University of Buenos Aires (UBA), under the supervision of Miguel Blesa. He worked as a postdoctoral fellow at the University of Paris VI with Prof. Clément Sanchez (1998–2003). From 2003, he is a CONICET staff scientist at CNEA, Buenos Aires, Argentina. He is Professor at the Dpt. of Inorganic Chemistry, UBA. He has been a fellow of CONICET, CNRS, UBA and Fundación Antorchas. His main current interest is the development of novel mesostructured multifunctional materials with applications in the environment, health and energy. More information can be found at http://www.qi.fcen.uba.ar/personales/soler-illia.htm.*

**Omar Azzaroni**

*Omar Azzaroni was born in 1974 in Bernal (Buenos Aires, Argentina). He received his degree in chemistry and completed his PhD in 2004 at Universidad Nacional de La Plata, under the supervision of Prof. Roberto Salvarezza. He worked in the Melville Laboratory for Polymer Synthesis (2004–2007 University of Cambridge, UK, Marie Curie Research Fellowship in Prof. Wilhelm Huck's group) and the Max Planck Institute for Polymer Research (Mainz, Germany, Alexander von Humboldt Research Fellow with Prof. Wolfgang Knoll). From 2008, he is a staff scientist of CONICET at INIFTA, where he holds a Max Planck Partner Group since 2009. His research focuses on supra- and macromolecular materials science and soft nanotechnology. More information can be found at: http://softmatter.quimica.unlp.edu.ar.*

 

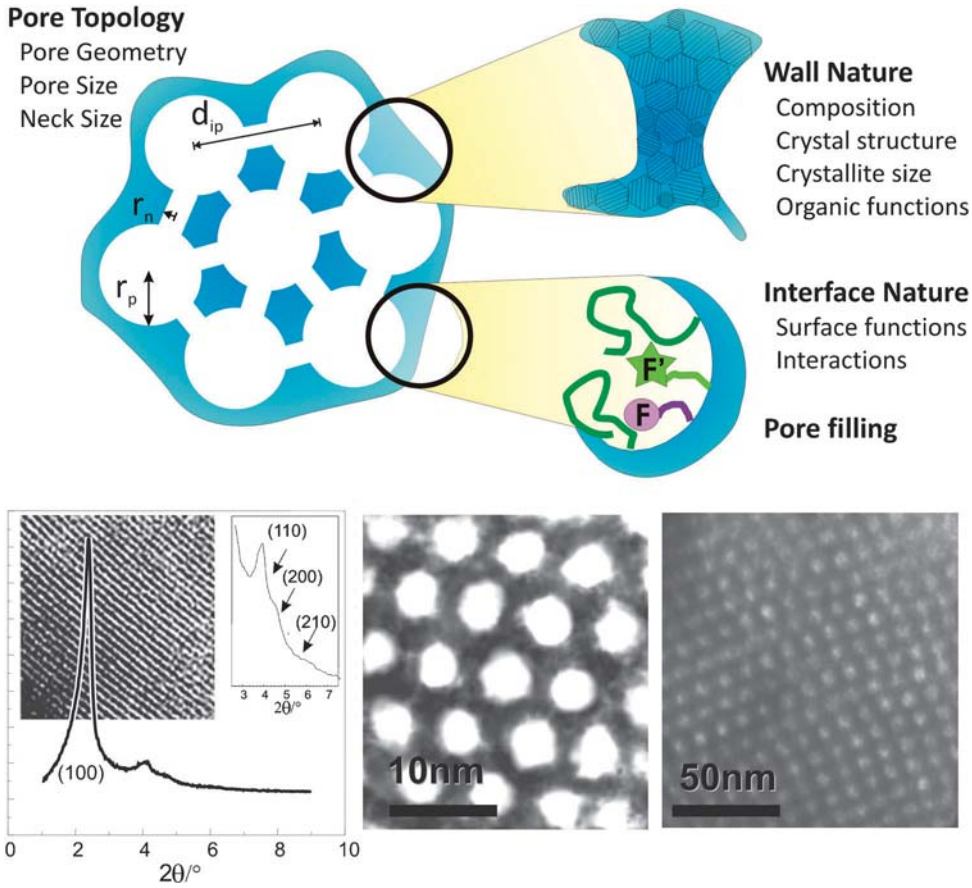


**Fig. 1** *Top*: Scheme of a mesoporous material and indication of the functional domains. *Bottom*: XRD diagram of an MCM-41 silica. Insets show the channel-like structure observed by TEM (left). TEM images of the hexagonal pore structure of a CTAB-templated titania powder (centre) and amino-functionalized zirconia thin film with cubic mesostructure (right).

modify materials' properties. In confined spaces of nearly molecular dimensions, all the adsorbed molecules are in close interaction with the surface, leading to remarkable consequences in their physical and chemical properties. Materials confined in nanoscale geometries show structures and dynamics different from those exhibited in bulk. The richness of chemical phenomena in confined environments[26,27] opens the path to advanced applications that rely on designed substrate–surface interactions. In particular, mesoporous materials provide a sound platform for the creation of large-area spatially-ordered arrays of monodisperse cavities that can be nowadays precisely designed and produced in reproducible fashion demanding very few synthesis steps. Such materials with a high and readily accessible specific surface can amplify certain functional chemical processes.

Within this context, the incorporation of macromolecular architectures into mesoporous media is emerging as an exciting area of investigation that would enable a precise control over the density and spatial arrangement of the functional groups incorporated in the pores. Considering the chemical diversity of polymers, the macromolecular building blocks can endow the mesoporous scaffold with built-in responses to a myriad of environmental chemical and physical stimuli, thus rendering them with, for example, catalytic, electronic or permselective properties. Exciting opportunities are revealed when we think in this manner. From a polymer chemistry viewpoint, the modification of the inner environment of mesostructured materials with highly functional macromolecular building blocks introduces a particularly interesting strategy to enhance active functions. Much more important—and also technologically relevant—as our array of synthetic tools grows, so does our repertoire to "engineer" macromolecules inside the mesopores. The ability to create new polymer–inorganic hybrid mesoporous materials from scratch will always be the distinguishing expertise of the chemist. However, crucial to the evolution of this field is the cross-fertilization between researchers from different disciplines that are approaching related structures from very different perspectives. In recent years the emphasis of mesoporous material design has dramatically changed towards a deeper understanding of the fundamental aspects of chemical and physical processes taking place in highly constrained geometries. As a consequence, a multidisciplinary and multi-technique approach is necessary to tackle the intriguing aspects of this emerging experimental scenario—controlling chemistry by geometry in nanoscale systems.

Although a review article of moderate size can only be illustrative of such burgeoning field, it is our hope that the juxtaposition of different perspectives and experimental systems in one place will stimulate and contribute to the ongoing

process of cross-fertilization that is driving this emerging area of molecular materials science. Taken all together, the above considerations have strongly motivated the idea of writing a critical review in which the interests of scientists, students, postdoctoral fellows, engineers and industrial researchers should be considered. To this end, this work is divided into three main sections. In the first, a brief introduction to mesoporous materials is provided. This section aims at providing the reader with the structural language, context and arguments that will be used in the subsequent discussion. Although several excellent reviews are available for this subject, we focused this section on the particular methods to achieve control over the materials' properties, presenting concrete examples and guiding the reader to specific references when necessary. The second part encompasses not only a description of the current synthetic strategies towards polymer–inorganic mesoporous materials, but also a discussion of the experimental tools that are required to fully characterize them. Selected interesting applications of polymer–inorganic mesohybrids which may deserve particular attention are included as "case studies" in the third part. The selection of "case studies" mirrors our appreciation for and belief in the impact of a boundary breaking, multi-disciplined interaction between different subfields of chemistry and physics. We strongly believe that even a casual reader of this critical review will not fail to be impressed by the wealth of synthetic strategies to new hybrid polymer–inorganic mesostructured materials as well as the broad range of experimental approaches for designing tailor-made functional materials from readily available building blocks.

## 2. A glimpse into mesoporous materials: formation, structure and modification

### 2.1 Synthetic pathways

Mesoporous and mesostructured phases presenting ordered structures at the 1–50 nm scale are built from the combination of the sol–gel process, and the templating effect of supramolecular systems. Overall, a mesostructured hybrid phase is produced in a first stage composed of inorganic building blocks and an entrapped organized supramolecular template. This step is followed by template removal, which leads to the actual mesoporous material. The formation of this first mesostructured hybrid phase is critical in obtaining a final mesoporous material with tailored features, in a reproducible way.

Control of the synthesis parameters of the inorganic species is in this context a central issue. We can exemplify this aspect with the sol–gel processes used for oxide production, which are based on the controlled polymerization of inorganic molecular precursors in mild conditions. Oxide formation by the sol–gel process implies generating metal–oxo or metal–hydroxopolymers in solution.[28] *Hydrolysis* of an alkoxy group attached to a metal center leads to hydroxyl–metal species (Reaction (1)):

$$M\text{–}OR + H_2O \rightarrow M\text{–}OH + ROH \quad (1)$$

The hydroxylated metal species can react with other metal centres leading to *condensation* reactions, where an oligomer is formed by bridging two metal centres. Condensation can lead to an *oxo bridge*, and water or alcohol is eliminated (Reaction (2)).

$$M\text{–}OH + XO\text{–}M \rightarrow M\text{–}O\text{–}M + X\text{–}OH,\ X = H \text{ or } R \quad (2)$$

In the case of *olation*, an addition reaction takes place, and a hydroxo bridge is formed (Reaction (3)).

$$M\text{–}OH + M\text{–}OX \rightarrow M\text{–}(OH)\text{–}M\text{–}OX,\ X = H \text{ or } R \quad (3)$$

Chemical control of sol–gel reactions (1–3) permits to tailor the size, shape and philicity (*i.e.* presence of polar –OH groups, or hydrophobic residues) of the inorganic building blocks. This last aspect is important, because it permits to tune the interactions with the organic templates. In silica-based systems, hydrolysis has to be catalyzed by submitting to low pH values; condensation is minimised at pH values between 1 and 3. For transition metal precursors, hydrolysis and condensation are fast processes, and highly acidic media (pH $<$ 1 for M(IV)) or complexing agents are required to avoid extended condensation.

A complex co-assembly of inorganic and organic building blocks that gives rise to well-defined framework walls and pore template regions takes place during the precipitation or gelation of the systems. Control of this first step is essential in order to define the characteristic interaction lengths that control the nascent mesophase. The main driving forces towards obtaining organized templated mesophases have been presented in the literature, and the relevant thermodynamic and kinetic factors have been analyzed.[16,29] The interactions between the inorganic components and the organic template are among the most important thermodynamic drivers, and usually determine the feasibility of mesostructure formation, and its topology. These interactions are in turn determined by the composition of the initial systems, and the adequate size and hydrophilicity of the inorganic building blocks, in order to properly locate both kinds of building blocks in space. Regarding the kinetics, the cooperative formation of an organized hybrid mesostructure is the result of the delicate balance of phase separation/organization of the template and inorganic polymerization. It has been proposed that processes linked to phase separation and organization at the hybrid interface between the inorganic building blocks and the template must be faster than the inorganic condensation that leads to "freezing" of a continuous matrix. Winning this "race towards order" leads to highly organized mesophases; if the inorganic condensation rate takes over the template self-assembly and the co-assembly at the hybrid interface, only poorly ordered mesophases will result.[29,30]

There are globally four routes leading to obtaining mesostructured materials: (1) direct precipitation,[2] (2) True Liquid Crystal Templating (TLCT),[31] (3) Evaporation-Induced Self-Assembly (EISA),[32,33] and (4) exotemplating,[34] which are sketched in Fig. 2. We must stress that the use of these synthesis routes has afforded a wealth of different structures with a great diversity of pore size and topology, and an impressive variety of frameworks, ranging from oxides to phosphates, sulfides metals, or polymers, have been produced so far. Each of the synthesis routes represents a certain synthetic strategy and has been developed for a given type of

 

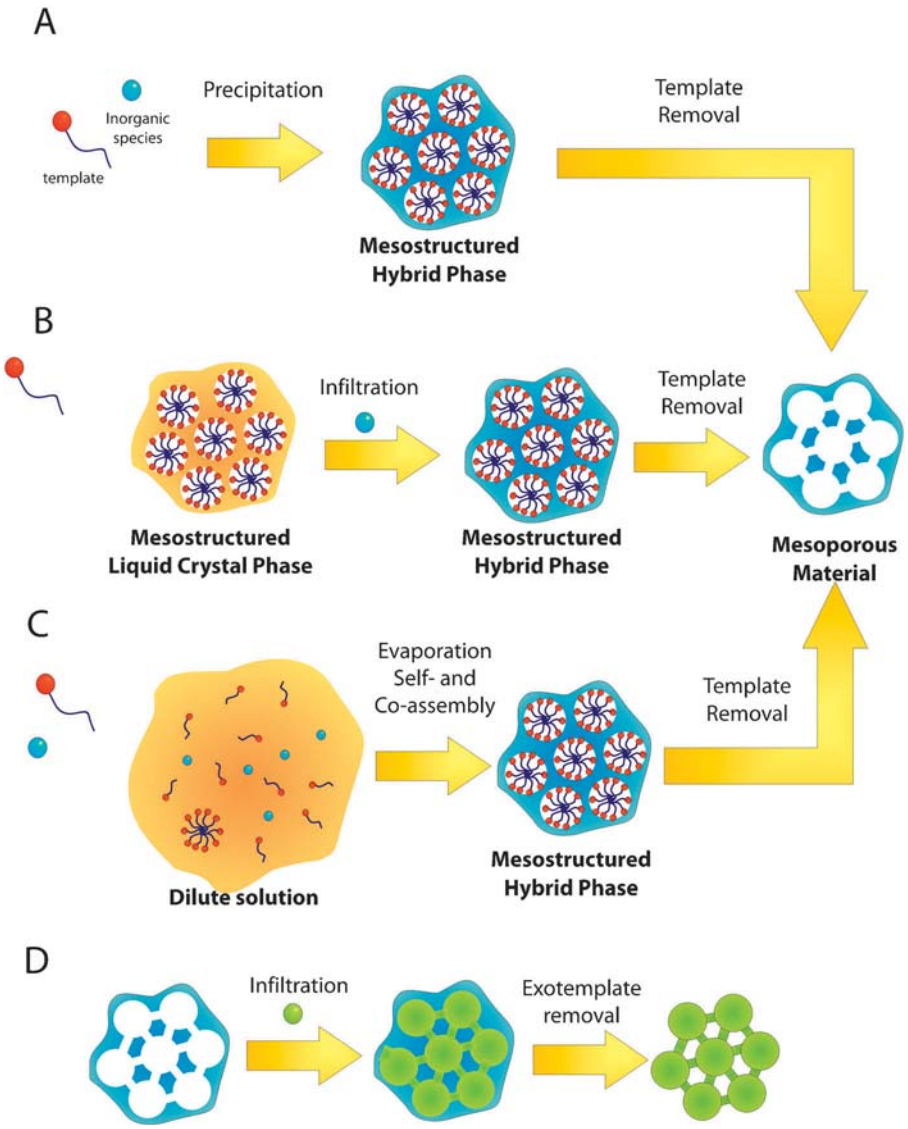


**Fig. 2** Scheme of the main synthesis routes to mesoporous materials: precipitation (A), True Liquid Crystal Templating, TLCT (B), Evaporation-Induced Self-Assembly, EISA (C) and Exotemplating (D).

framework-template combination. In addition, each route is suited to the final desired shaping of the material (*i.e.* powders, films, membranes, gels, *etc.*). Therefore, these two central aspects: *structural control* (at the molecular and meso-scale level) and *desired shaping-processing* (at the micronic–macroscopic scale) of the final material dictate the choice of a given synthetic route.

**Precipitation.** This first developed route relies on the cooperative assembly of the mineral precursors and the supramolecular template that occurs upon hydrolysis and condensation of the inorganic species. In the case of oxides, evidence provided by *in situ* measurements (SAXS, NMR, fluorescence) demonstrated that a variety of complex concurrent processes implying aggregation of micelles and partially condensed metal–oxo species take place before leading to a mesostructured material, constituting a complex mechanism.[29,35–37] However, a general rule for most cases seems to be that a mesophase with local order is formed first; rearrangement of this mesophase upon aging leads to highly ordered mesostructured materials; coexistence of highly ordered and locally ordered domains is possible, and rearrangements between these two phases with different ordering are responsible for the highly ordered mesostructures obtained upon aging.[38] In order to obtain highly ordered pore systems, it is thus essential to control the inorganic hydrolysis and condensation, leading to produce hydrophilic oligomers that are able to interact favourably with the templating species, which is typically present in concentrations above the critical micellar concentration. To this end, the synthetic conditions such as solvent, pH, precipitant, temperature and aging must be optimized. For example, silica can be obtained either in alkaline[2] or acidic media,[39] in which the size and hydrophilicity of Si–oxopolymers can be adequately controlled. Silica synthesis in nearly neutral medium has been achieved by using small fluoride quantities that permit a fast hydrolysis and slower, controlled, condensation.[40] In order to obtain mesoporous oxides derived from the more reactive transition metals, condensation should

be delayed by lowering the pH, or by adding complexing agents. For example, alkylphosphate surfactants were first used with the double function of templates and condensation controllers in the synthesis of mesoporous titania by the so-called ligand-assisted templating approach.[41] Other complexing agents such as atranes,[42] acetylacetonate[43] or peroxide[44] have also been used in order to moderate $Ti^{IV}$ reactivity and optimize the metal–template interactions, leading to highly ordered mesoporous titania, or other transition metal frameworks. While precipitation methods are straightforward and large quantities are obtained, mesoporous phases obtained from precipitation can only be processed as powders, and reproducibility is still an issue in the case of non-silica materials.

**True liquid crystal templating (TLCT).** This route developed by Attard *et al.*[31] implies three steps: the formation of a liquid crystalline mesophase, infiltration of this mesophase with the mineral precursor, followed by the formation of the mineral walls in the aqueous regions between the micelles by inorganic condensation (oxides, sulfides) or electrodeposition (metals). While this flexible method is useful for the production of mesoporous metal electrodes,[45] the procedure is delicate, and the initial lyotropic liquid crystal can be disrupted by the addition of metal precursors, or by the release of low weight alcohols upon hydrolysis, limiting the applicability of the method.

**Evaporation-induced self-assembly (EISA).** This method is based on the formation of a hybrid mesostructured phase after solvent evaporation from dilute solutions containing inorganic precursors, the templating agent and other additives.[32] The solution can be casted, in order to form mesostructured gels, dip- or spin-coated to form mesoporous thin films, or sprayed, in order to form mesoporous microparticles. This evaporation-based procedure permits one to avoid the diffusion problems encountered when infiltrating a real LC structure with a metal precursor, which constitutes a limitation of the TLCT method. The mineral-template hybrid mesophase formed upon solvent evaporation is flexible as-synthesized, due to the incomplete inorganic polymerization. Aging of these soft hybrid mesophases under controlled humidity conditions and low temperature helps to improve ordering.[46] Inorganic condensation can be "turned on" in a subsequent step by heating or adding a condensation enhancer (ammonia), leading to a condensed inorganic framework. This procedure allows for a very flexible material processing in the shape of xerogels, monoliths, aerosols[47] or thin films.[30,48] This route is also interesting for the chemical variety of frameworks that can be obtained. In particular, this is the method of choice for transition metal oxide-based materials, in which the inorganic condensation can be readily controlled by addition of an acid, which is subsequently eliminated by evaporation.[33] In addition, this method is the natural choice for producing mesoporous transparent thin films (20–500 nm) with excellent substrate adhesion, in the form of monolayers or even complex multilayers.[49]

**Exotemplating.** The templating pathways presented above rely on supramolecular porogens that are added to the initial synthesis mixtures. Upon precipitation, TLCT or EISA methods, the soft templates remain occluded in the solid and leave a pore system after their removal. These routes have been extremely useful for producing a number of inorganic or hybrid matrices. However, there are some limitations towards these "soft mesotemplating" procedures, especially in obtaining materials that tend to disrupt a templating liquid crystalline phase (*e.g.*, organic precursors with hydrophilic–lipophilic balances close to those of the templates) or to crystallize upon precipitation (typically, first series transition metals that readily form basic salts after hydrolysis-condensation). Therefore, an alternative two-step path has been developed, in which porous materials act as "hard templates" for the synthesis. The first step consists in loading a previously formed mesoporous matrix, which acts as the "exotemplate", with the necessary precursors for the desired phase. In a second step, the exotemplate is removed, leading to a continuously porous solid or finely divided particles, depending on the connectivity of the template and the loading. The obtained material presents a mesostructure that is the "negative" of the exotemplate used. An adequate choice of the exotemplating procedure implies three factors: (a) chemical compatibility of the desired phase and the exotemplate, (b) optimization of the filling process (including wetting of the exotemplate by the filling solution), (c) the judicious selection of a template removal process. The latter limiting step is mostly based on selective solubility. A very accurate control of the structure and texture on length scales between nanometres and micrometres has been achieved

**Table 1** Description of most usual structures

| Name | Process | Symmetry | Framework | Route[a] | Surface area ($m^2\ g^{-1}$)[b] | Pore volume ($cm^3\ g^{-1}$)[b] | Pore size (nm)[b] | Ref. |
|---|---|---|---|---|---|---|---|---|
| MCM-41 | Particles | *P6m* | silica | P | 1040 | 0.7 | 1.5–10 | 2a |
| MCM-48 | Particles | *Ia3d* | silica | P | | 0.6 | 2.6–2.8 | 52 |
| SBA-15 | Particles | *P6m* | silica | P | 690–850 | 0.56–1.17 | 4.7–8.9 | 53 |
| SBA-16 | Particles | *Im3m* | silica | P | 740 | 0.45 | 5.4 | 53 |
| MSU-1 | Particles | Local order | silica | P | 644–1121 | 0.31–0.82 | 2.4–4.7 | 54 |
| CMK-1 | Particles | *Ia3d* | carbon | EXT | 1380–2000 | 1.06 | 2.9 | 55 |
| FDU-17 | Cast gels | *Fd3m* | carbon | EISA | 500–900 | 0.33–0.55 | 3.2–7 | 56 |
| — | Cast gels | *Im3m* or *p6m* | Various $MO_2$ (M = Ti, Zr, Hf, Sn,...) | EISA | 150–500 | 0.43–0.63 | 3.5–14 | 57 |
| — | Film | *Im3m* or *p6mm* | $SiO_2$ | EISA | 580–970 | 0.45–1.13 | 3.5–9 | 58 |
| — | Film | *Im3m* or *p6mm* | $TiO_2$ | EISA | 150 | 0.3–0.5 | 3–8 | 59 |

[a] Routes: P: precipitation, TLCT: True Liquid Crystal Templating, EISA: Evaporation-Induced Self-Assembly, EXT: Exotemplating. [b] Representative values.

 

over the last few years.[34] In particular, this method is extremely useful in two cases: mesoporous carbons[50] and low-valence transition metal oxides.[51] In addition, an exotemplated material can also be replicated through another filling-removal step, leading to a replica of the initial matrix.

Table 1 presents a quick overview of the most usual and reproducible structures obtained, along with their synthesis routes, pore topology, and typical values of surface area, pore volume, and pore diameter.

### 2.2 Structural control

The most relevant structural features of a mesoporous material are summarized in Table 2, along with the preferred methods employed to control them. Below we will briefly discuss these aspects by presenting selected classical examples. A detailed discussion of each of these parameters is out of the scope of this work, and authors are encouraged to refer to comprehensive reviews dealing with the synthesis parameters[60] and chemical strategies[16] leading to optimization of the synthesis.

**2.2.1 Pore topology.** The *shape*, *spatial distribution and interconnectivity of pores* constitute a central aspect, which is controlled by a variety of synthesis and processing variables. The first reports on mesoporous materials used cationic cetyltrimethylammonium bromide (CTAB) as a supramolecular template. CTAB is a cationic template with a compact headgroup that leads to a variety of silica mesostructures: MCM-41 (2D hexagonal *p6m*) and MCM-48 (bicontinuous cubic *Ia3d*) and lamellar powders can be obtained by increasing the surfactant to silica ratio.[2] Film processing permits to obtain these mesophases as well as 3D hexagonal (*p63/mmc*), or micellar cubic (*Pm3n*).[33] The shape of the template can be selected by the adequate choice of surfactants with different head-to-tail volume ratios, or hydrophilic–lipophilic balance (HLB).[61] Gemini surfactant templates with a bulkier hydrophilic head with respect to CTAB lead to three-dimensional mesophases with higher curvature.[62] The nature of the framework precursors is also important, as the organized mesophases are formed by the co-assembly of the template and the framework building blocks. For example, control of the hydrolysis and condensation of silica precursors is one of the key points that can direct to disordered or ordered structures in mesoporous thin films, due to the changes in the charge, size, hydrophilicity and flexibility of the inorganic precursors that take place during aging of the precursor sols. These features control in turn the silica–template interactions that lead to an optimum assembly of both kinds of building blocks.[30,63,64]

*Interconnectivity between mesopores* is a fundamental feature regarding pore accessibility of molecular probes,

**Table 2** Essential features of mesoporous materials, and their control

| Feature | | Control | Ref. |
|---|---|---|---|
| **Pore topology** | Symmetry of the pore system | Template nature (molecular shape) | 2, 30, 33, 61–64 |
| | Pore interconnectivity and accessibility | Template : framework precursor ratio<br>Precursor hydrolysis-condensation | 53, 65–71 |
| **Pore size** | Pore diameter | Template size<br>Post-treatment and aging<br>Thermal treatment<br>Swelling agents | 2, 16, 69, 72, 73, 76 |
| | Neck diameter | Template : framework precursor ratio<br>Post-treatment and aging<br>Thermal treatment | 70, 76 |
| | Micropore : mesopore ratio | Template type<br>Post-treatment and aging<br>Thermal treatment | 74, 75 |
| **Framework** | Composition | Precursors ratio<br>Additives for condensation control | 16, 78–81 |
| | Crystalline structure | Thermal treatment<br>Substrate (thin films) | 83–86 |
| | Wall thickness | Type of template<br>Template : inorganic precursor ratio (*s*)<br>Condensation degree of framework | 69, 70, 82 |
| **Pore surface** | Specific surface | Template type<br>Post-synthesis treatment<br>Thermal treatment | 48, 87–94 |
| | Surface philicity | Thermal treatment<br>Addition of organic functions | 87–91 |
| | Surface reactivity | Exposure of functions<br>Surface–function interactions | 87–90 |
| **Pore modification** | Solvent uptake | Surface modification<br>Mesopore size | 95 |
| | Inclusion of chemical functions | Precursor adsorption<br>Grafting of functional groups<br>Co-condensation<br>Reactivity of precursors or grafted species<br>Accessibility of pore system | 89–92 |
| | Nanoparticle inclusion | Precursor adsorption<br>Precipitation or reduction method<br>Accessibility of pore system | 96–98 |

functional groups, monomers or polymers to the pore system, in order to produce polymer-functionalized mesoporous materials. This aspect is also a consequence of the spatial pore distribution, and therefore it can be tailored mainly by the adequate choice of template nature and concentration. Bidimensional hexagonal mesophases (*p6m*) present long cylindrical-like pores, which lead to less accessible pore systems, due to diffusional constraints. Reactions tend to take place near pore openings, which is a limitation when an even distribution of organic functional groups is desired.[65] However, micropores or defects in the inorganic walls are at the origin of molecule diffusion between pores. It is known that cylindrical pores in block-copolymer templated silica are interconnected by smaller micropores located in the walls.[66] These cavities are due to the interpenetration of the template with the inorganic matrix, which actually forms a microporous corona around the mesopores.[67] Three-dimensional pore arrays present in principle improved accessibility; typical cubic (*Pm*3*n*, *Im*3*m* or bicontinuous *Ia*3*d*) or 3D hexagonal (*p*63/*mmc*) symmetries obtained from block copolymers display more accessible pores, interconnected by periodic interpore necks.[68]

In addition to pore symmetry control, exerted by changing the template (*i.e.*, the molecular packing parameters), pore interconnectivity can be adjusted by changing the template : precursor molar ratio, *s*. While smaller values of *s* lead to three-dimensional pore distributions, derived from spherical micelle templating, larger *s* values lead to less curved micelles with tubular or even lamellar features, bicontinuous phases being an intermediate case.[53,69] Interpore necks are formed either as a consequence of the symmetry of the templating lyotropic phase itself, or can develop after aging or further template addition, as will be discussed in the next section.[70] It shall be noted that the existence of a 3D pore arrangement is not necessarily a guarantee of pore interconnection and accessibility. In the case of using low quantities of template, an array of highly ordered isolated pores with three-dimensional spatial distribution can be obtained, with little or no interconnectivity.[71]

**2.2.2 Pore size.** This feature is essential to the properties of mesoporous materials. Confinement-derived effects such as capillary condensation, size selectivity or perm-selectivity can be regulated by tailoring the sizes and shapes of the mesopores and the constrictions between them. Pore diameter is also related to the pore topology, and generally regulated by the template size. Micellar templates are indeed uniform nanometric entities, composed by a well defined aggregation number. Within a given mesostructure symmetry, pore size will mostly depend on the template size, and therefore selection of the templating molecule is essential to size tailoring. The first efforts to tailoring pore size relied in the use of ionic templates with different hydrophobic chain lengths, leading to small pore sizes (2–4 nm) and thin inorganic walls, such as the MCM families and derived materials.[2] The introduction of amphiphilic block copolymer (ABC) templates permitted a more flexible tailoring in the 5–20 nm pore diameter range, opening the way to the SBA-15 and related families of large-pore mesoporous materials. Precise tailoring of the template size can be achieved by regulating the polymerization degree of the hydrophilic or hydrophobic polymeric blocks. In addition, ABC are capable to impart thicker walls, apart from being industrially available, hazard-free and easy to remove from the mineral framework by thermal treatment or solvent extraction.[69,72,73]

Micropores are usually present in mesoporous materials, as a consequence of the use of sol–gel soft methods.[74] The incomplete condensation of the inorganic framework, or the trapping of solvent or template molecules invariably lead to a texture in the subnanometre scale, which can be readily derived from nitrogen adsorption–desorption curves. Micropores can be desired, or an unwanted problem. In the first case, methods have been developed to produce zeolite-based materials presenting controlled micropores and mesopores, as a hierarchical ensemble.[75] In the most common case of sol–gel derived microporosity, the micropore to mesopore ratio can be varied by thermal treatment of the mesoporous material, but also by submitting to a careful post-synthetic treatment. The choice of the template also influences the presence of micropores, non-ionic templates being more prone to originate microporosity (see below).[69] Pore shape will also depend on the topology, and the template nature and *s* are essential factors, as previously discussed. Increase of surfactant concentration (therefore, higher *s* ratio) can lead to two different effects, depending on the template used. For ionic templates, a higher template molecule concentration will mostly result in more micelles; the interpore distances will shorten, but pore size will remain essentially constant, as well as the constrictions.[76] The case of non-ionic templates that give rise to cage-like structures like SBA-16 is different, and strategies have been developed to independently tailor pore size and interpore constrictions. An increase in *s* can result in the development of wider interpore necks (also called *pore entrances*), presumably by incorporating the additional template molecules to the developing connections between the micelles; this neck widening behaviour has also been achieved by adding a second surfactant.[70] Some of the cubic mesophases (*Im*3*m* or *Ia*3*d* symmetry) can be considered as infinite periodical minimal surfaces.[77] Although in principle pore size can be arbitrarily tuned by the molecular weight of the porogen molecule, the use of surfactants as supramolecular templating agents presents a practical limit in the 10–20 nm pore diameter range. Larger size, more complex molecules can segregate from solution, leading to inhomogeneous assembly with the inorganic building blocks and therefore to irregular pore formation. In addition, larger molecules exhibit a wider conformational landscape, and tend to present slow assembly kinetics with the inorganic components. This results generally in systems where the organic molecule acts as a polymeric spacer rather than an assembled template, and results in poorly defined pores. Routes towards organised, larger pores imply therefore the use of the usual porogens with the addition of swelling agents such as trimethylbenzene (TMB) or similar molecules.[73]

**2.2.3 Nature of the inorganic framework.** Since the beginning of this field, production of mesoporous silica and materials derived thereof has been the most exhaustively

 

explored topic. This is mostly due to the intrinsic interest in silica materials as potential substrates towards high surface area catalysts, and also to the existence of several reliable synthesis routes towards the well-known MCM, SBA, MSU or other materials. Moreover, the use of a variety of versatile silicon or organosilicon precursors opened the path to hybrid silica based hybrid frameworks. In addition, in the last years, a whole palette of mesoporous frameworks such as non-silica oxides,[78] sulfides,[79] phosphates,[80] carbons,[81] or even microporous inorganic or organic frameworks[75] has been developed. This wide range of framework compositions is possible thanks to the use of different synthesis routes, as well as the thorough chemical control of several synthesis parameters.[16] An accurate control of the hydrolysis-condensation processes of silicon(IV) or high valence metals (Ti(IV), Zr(IV), Nb(V), Al(III)), permit to produce pure and mixed mesoporous oxides in which framework composition is in principle controlled by the adequate mixture of the inorganic precursors (typically, chlorides, alkoxides or acetylacetonates) that present similar high acidity. It has to be noted that these high-valence inorganic centres tend to yield amorphous or low-crystallinity mesostructured frameworks upon precipitation or related sol–gel soft processing. In the case of low-valent metals (such as the first transition series: $M^{II}$, M = Mn, Fe, Co, Ni, Cu, Zn,...), very few reliable reports of ordered mesoporous materials by direct synthesis exist. In this case, precipitation often leads to obtaining non-mesostructured crystalline basic salts. Wall thickness can be controlled by several parameters, the most usual is the template size, and the template : metal ratio that influences the intermicelle distance. The very nature of the template also influences the wall thickness: while ionic templates lead to thinner walls, non-ionic surfactants (for example, polymeric ABC) give rise to thicker walls, due to a less defined inorganic–organic interface.[69] Notwithstanding, the use of non-ionic templates often leads to micropores, due to the strong interactions between their hydrophilic heads and the uncondensed inorganic building blocks.[67,82] Aging at moderate temperature or under hydrothermal conditions enhances inorganic condensation and permits a better phase separation between the inorganic and organic components, leading to denser walls, and well-defined pores with less or no microporosity.[70] Control of the thermal treatment of the initially obtained mesostructured precursors is essential in order to keep the high surface area and well defined mesopores, while ensuring nanocrystalline walls, in the case of non-silica. Low temperature treatment (<250–300 °C) results in low porosity, due to partial template removal, and to poor mechanical and chemical stability, due to incomplete condensation of the inorganic frameworks. Temperatures higher that 300–350 °C are necessary to completely remove the templates. At these temperatures, framework condensation is complete, in the case of oxides, therefore toughening the mesostructure. In this high temperature range, pore coarsening can begin to take place, resulting in loss of microporosity, and changes in the pore and neck shape. In the case of silica systems, evolution to higher temperatures (600–700 °C) leads to a decrease in hydrophilicity due to dehydration of surface silanol groups.

Non-silica oxides begin to undergo crystallization in the 300–400 °C range. Extended growth of crystallites constitutes a problem, for it might lead to the total loss of surface area and porosity. Detailed studies carried out on mesoporous titania thin films showed that restricted crystallization of the anatase phase takes place through nucleation-growth processes in the confined environments of the mesopore walls. The mesopore system geometry determines the final shape and size of the anatase nanocrystals. Rapid anatase nucleation is followed by confined growth, the limits to which are set by the pore interfaces. Oriented growth and rearrangement occur because of these limitations, and the final pore and crystallite structures are intimately related to the low-temperature structures.[83] Along thermal treatment, the surface area decreases, while the pore and neck sizes increase by coarsening. If the nucleation and growth processes can be controlled through gentle heating, a mesoporous, nanocrystalline, robust, and highly accessible titania framework can be achieved, which keeps the structure and topology of the original mesoporous system. Too high temperatures result in extended crystallization, and the original mesoporous structure can be lost. Therefore, an optimised thermal program is needed in order to take advantage of the concurrent processes of crystallization and pore coarsening for interesting properties such as photocatalysis.[84] Other strategies for obtaining mesoporous crystalline materials include controlled thermal treatment under an inert atmosphere, leading to partial template carbonization,[85] or the use of templates that decompose at temperatures comparable to the crystallization threshold.[86] In both cases, the soft template serves as an organic or carbonaceous scaffold that holds the mesostructure in place during crystallization and sintering, in order to avoid extended crystallite growth that would lead to disruption of the pore structure.

**2.2.4 Control of pore surface.** The high surface area of mesoporous materials is central, for it largely contributes to their energetics. Surface energy, represented by an energy term of the type $dG_{surf} = \gamma dS$, indeed controls thermodynamic and kinetics aspects (globally, stability and reactivity), that will greatly influence the materials' properties, such as wettability, adsorption, or dissolution rate. Two important features are the pore specific surface area and the surface energy, represented by $\gamma$. These parameters can be independently tailored by adjusting synthesis and processing variables. The amount of surface area is generally controlled by the template choice, the $s$ ratio and the thermal treatment, which also affects pore size, as discussed above. The nature and reactivity of the pore surface can be tailored by several means: in the case of oxides, the density of M–OH groups (thus, the hydrophilic character) can be controlled by exposure to solvents, and thermal treatment; high temperatures can lead to dehydroxylation, resulting in a hydrophobic surface, as discussed above. Surfaces with different philicity, and thus different reactivity can incorporate a wealth of chemical species, such as inorganic cations or anions, or bifunctional molecules such as silanes, silazanes, diones, phosphates, carboxylates, *etc*. It has to be pointed out that mesoporous materials tend to strongly adsorb species in solution, leading to partition and preconcentration

of reagents in the pore networks. Molecules can remain just adsorbed, or react with the surface groups, leading to functionalized pore surfaces, which will present a modified behaviour.[87–89] The differential reactivity of the grafting group towards the surface species can be exploited in order to generate selective functionalization.[90,91] Pore surface modification of mesoporous materials has vast implications in tailored materials for a wealth of applications such as adsorbents, catalysts, selective membranes, optical materials, biointerfaces, new electronics, *etc*. This is a wide and thriving field, and although some specific examples will be commented in Sections 3 and 4, the reader is referred to several specific reviews dedicated to this subject.[48,87,92–94]

**2.2.5 Pore contents.** Pore filling of mesoporous materials with liquids, molecules, polymers or nanoparticles leads to dramatic changes in their properties. Capillary condensation of vapours takes place after a critical pressure that is dependent on pore size and shape, and on the energy surface, $\gamma$, and can be explained by a modified Kelvin model.[95] Nitrogen, argon or krypton adsorption has been used as a major pore size characterization tool. In addition, solvent condensation within mesopores leads to an important rise in material density, and subsequent loss of density contrast between walls and pores. Modification of pore size, shape and surface nature change the threshold pressure ($P_c$) at which capillary condensation occurs. This parameter is roughly proportional to the inverse of the pore radius and directly proportional to the surface energy of the vapour at the material interface. Modification of pore volume also changes the electron density contrast between the empty and the filled porous structure. These effects have been advantageously used in mesoporous transparent thin films, in order to perform optical sensing.[49b,c]

Repeated pore loading cycles permit inclusion of molecular compounds, beyond pore surface modification. In this way, nanosized entities can be produced within the pore systems, with properties different from the bulk. For example, a remarkable confinement effect has been reported for MCM-41 loaded with ibuprofen, which presents quasi-liquid-like behaviour at ambient temperature, modifying its drug release performance.[96] Inclusion of metal, semiconductor or carbon nanoparticles (NP) within mesoporous materials has been reported, with particular interest in the catalysis or optics fields. NP have been incorporated to the pore array either by capillary inclusion (limited to small nanoparticles in very accessible pore systems), or by *in situ* production. The second choice is the most frequently used, and soft chemical reduction, sequential precipitation or electrochemical methods have been followed in order to load the mesoporous matrix with the desired NP.[97,98] One the most important features is an excellent pore accessibility and interconnectivity. Repeated cycles composed of precursor uptake followed by precipitation or reduction steps must be performed in order to achieve the desired NP loading. Thus, it is crucial to control the surface charge, in order to optimise the adsorption of the precursor species that will lead to the final nanocomposite material. In addition, suitable techniques have to be used to assess pore loading, and its effects on the variation of pore radius. Inclusion of polymers permits to separately control the functions at the pore surface and the pore interior, leading to multifunctional hybrid materials, and will be treated in detail in section 3.

### 2.3 Formation of mesoporous hybrid materials (MPHM)

The chemical strategies for the production of mesostructured and mesoporous hybrid phases have been presented in detail in several reviews and themed issues,[1] comprising general approaches and concepts, and specific routes towards mesoporous hybrid materials (***MPHM***), processed as powders, gels or thin films.[30,48,64,87,92,99,100] The organic components can be added during the synthesis of the mesostructure, or in a subsequent functionalization step, constituting the so-called "one-pot" or "two-step" methods. The "one-pot" (or direct) synthesis implies the co-condensation of a functional inorganic precursor, such as an organosilane with a non-functional precursor in the presence of the supramolecular templates. The "two-step" (or post-grafting) route involves addition of the organofunction by post-synthesis treatment of a mesostructured or mesoporous material, either by solution impregnation or by exposure to volatile vapours. The use of bridged organosilica hybrid precursors permitted the emergence of the very active area of Periodic Mesoporous Organosilica materials (PMO) presenting walls that contain organic functional groups, cross-linked by Si–O–Si bonds.[101] Although the synthesis of PMO can be considered a "one-pot" path, the different nature of the precursor and the possibility of locating organic groups within the pore walls make it stand out from ordinary direct synthesis, and will be treated separately. These three main routes leading to ordered MPHM are schematised in Fig. 3, and will be briefly commented upon below, focusing on the oxide-based mesoporous hybrid materials, which is the most extensively studied field.

**Post-grafting approach (Fig. 3, route A).** Mesoporous matrices present large surface areas rich in silanols or other M–OH groups; for example the Si–OH surface group density is of *ca*. 1–2 $nm^{-2}$ in the case of mesoporous silica.[102] This highly accessible surface provides a simple and immediate way to functionalise the pores by adding adequate bifunctional molecules with a variety of anchoring groups. Alkoxysilane or silazane anchoring groups are the usual choice for silica surfaces (chlorosilanes are more reactive); carboxylates, phosphates or acetylacetonates are used for transition metal oxides, and thiols for metals. A clear advantage of this method is that all functional groups actually protrude into the pores due to the surface reactions involved. However, in order to achieve an even surface coverage and strong grafting, three features have to be controlled: (a) tune the philicity and reactivity of the surface with the organofunction, to avoid localized condensation that leads to the formation of function "patches", (b) avoid competition of the anchoring group with other species in solution, for example, nucleophiles such as water in the case of mesoporous silica, (c) avoid autocondensation of the functional molecules that can lead to pore blocking due to the formation of $(R\text{-}SiO)_x$ polymers in the pore entrances.[65] Post-grafting proceeds typically in

 

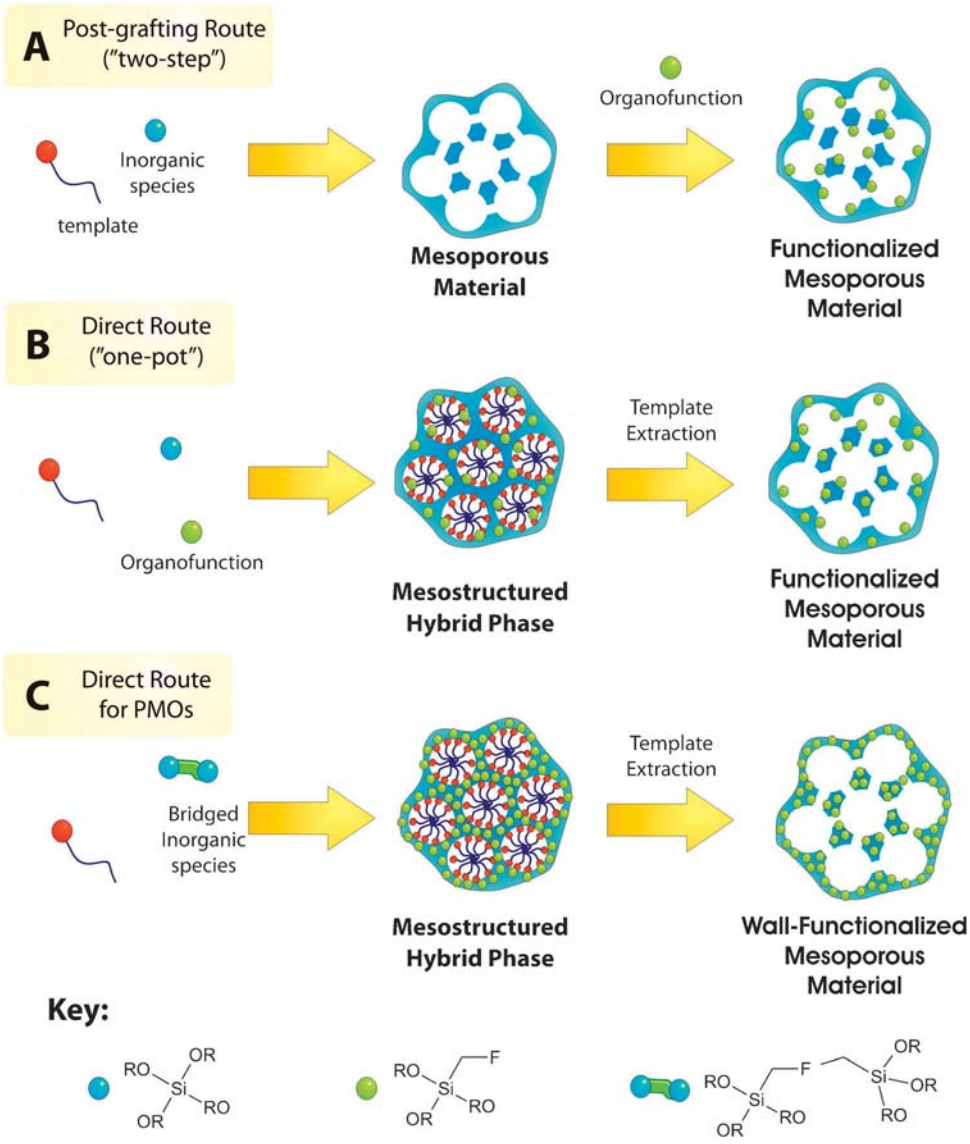


**Fig. 3** Scheme of the conventional routes towards mesoporous hybrid materials carrying organic functions. Below are representative silicon precursors, although other alkoxides might be used as network formers or modifiers.

anhydrous conditions, in which clustering is minimised; in some cases, post-grafting can also take place by breaking Si–O–Si bonds, through nucleophilic displacement at the surface silicon atom by the entering alkylsiloxane.[103] Depending on the post-grafting conditions (solvent, function solubility *etc.*), the framework can be partially dissolved or M–O–M bonds can be cleaved in the procedure.

**One-pot synthesis (Fig. 3, route B).** This route involves including an organofunctional precursor in the initial solutions, which carries the desired functional group to be incorporated. Co-condensation of the inorganic (typically TEOS, TMOS, other metal alkoxides or chlorides) and the organofunctional precursor (typically, organotrialkoxysilanes) takes place either in the initial solutions or during the assembly process, during precipitation or the formation of the liquid crystalline mesophase. This is an attractive synthesis, as it constitutes the easiest way to grant incorporation of organic groups embedded within the metal–oxo skeleton. However, certain aspects should be taken into account in order to design a proper synthesis procedure:

(a) Template removal must be performed under mild conditions, in order to avoid damaging the organic function. Even if methyl or phenyl groups are able to withstand the typical temperatures used to remove the template (250–350 °C), other groups are destroyed. Template removal for this route is typically a two step process. First, the mesostructure is heated at 150–200 °C, which enhances condensation, consolidating the framework. Subsequently, the template is extracted in a suitable solvent (acidic low weight alcohols, toluene, *etc.*).

(b) The functional alkoxides can introduce remarkable changes in the co-assembly thermodynamics and kinetics. The dangling organic functions often lead to a change in the hydrophilic–lipophilic balance of the reaction mixtures, modifying the interactions at the template–framework hybrid interface, and thus the relative stability of the possible

mesophases. In most cases, inclusion of organic containing precursors deteriorates mesostructure ordering; therefore, the organic contents should be kept low (below 30–40% mole fraction), in order to reproducibly obtain ordered mesostructures. The presence of polar organofunctions can lead however to a good organisation, and even to a change of mesostructure, as observed in nitrogen-containing mesoporous hybrid thin films derived from co-condensation.[104]

(c) The hydrolysis and condensation rates of the functional alkoxides and the inorganic precursors can be markedly different, and must be tuned, in order to avoid the formation of clusters with different concentrations of organics, which lead to irregular chemical composition of the material. For example, an alkaline and nucleophilic function such as a propylamino group in $(EtO)_3Si–(CH_2)_3NH_2$ can accelerate the inorganic condensation kinetics, eventually leading to less ordered mesostructures, unless the synthesis is performed in acidic conditions, in which the nitrogen atom is protonated.

(d) As a consequence of the composition of the initial mixtures, an important fraction of the incorporated organic functions is partially buried in the inorganic walls. This brings consequences in the mechanical and chemical properties of the materials, due to the connectivity of the hybrid framework, which is different than in the pure inorganic case.[64] In addition, only a minor proportion of the organic groups are available to react at the surface. Recent work in amino-containing mesoporous thin films showed that *ca.* 37% of amine groups are available for quantitative reactions with organic functions in post-grafted films whereas only about 16% are reactive in the materials obtained from co-condensation. This result can be understood in terms of the different distribution of functionalities obtained in both reaction routes.[105]

**One-pot synthesis with bis- or polysilylated precursors (Fig. 3, route C).** This route is analogous to Route B, but generally implies the condensation of a single-source bridged precursor, typically a bis-trialkoxysilyl-organosilane molecule (*i.e.* $(RO)_3Si–R'–Si(OR)_3$), although multi-silylated precursors can also be used. Synthesis conditions involve hydrothermal treatment and extreme pH conditions, in which sometimes integrity of the Si–C bonds might be damaged. An advantage of this route is that organic functions are integrated within the framework walls: organic functions are accessible but do not modify pore size. In some cases, and depending on the size and shape of R′, assembly at the molecular scale also takes place. Inagaki *et al.* reported an ordered benzene–silica hybrid material presenting a hexagonal array of 5.2 nm diameter mesopore channels, and crystal-like pore walls exhibiting structural periodicity with a spacing of 7.6 Å along the channel direction. This periodicity at the molecular scale is driven by the π–π stacking of benzene residues that provides a structure-directing driving force that enters in synergy with the interactions between the precursor molecules and the surfactants, determining the ordering at two different length scales.[106] Co-condensation of a bridging precursor and a terminal organotrialkoxysilane (*i.e.* $(RO)_3Si–R''$), or a second bis-silylated precursor can lead to a rich variety of bifunctional materials that permit a variety of function exposure at the pore surface or double functions within the walls, respectively.[100] An additional advantage of PMOs is the possibility to perform chemical reactions on the hybrid framework, and several examples with applications in catalysis have been recently reviewed.[107]

In summary, co-condensation and post-grafting routes are complementary, and their application depends on the features desired for the mesoporous system. Post-functionalisation has several advantages: a higher fraction of active surface species is available, grafted on a well-defined, robust mesoporous framework. However, the reactivity of surface silanols is not always easy to control, due to the different reactivity of isolated, terminal, geminal or hydrogen bonded surface species. The control of the extent of grafting reactions is an important drawback of post-functionalisation. On the other hand, ''one-pot'' synthesis is somehow complicated by the presence of organically modified alkoxides with different reaction rates and philicity that can modify or even hinder the formation of highly ordered pore arrays upon co-assembly of the framework building blocks with the template. Degradation of the organic groups during thermal treatment also has to be taken into account, and a large fraction of the functional groups remains buried. However, direct methods bring out the possibility of obtaining homogeneous function distribution, and the use of bridged precursors opened the rich field of PMOs. Overall, both routes can be combined in order to obtain complex multifunctional pores. For example, the consecutive application of one-pot and post-grafting permits to produce bifunctional mesoporous films.[108]

The ultimate goal of MPHM synthesis is to use all the possible synthetic tools described above in order to design controlled size pore systems with any desired functional groups attached to the surface or within the pore walls, and to control the interactions between those functional groups in the confined conditions imposed by the pore size and shape. In particular, the control of spacing between the organic functions, and their spatial location in the macroscale are central features, if advanced multifunctional systems are sought. A vast catalogue of construction rules are ready to be used for building up designed multifunctional MPHM, which includes total pore control, selective reactivity, tuning of surface charge or philicity, formation of self-assembled monolayers, and positional control of functional groups.[99,109,110] The intelligent choice among these nanoscale-molecular scale tools permits to imagine complex systems with well-crafted chemical species located in spatially arranged functional domains. The next section will be dedicated to the analysis of exemplary systems that will illustrate this powerful concept.

## 3. Incorporation of macromolecular building blocks into mesoporous materials: synthetic strategies towards functional hybrid polymer–inorganic mesostructures

### 3.1 Monomer impregnation/inclusion followed by polymerization.

A straightforward strategy to incorporate macromolecular building blocks into mesoporous materials relies on the *in situ* polymerization of monomer-loaded mesopores. In a

 

seminal work, Bein and collaborators developed a simple but effective protocol to build up functional macromolecular units within mesoporous frameworks.[111,112] Conducting filaments of polyaniline were prepared into 3-nanometre-wide mesochannels by adsorption of aniline vapor into the dehydrated host, followed by reaction with peroxydisulfate, thus leading to encapsulated polyaniline macromolecular chains bearing several hundred aniline rings.[113] This approach based on the gas-phase incorporation of monomer units into the mesochannels was extended to different functional units leading to a plethora of hybrid platforms in which the polymeric building blocks were selectively confined within the pores.[114] For example, Bein *et al*. reported the synthesis of host–guest nanocomposites by the adsorption of methyl methacrylate (MMA) and its conversion to PMMA in the presence of benzoyl peroxide within MCM-41 and MCM-48 mesochannels.[115] Nitrogen sorption isotherms confirmed the filling of the mesopores with the polymer while thermogravimetry evidenced that the polymer content of the composites increased with increasing pore volume. More important, scanning and transmission electron microscopy confirmed that polymer deposition did not occur on the external host surface, thus evidencing that monomer preconcentration in the mesopores is a key step to attain spatial control over the polymerization reaction. Furthermore, polymers confined in the mesochannels did not show characteristic bulk behavior with respect to their glass transition temperature. The absence of a glass transition event in the composites prepared *via* gas-phase adsorption could be ascribed to nanoconfinement effects due to strong polymer–host interactions at the nanometre scale.

Hyeon *et al*.[116] exploited this methodology to create polypyrrole/poly(methyl methacrylate) coaxial nanocables through the sequential polymerization of methyl methacrylate and pyrrole monomers inside the channels of mesoporous SBA-15 silica, followed by the removal of the silica template SBA-15 (Fig. 4). The strategy consisted of incorporating methyl methacrylate (MMA) into the pores of SBA-15 silica by heating for 5 h at 90 °C under reduced pressure. Then, MMA was polymerized in the presence of benzoyl peroxide under an argon atmosphere at 70 °C for 2 days and then 120 °C for 2 h, followed by evacuating in a vacuum oven at the same temperature for 18 h. Next, pyrrole was loaded into the pores of the PMMA/SBA-15 composite using the same conditions as in the MMA incorporation, and then polymerized with 20 mL of 0.81 M aqueous $FeCl_3$ solution for 3 h. The resulting solid was retrieved by filtration, followed by drying under vacuum at room temperature for 12 h. To remove the silica template, the PPy/PMMA/SBA-15 composite was dispersed in an aqueous HF solution (48 wt%), and was stirred overnight.

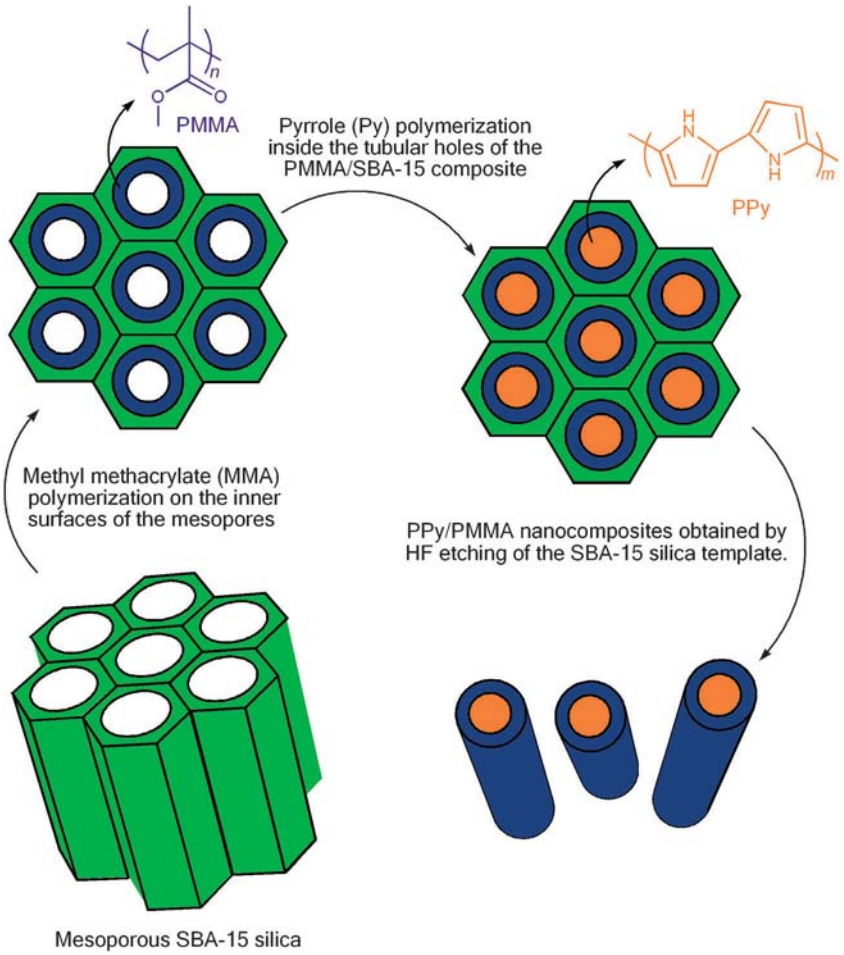


**Fig. 4** Sequential synthesis of polypyrrole (PPy)-polymethacrylate (PMMA) composite architectures into the inner channels of mesoporous silica.

Sequential polymerization reactions within mesopores can also lead to nanoconfined polymer blends. Kelly *et al*. described the formation of poly(3,4-ethylenedioxythiophene) (PEDOT) blended with poly(furfuryl alcohol) (PFA) by a sequential infiltration–polymerization approach.[117] The PEDOT-modified mesoporous silica was prepared by filling the mesoporous silica with a toluenic solution of EDOT (Fig. 5). The silica was previously heated to 120 °C for 2 h to remove adsorbed water and then cooled to room temperature. The EDOT solution is incorporated gradually to completely fill the pore volume of the silica by using a micropipette, and the mixture was agitated with a spatula for several minutes. The powder was transferred to a vial and dried at 60 °C for a period of 1 h, after which an aqueous solution of sodium persulfate was added to initiate the polymerization. Once the samples were purified, the polymerization of poly(furfuryl alcohol) was accomplished by drying *in vacuo* the PEDOT-modified samples at 85 °C for 2 h followed by the incorporation of furfuryl alcohol to completely fill the remaining pore volume of the mesoporous host. Finally, the monomer was polymerized by heating at 150 °C for 3.5 h. The filling of the mesopores and the polymer distribution within individual mesoporous particles were determined by a combination of energy-dispersive X-ray microanalysis, X-ray photoelectron spectroscopy, and nitrogen adsorption. The results suggest that when PEDOT is added to the silica host, followed by PFA, the phase separation of the two immiscible polymers is constrained by the dimensions of the silica mesopores, ensuring nanoscale contact between the two phases. The silica template can be removed by etching with 25% hydrofluoric acid, leaving behind a blended polymer microparticle. The etched microparticles exhibit macroporous morphologies different from that of pure PEDOT particles prepared by a similar route. The blended microparticles also appear to undergo limited phase separation provided that no evidence of polymer domain segregation was observed. Interestingly, when PFA is added to the host first, followed by PEDOT, the final composition of the blend is drastically altered. The reversal of the blending order results in a more amorphous, phase-separated material, thus demonstrating that nanoconfinement effects arising from the interaction of the polymers with the mesopore walls may dictate the factors that govern the structural reorganization of the constrained polymer blend.

The synthesis of nanocomposites by sequential chemical reactions within mesopores has been also extended to the construction of nanoconfined inorganic-hybrid architectures. Zhang *et al*. reported the fabrication of ZnO quantum dot/polythiophene (ZnO/PTh) into mesoporous silica (SBA-15) *via* a simple wet chemical two-step approach.[118] First, the SBA-15 was thermally treated at 120 °C to remove the physically adsorbed water and then immersed in a thiophene solution (in methylene chloride). After sonication, the solution is slowly evaporated at 30 °C during a period of 24 h. This protocol enables the efficient incorporation of monomer units into the mesochannels. Then, the monomer-loaded mesoporous material was treated with an ethanolic solution containing $H_2O_2$ and $FeCl_3$ in order to initiate the polymerization of the confined monomers. Finally, the preparation of the ZnO/PTh/SBA-15 nanocomposites was accomplished by immersing the PTh/SBA-15 composites in an ethanolic solution of zinc acetate followed by treatment with an aqueous solution of LiOH to form ZnO quantum dots into the PTh-modified mesochannels. The photoresponse of ZnO/PTh/SBA-15 nanocomposites was studied with respect to its incident photon-to-collected electron conversion efficiency (IPCE) and morphology. The large increase in IPCE indicated that the ordered ZnO/PTh/SBA-15 hybrid architecture greatly improved the ability of charge collection and transportation. In addition, the presence of SBA-15 proved to be critical for controlling the interfacial morphology and hence enlarging the interfacial area of the inorganic–organic heterojunction. These results highlight the importance of hybrid nanostructured platforms as key enablers to photovoltaic cells provided that they are able to create more charge transfer junctions with high interfacial area.

Polymerization of mesopore-confined monomers can be also carried out by electrochemical (instead of chemical) means to produce, for example, mesoporous silica filled with

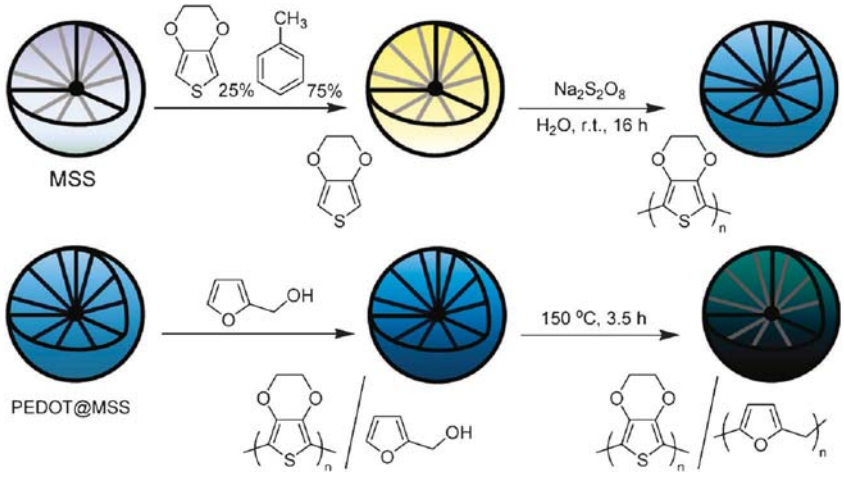


**Fig. 5** Sequential infiltration–polymerization steps necessary to accomplish the synthesis of PEDOT/PFA-mesoporous hybrids. Reproduced with permission from T. L. Kelly, S. P. Y. Che, Y. Yamada, K. Yano, M. O. Wolf, *Langmuir*, 2008, **24**, 9809–9815. Copyright 2008 American Chemical Society.

 

polypyrrole.[119] In this case, prior to monomer adsorption, the mesoporous host (silica particles—SBA 15) required prolonged heating (300 °C for 3 h) to remove air and water in the channels. The host matrix and pyrrole monomer were separately placed in two glass tubes which were connected into a self-regulating system and kept at equilibrium under vacuum at room temperature for 24 h. Thereafter, pyrrole molecules were driven into the channel leading to the pyrrole/SBA-15 nanocomposite. Then, the pyrrole/SBA-15 nanocomposite was dispersed in water and the suspension was dropped on the surface of a glassy carbon electrode. The pyrrole/SBA-15 modified electrode was subject to continuous cyclic electrode potential scans. Pyrrole molecules adsorbed in the channels of SBA-15 were electropolymerized and the PPy/SBA-15 modified electrode was obtained. The XRD, SEM, TEM, $N_2$ adsorption/desorption and FT-IR studies confirmed that the ordered mesostructure of SBA-15 remained unchanged after encapsulation and PPy was located in the channels of SBA-15.

Previous approaches were mostly based on the incorporation of monomer units *via* gas-phase adsorption. Even though this methodology has been proven successful by different authors,[120] it requires careful preconditioning of the mesostructured host, *i.e.*: heating and vacuum, provided that air and moisture can seriously affect the incorporation of hydrophobic monomers into hydrophilic pores. The disadvantages of "gas-phase" inclusion methods can be overcome by "wet" strategies based on the use of monomer units displaying affinity to the pore walls.[121] Recently, Wolf *et al.* reported a new poly(*p*-phenylenevinylene) (PPV) composite material obtained through the incorporation of insoluble PPV polymer chains in the pores of monodisperse mesoporous silica spheres through an ion-exchange and *in situ* polymerization method.[122] The mesopores were templated by the alkylammonium surfactant leading to a scenario in which the interior of the mesopores contains alkylammonium–siloxide ion-pairs. Then, the surfactant-filled mesoporous silica spheres were refluxed in a methanolic solution of *p*-xylylenebis-(tetrahydrothiophenium chloride) to promote the ion exchange of the alkylammonium surfactant inside the pores for the doubly charged monomer. The basic siloxide sites were then able to deprotonate the monomer and cause it to undergo polymerization. Subsequent heating of the pPPV intermediate at 200 °C *in vacuo* produced the fully conjugated PPV material confined in the mesoporous structure.

The use of "wet" chemical routes to incorporate the monomers and proceed with the polymerization reaction has been also extended to the use of free radical polymerization as a tool to build up mesopore-confined polymers. Ryoo *et al.*[123] exploited this straightforward route through radical polymerization of vinyl monomers inside mesoporous silica to prepare composite functional materials without altering the well-defined mesoporosity and locating the polymer entities selectively onto the silica mesopore walls (Fig. 6). The experimental protocol demanded the incorporation of vinyl monomers, cross-linkers, and radical initiators onto the pore walls of mesoporous silica *via* the wet impregnation method, followed by equilibration under reduced pressure in order to achieve uniform distribution. Then, the monomers predominantly incorporated/adsorbed on the mesopore walls were subsequently polymerized with heating to form a uniform polymer layer on the surface of the silica framework. Finally, the polymer–silica composite materials were washed with chloroform and ethanol in order to remove remaining monomers and loosely adsorbed polymers. $N_2$ adsorption isotherms and XRD characterization revealed that *in situ* polymerization of nanoconfined monomers led to uniform films on silica walls. This strategy enables a certain degree of control over the location of the confined polymers by tailoring the mesostructure of the silica framework as well as the polymerization conditions.

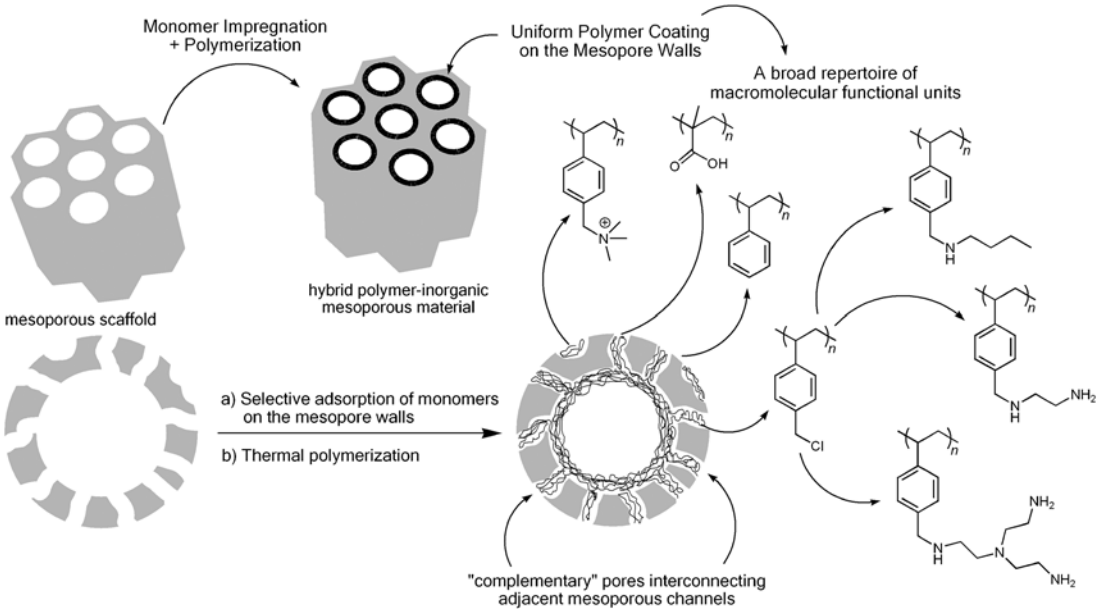


**Fig. 6** Synthetic strategy based on selective monomer adsorption followed by thermal polymerization for obtaining uniform functional polymer coatings on mesoporous frameworks.

In this regard, it is worthwhile indicating that, even though free radical polymerization is the most versatile method for the polymerization of vinyl monomers, the propagation reaction is generally more difficult to control than ionic processes due to the irreversible termination of the growing polymer radicals through recombination and disproportionation reactions. However, diverse chemical and physical strategies have been devised to suppress such termination reactions. The former utilize transition metal complexes to stabilize growing polymer radicals *via* reversible interaction, while the latter employ restricted spaces such as micelles to provide an isolated reaction environment for each growing polymer radical. From the latter point of view, mesoporous materials displaying uniform arrays of nanoscopic channels may provide a confined but adequately large space for the synthesis of macromolecular building blocks. Along these lines, experimental work by Aida and co-workers[124] on the free radical polymerization of methyl methacrylate (MMA) within mesopores revealed that the confined growth of high molecular weight polymer (PMMA) as well as the formation of long-living propagating polymer-radicals, as observed by electron paramagnetic resonance (EPR), is feasible. The molecular weight of PMMA within the mesopores could be controlled over a wide range by changing the monomer-to-initiator mole ratio. This indicates that mesopore-confined free radical polymerization enables the formation of a whole set of hybrid materials by simply choosing the adequate mesostructure and the desired monomer units.[125] Various commercial monomers are available, and their copolymerization can be a route to prepare multifunctional materials, including polyelectrolytes, hydrophobic and thermoresponsive polymers. Hence, depending on the monomer, the resultant confined polymers can easily be post-functionalized to incorporate diverse functional groups in high density, due to the open porous structure allowing facile access for the chemical reagent.

Kleitz *et al.* described the tailoring of mesoporous amine-functionalized polymer–silica composites by a two-step confined polymerization technique.[126] A functional vinyl monomer, chloromethylstyrene (CMS), was polymerized within the mesostructure leading to a uniform coating on the mesopore surface. In the second step, diverse amine-based moieties were attached to the polymer surface by nucleophilic substitution, generating a variety of nanoporous amino polymer–silica composites. This approach allows for a tuning of surface concentration of the organic groups either by varying polymer loading or by copolymerization of the CMS monomers with non-reactive monomers (styrene) as well as the facile incorporation of diverse types of amine groups, *e.g.* secondary amines, diamines, linear or branched polyamines. These composite materials were shown to be active as catalysts in the Knoevenagel condensation reaction confirming their potential in liquid phase heterogeneous catalysis. Experimental evidence also reveals that the nature of the mesoporous framework and the polymerization conditions can lead to the appearance of blocking effects. The distribution and uniformity of the polymer layer along the channel walls depend on the content of polymer in the composite, which can be controlled by altering the polymerization conditions during the synthesis. At higher content, the polymer layer is formed heterogeneously in thickness along the channels, resulting in pore plugging and heterogeneous pore size, but without altering the ordered hexagonal mesostructure of the material.[127] The synthesis strategy using vinyl monomers can introduce remarkable advantages by incorporating organic moieties within the mesoporous silicas *via* the formation of a robust C–C bond rather than hydrolysis-susceptible siloxane bonds. However, polymers are not actually "grafted" to the pore walls but physically confined within the mesostructure. The presence of "complementary" pores interconnecting adjacent mesoporous channels is important for fixing the polymer phase provided that macromolecular layer can acquire high stability through the formation of an interpenetrating network between the mesoporous framework and the polymers.

### 3.2 Functionalization of mesoporous materials with dendrimers and dendronized macromolecules

Dendrimers are macromolecular building blocks characterized by a regularly branched structure synthesized by step-by-step reactions. There are several distinctive features that make them attractive functional units for molecular design of mesopores, these are: accurate control over the whole molecular architecture, high level of monodispersity and nanoscale dimensions. Synthesizing dendrons and other dendritic architectures within the mesoporous framework[128] introduces the possibility of generating hybrid materials displaying a high density of predesigned active sites that might be useful for designing catalytic platforms[129] or "active" membranes,[130] just to name a few examples. Polyamidoamine (PAMAM) dendrimers up to the third generation were grown from amino-functionalised mesoporous silica *via* sequential Michael addition of methyl acrylate followed by amidation in the presence of ethylenediamine.[131] In-depth characterization of dendrimer-modified mesoporous silica using nitrogen adsorption, solid state NMR, FTIR, thermogravimetry, and chemical analysis revealed that dendrimer growth took place inside the channels with an average yield higher than 97%, all synthesis steps being included. The third generation was found to almost completely fill the pore system. These materials were then used as nanostructured supports to anchor rhodium species leading to rhodium-complexed polyamidoamine (PAMAM) dendrimers grown inside the channels of MCM-41. This was accomplished by phosphinomethylating and then complexing generations 0, 1 and 2 with rhodium. The Rh-PAMAM-G(0) and Rh-PAMAM-G(1) nanomaterials displayed very good activity in hydroformylation of 1-octene (turnover frequency of 1800 $h^{-1}$ at 70 °C) and the catalyst could be recycled several times without loss in activity (Fig. 7). These functional aspects make them excellent candidates for recyclable catalysts in olefin hydroformylation reactions. The use of dendritic mesoporous silicas is gaining increasing interest in catalysis. For example, by changing the chemical nature of dendritic networks (aliphatic or aromatic), it is possible to have predominantly base catalysts within a large range of well-defined controlled basicities. The hydrophobic nature of the dendritic mesostructures is advantageous in increasing reaction rates by altering local water concentration

 

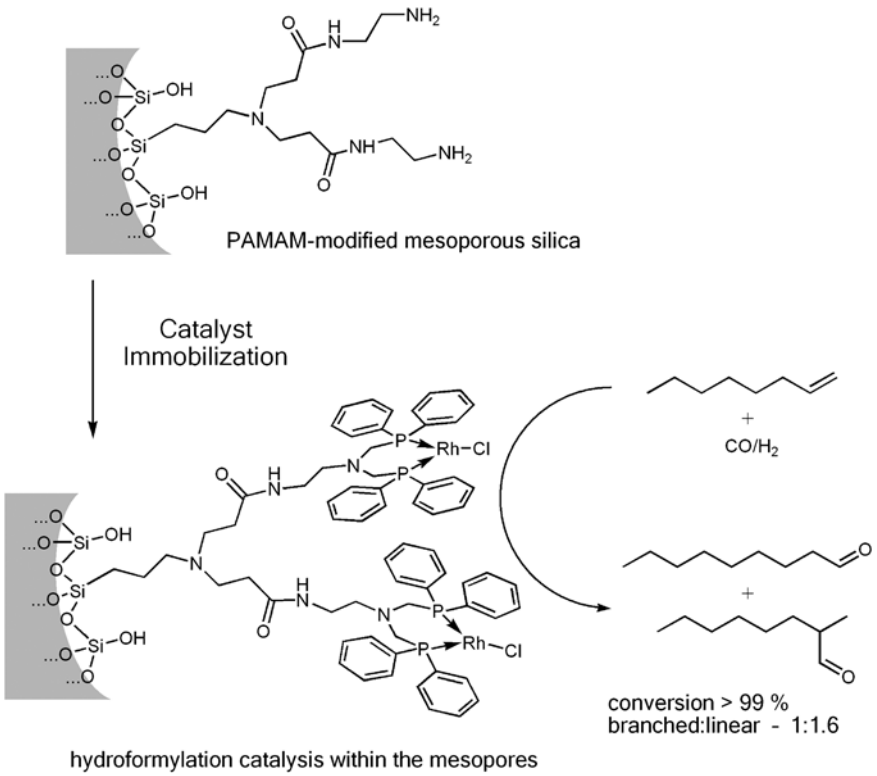


**Fig. 7** Scheme describing the construction of PAMAM–MCM-41 hybrids, their phosphinomethylation and complexation with rhodium and subsequent use as catalytically active material for olefin hydroformylation.

in the Knoevenagel condensation reaction.[132] Higher generation dendrimers were supposed to exhibit a higher density of active sites, but instead, they were found to be less effective than catalysts of lower generation. This can be attributed to steric crowding. Beyond generation 3 (G3), the mesoporous channels were essentially blocked and the dendrimer stopped growing. These data indicate that the pore system plays an important role in the synthesis of supported dendrimers of a desired generation.

Using larger pore (8.3 nm) SBA-15 silica with less-grafted propylamine, Shantz and co-workers synthesized up to G4 melamine-based dendrimers inside the support channels.[133] The porosity of the hybrid material can be modified either by using dendrimers of different generations (Fig. 8), using different linkers in the dendrimer structure, or by controlling dendrimer loading.

Porosimetry measurements indicated that the effective pore size of the hybrid and the total pore volume of the material can be controlled independently of one another. Copper sequestration was used as a probe to demonstrate that the terminal amino groups of the dendrimer are accessible and able to bind Cu(II).[134] These melamine-based dendrimers[135] confined in the mesoporous structure have also shown interesting applications as $CO_2$ absorbers[136] as well as effective solid base catalysts for a diverse range of chemistries, which include aldol chemistry and transesterification reactions. The dendron-modified mesoporous materials are active in both the nitroaldol (Henry) reaction and the transesterification of glyceryl tributyrate to afford methyl esters.[137] In both reactions it is observed that dendrons terminated with primary amines are more catalytically active than samples containing dendrons terminated with secondary amines. The first generation dendrons are the most active for both chemistries and larger pores displayed a higher activity than the smaller ones indicating the critical role of molecular transport and diffusion resistance in the catalytic functional properties of hybrid polymer–inorganic mesoporous films. The experimental results reported by Shantz and co-workers indicate that dendron catalysts are much more active and stable than simple amines attached to silica in the transesterification of triglycerides.

A different strategy to functionalise the mesoporous network with dendrimers relies on the implementation of a post-synthesis method using a novel amine dendritic precursor.[138] The synthesis of such building blocks is based on the introduction of a spacer unit with a terminal T-silyl function on some of the peripheral amine groups of poly(propyleneimine) dendrimers. These precursors can react with silanol groups on the pore walls leading to the covalent modification of the mesoporous films with predesigned dendritic units. The post-grafting reaction should be carried out under anhydrous conditions in order to avoid self-condensation of dendritic precursors in the presence of water. This synthetic route represents an alternative to the preparation of amine-functionalized and dendrimer-functionalized mesoporous silica with a highly dense population of amine groups, avoiding several reaction steps of the iterative procedure usually followed for dendritic growth inside the channels of mesoporous materials. The use of different dendrimer generations and nominal degrees of surface functionalization can be exploited with simple experimental variables to finely tune the incorporation of amino group into the mesoporous framework. On the other hand,

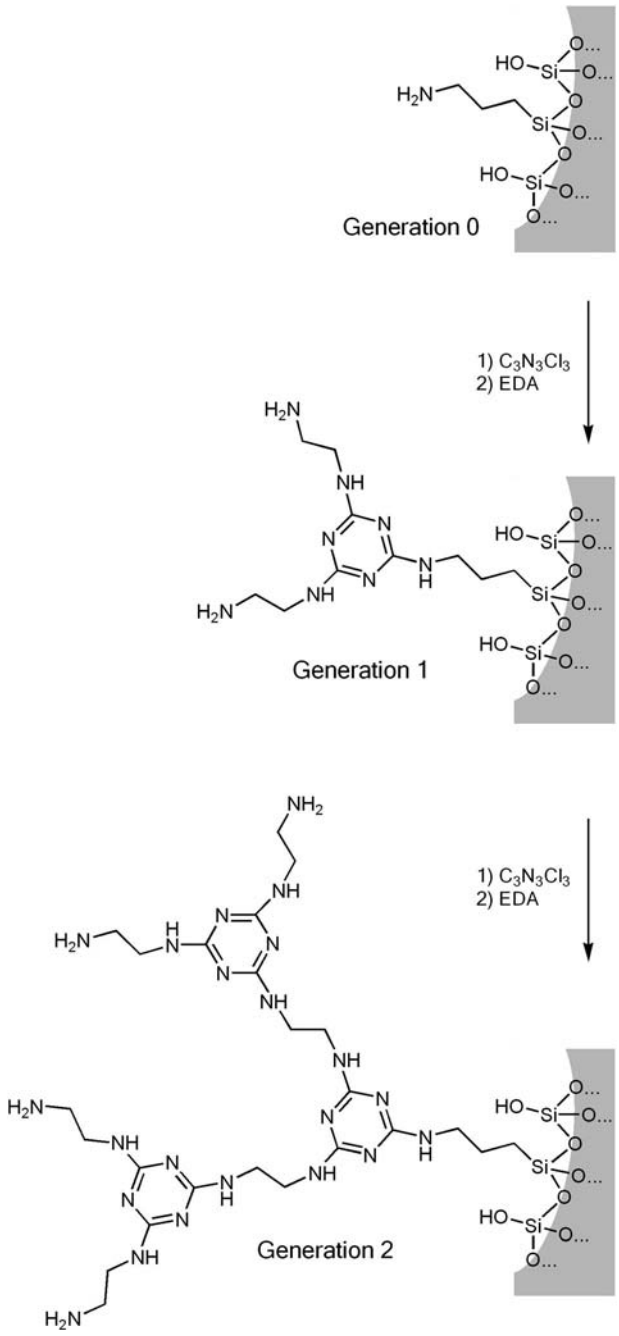


**Fig. 8** Synthesis of different generations of dendrimer-mesoporous hybrids through sequential reactions on the mesopore walls.

hyperbranched polymers prepared in a one-pot synthesis also constitute a valuable alternative to functionalize mesoporous frameworks with dendritic macromolecules. Linden and co-workers proposed a simple method based on hyperbranching polymerization for functionalizing mesoporous silica with high loading of amine groups.[139] These authors used an acid-catalyzed hyperbranching polymerization approach to produce reactive primary amino groups on the surface of mesoporous silica in the form of a surface-grown polyethyleneimine (PEI), as depicted in Fig. 9.

The polymer has been grown directly from the surface silanol groups utilizing a highly reactive, non-bulky monomer, aziridine. This technique can be implemented through the introduction of acetic acid into the mesoporous silica together with the monomer before polymerization or by using COOH-functionalized silica as the substrate for the polymerization in order to aid a complete surface functionalization. The surface polymerization of aziridine was straightforwardly performed with toluene as solvent, in which the SBA-15 substrate was suspended in the presence of catalytic amounts of acetic acid. The presence of the catalytically active COOH function on the pore walls enables a homogeneous growth of PEI. In this regard, due to the high amine loading, hyperbranched PEI-modified mesoporous silicas have shown interesting properties for $CO_2$ capture and could be extended as promising new materials for acid gas capture. The advantage of this hybrid material over previously reported adsorbents rests in its large $CO_2$ capacity and multicycle stability. The material was recycled by thermally desorbing the $CO_2$ from the surface with essentially no changes in capacity. Furthermore, the organic groups on the surface were stable in the temperature range between 25 and 130 °C due to the robust covalent attachment between the mesoporous support and the hyperbranched polymer.[140]

Confinement of fluorescent functional groups within mesopores brings the possibility of exploiting the optical properties of dendrimer-containing thin films for sensing applications. Phosphorus-containing dendrimers presenting fluorescent groups were grafted onto nanocrystalline mesoporous titania thin films. This system presents enhanced response to phenolic molecules that quench the fluorescence of the dendrimer more efficiently in the solid state than in solution. This effect is a result of the increased spatial proximity of the fluorescent molecules, which is induced by pore confinement that makes the formation of hydrogen bonds between the hydroxyl moieties of the quenchers and the carbonyl groups of the dendrimer easier. This strategy is useful to design a new hybrid sensor exhibiting high sensitivity to resorcinol and 2-nitroresorcinol.[141]

### 3.3 Molecular assembly of polymerizable structure-directing agents

An attractive approach to build up macromolecular functional units within mesoporous materials is to utilize structure-directing agents bearing polymerizable groups.[142] Pioneering work by Brinker and co-workers described the use of polymerizable surfactants as both structure-directing agents and monomers in the evaporation-driven self-assembly of mesostructured materials (Fig. 10).[143] Synthesis of polymerizable amphiphilic diacetylene molecules enabled the self-assembly of conductive, conjugated polymer/silica nanocomposites in thin-film forms suitable for integration into devices. The progressively increasing surfactant concentration drives self-assembly of diacetylene/silica surfactant micelles and their further organization into ordered, three-dimensional, liquid crystalline mesophases. Ultraviolet-light-initiated polymerization of the diacetylene units, accompanied by catalyst-promoted siloxane condensation, topochemically converts the colourless mesophase into the blue polydiacetylene/silica nanocomposite, preserving the highly ordered, self-assembled

 

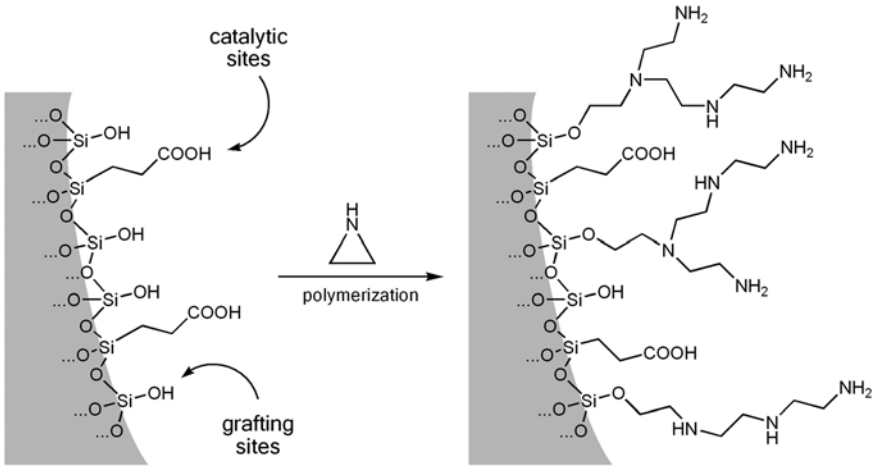


**Fig. 9** Schematic representation of the surface polymerization of aziridine in the mesopore.

architecture. In a similar vein, responsive mesoporous silica was also synthesized through cooperative assembly of cetyltrimethylammonium bromide and silsesquioxanes containing a bridged diacetylenic group. The construction process involved the spontaneous organization of diacetylenic molecules around the surfactant liquid crystalline structure, forming a mesoscopically ordered composite with molecularly aligned diacetylenic units. Subsequent surfactant removal followed by topo-polymerization gave rise to the responsive mesoporous silica embedded with polydiacetylene (PDA), a polymer that chromatically responds (*e.g.*, blue to red) to a wide range of external stimuli.[144]

Aida *et al.*[145] reported the synthesis and self-assembly of polypyrrole/silica nanocomposite material, templated by a pyrrole-containing surfactant, where polypyrrole domains segregated and insulated by one-dimensional silicate nanochannels were obtained after oxidative polymerization in the presence of $FeCl_3$. Along these lines, in recent years different groups explored the use polymerizable surfactants as building blocks to create mesostructured functional materials displaying photoluminescent or electrochemical properties.[146]

### 3.4 Confined polymerization at "activated" mesoporous walls

Aida *et al.* reported the synthesis of crystalline polyethylene fibers (diameter 30–50 nm) by the polymerization of ethylene within mesoporous supports modified with titanocene and methylaluminoxane (MAO) as a cocatalyst.[147] The polymerization of ethylene within this nanoconfined reactive environment gave a cocoon-like solid mass consisting of fibrous

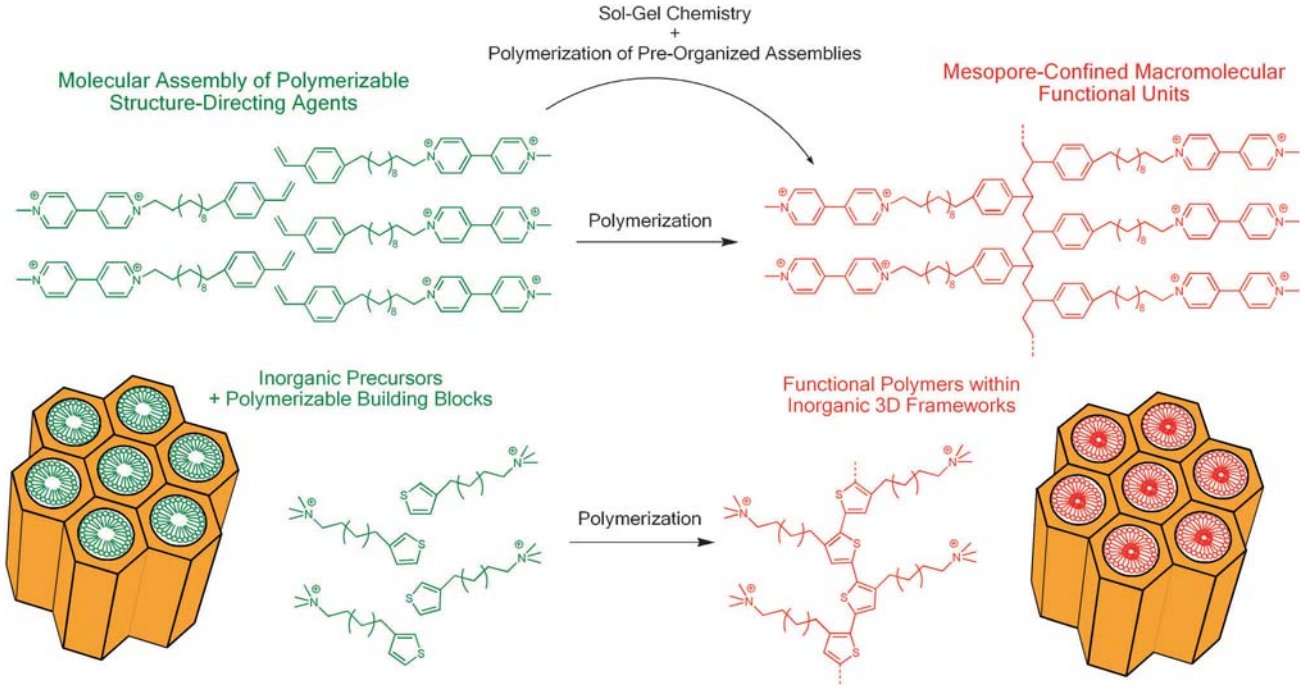


**Fig. 10** Scheme describing the formation of mesopore-confined macromolecular functional units through the molecular assembly and reaction of polymerizable structure-directing agents.

polyethylene (PE). Polarization microscopy of the PE fibers showed a clear birefringence in the fraying edge region, which suggests that the fibers are crystalline. These authors postulated that the formation of the crystalline PE fibers within the reactive mesopore can be explained by an "extrusion polymerization" mechanism similar to the biosynthesis of crystalline cellulose (Fig. 11).

Polymer chains, formed at the activated titanocene sites within the individual mesopores, are extruded into the solvent phase and assembled to form extended-chain crystalline fibers. As the pore diameter of the mesoporous material ($\sim$3 nm) is much smaller than the lamellar length of ordinary PE crystals ($\sim$10 nm), the nascent polymer chains cannot fold within the narrow reaction channels of the support and therefore grow out of the porous framework before they assemble, resulting in the formation of extended-chain crystalline fibers. By using regularly arranged nanoscopic, one-dimensional polymerization reactors, the authors thus achieved oriented growth of polyethylene macromolecules that normally requires post-processing steps. Chromium acetylacetonate [$Cr(acac)_3$] complexes have been also grafted onto mesoporous materials resulting in a catalytic system, which is able to polymerise ethylene under nanoconfinement at relatively low pressures.[148] This strategy also enables the formation of polymer blends with nanoscaled dispersion through space-confined polymerization of two monomers in mesoporous environments displaying dual catalytic sites. The dual catalysts offer independent active sites during the polymerization so as to generate the ultimate blends of the two polymers. Loading two catalytic systems within mesopores to make two polymers represents an attractive synthetic methodology to blend two polymers to nanoscale range through direct reaction without the need of a compatibilizer. The experimental protocol would simply rely on supporting the suitable catalysts/initiators onto the mesoporous framework and the dual catalytic system would be then exposed to two monomers simultaneously to generate polymer blends. Along these lines, Chan *et al.*[149] reported the blending of ethylene and syndiotactic polystyrene by pretreating the mesoporous support with the adequate catalysts. Ethylene homopolymer is made from a catalyst prepared by pretreating the mesoporous support with the cocatalyst, methylaluminoxane (MAO), prior to adding the metallocene precursor, zirconocene dichloride. On the other hand, syndiotactic polystyrene (sPS) is polymerized by pentamethylcyclopentadienyl titanium trimethoxide and MAO supported on mesoporous silicate. The combination of both catalytic systems led to the generation of binary polymer systems displaying unusual physical properties arising from nanoconfinement. PE and PS nanoblends demonstrated more significance in blending effectiveness when using space-confined polymerization. When PE and sPS are made simultaneously by dual catalysts within mesoporous channels, the crystallinity of PE is suppressed dramatically, as demonstrated by both DSC and XRD, while the physical blends usually merely show crystallinity reduction in proportion. Widenmeyer *et al.* applied surface organometallic chemistry to generate Sm(II) alkoxide, indenyl, and alkyl surface species *via* ligand exchange at mesoporous substrates.[150] Interestingly, Sm(II) grafting and subsequent ligand exchange did not markedly change the morphology and the microstructure of the samples. Such Sm(II)-modified organometallic–inorganic hybrid materials were able to initiate the graft polymerization of methyl methacrylate *via* a radical-initiated anionic coordination polymerization mechanism involving sterically unsaturated surface-confined samarium enolate moieties. The local environment of the Sm(II) surface centers (coordination sphere) may strongly affect their reactivity and, hence, the efficiency of MMA polymerization. Hybrid materials featuring the 'smallest' ligands (methyl, methoxy) acted as the best initiators for graft polymerization. The polymer–inorganic nanocomposites revealed complete pore filling or blockage of the pore entrances as indicated by $N_2$ physisorption and scanning electron microscopy. The use of "activated" mesoporous walls to synthesize polymer chains under confinement has been also extended to the use of modified aluminium MCM-41 (Si/Al = 13, pore size = 3.2 nm) in which Ni(II) or Zn(II) species were introduced by ion exchange with aqueous salt solutions.[151] When these mesoporous aluminosilicates are evacuated to remove water and oxygen at 300 °C (0.1 Torr, 24 h), followed by exposure to alkyne vapor at 1 atm at various temperatures and time periods, an exothermic uptake of reagent produced dark brown or gray products. Combustion elemental analysis of the resulting solids revealed that approximately three-quarters of the pore volume can be filled with polymer. Although some polymer is formed at low temperatures with ethyne, significant pore loading is achieved above 150 °C. Control experiments performing ethyne polymerization on unmodified Al/MCM-41 (no Ni(II) or Zn(II) ions) did not reveal any evidence of polymer growth, thus indicating the requirement for Ni(II) or Zn(II), and the positive influence of porosity and confinement on ethyne polymerization. Zn(II)/MCM-41 treated with ethyne at 250 °C for 24 h generated the greatest polymer

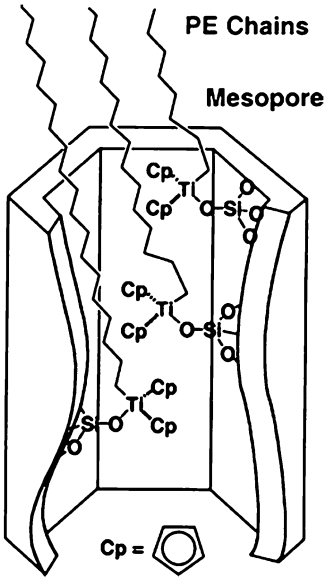


**Fig. 11** Simplified description for the growth of crystalline polyethylene nanofibers formed by the polymerization of ethylene within mesoporous silica modified with titanocene catalysts. Reproduced with permission from K. Kageyama, J.-I. Tamazawa, T. Aida, *Science*, 1999, **285**, 2113–2115. Copyright 1999 American Association for the Advancement of Science.

 

occupancy. Interestingly, Zn(II) ions have been reported not to catalyze such polymerization, furthermore their Lewis acidity (as has been suggested) cannot be the sole factor leading to ethyne polymerization, as many other M(II) or M(III) ions when incorporated into the mesoporous material failed to produce polymer. Hence, these experimental results evidence the emergence of interesting confinements effects that enhance the reactivity of Zn(II) ions, and consequently render them suitable species to promote the confined polymerization of ethyne. The rate and extent of polymerization within the mesoporous channels directly depend on the spatial distribution of catalytic sites as well as the diffusion rate of monomeric precursors and their local concentration near the catalytic sites.[152] Both factors can be adjusted by varying the pore size and by tailoring the catalytic activity of the surface through proper functionalization. To examine how these factors influence the nanoconfined polymerization of functional polymers, Pruski *et al.* studied the oxidative polymerization of 1,4-diethynylbenzene within two $Cu^{2+}$-activated mesoporous systems: silica and alumina materials (Cu-MCM and Cu-MAL, respectively) with different pore sizes and two different methods of $Cu^{2+}$ surface functionalization (Fig. 12).

One approach consisted of preparing the $Cu^{2+}$-incorporated MCM-41 silica material (Cu-MCM) by co-condensation using a $Cu^{2+}$-chelating molecule, *N*-[3-(trimethoxysilyl)propyl]ethylenediamine, as the precursor, whilst the other approach consisted of impregnating the mesoporous alumina with $Cu^{2+}$ ions. Experimental evidence provided by solid-state NMR and photophysical studies revealed that the preparation of the reactive mesopore environment has a strong influence on polymerization reaction. The conjugated poly(phenylene butadiynylene) polymer (PPB) synthesized within the Cu-MAL substrates displayed characteristic features of polydiacetylene-type cross-linking and conformational heterogeneity in the three dimensional arrangements of the polymeric chains. Conversely, the characterization of PPB polymer chains synthesized within the Cu-MCM provided sound evidence of the formation of isolated molecular wires (lack of cross-linking).

Spange *et al.* exploited the intrinsic reactivity of mesoporous walls to perform polymerization reactions under conditions of constricted geometry (Fig. 13).[153] The cationic polymerization of suitable vinyl monomers can be initiated either by active protons derived from acidic surface groups or by immobilized cationic-active surface initiators. In particular, proton ($H^+$) surface initiation has been observed for aluminosilicates and for protic acids adsorbed on silica.

Pure silicate materials are usually unable to initiate directly the cationic surface polymerization of *N*-vinylcarbazole (NVC), styrene, or other vinyl monomers, even suspended in solvents which are established for cationic polymerization, *e.g.*, dichloromethane, toluene, or hexane. However, suitable initiators for cationic surface polymerization are halogenoarylmethanes which become cationically active on acidic surfaces. The mesopores are prone to preconcentrate species with strong affinity to the pore walls; hence, preferential polymerization in the mesochannels is feasible by keeping the concentration of the carbenium ion in the surrounding solution, or on the outer surface, as small as possible. Arylmethyl halides are essentially inactive in solution but are activated specifically on the inner surface of the mesopore. The synthesis of poly(vinyl ether)s or polyvinylcarbazole under the conditions of constricted geometry can be achieved by means of cationic host–guest polymerisation of the corresponding monomers in the pores of MCM-41 (pore diameter 3.6 nm), MCM-48 (pore diameter 2.4 nm) and in nanoporous glasses (Gelsil with a pore diameter of 5 nm) with bis(4-methoxyphenyl)methyl chloride (BMCC) or triphenylmethyl chloride as the internal surface initiator.

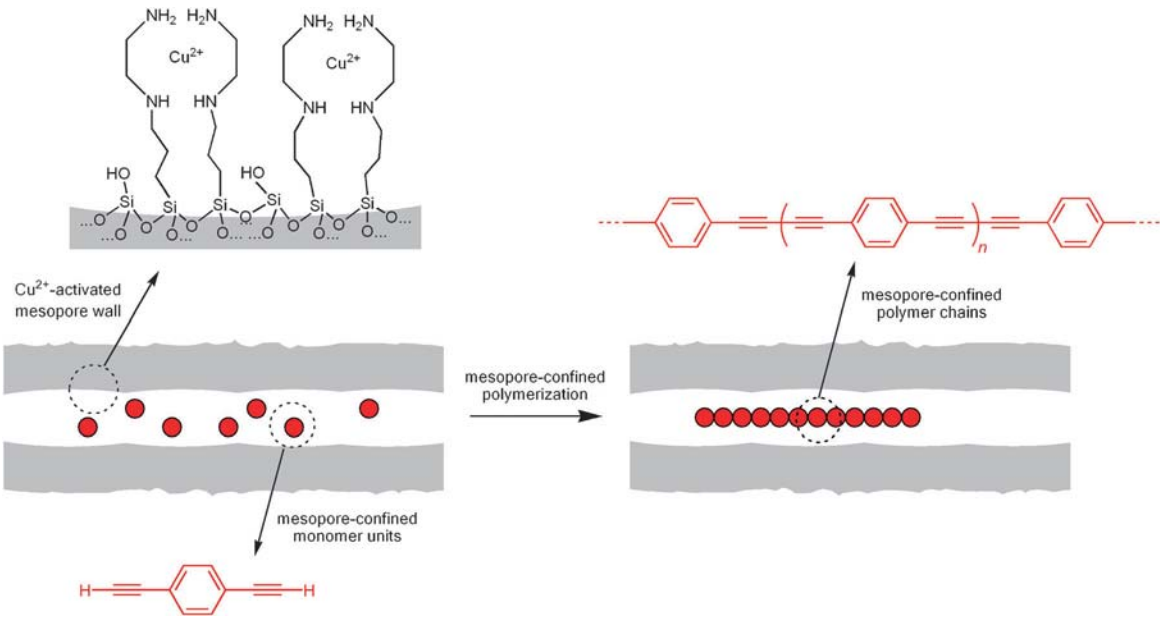


**Fig. 12** Simplified representation of the mesopore-confined oxidative polymerization of 1,4-diethynylbenzene into conjugated oligo(phenylene butadiynylene) in the presence of $Cu^{2+}$-functionalized mesoporous silica.

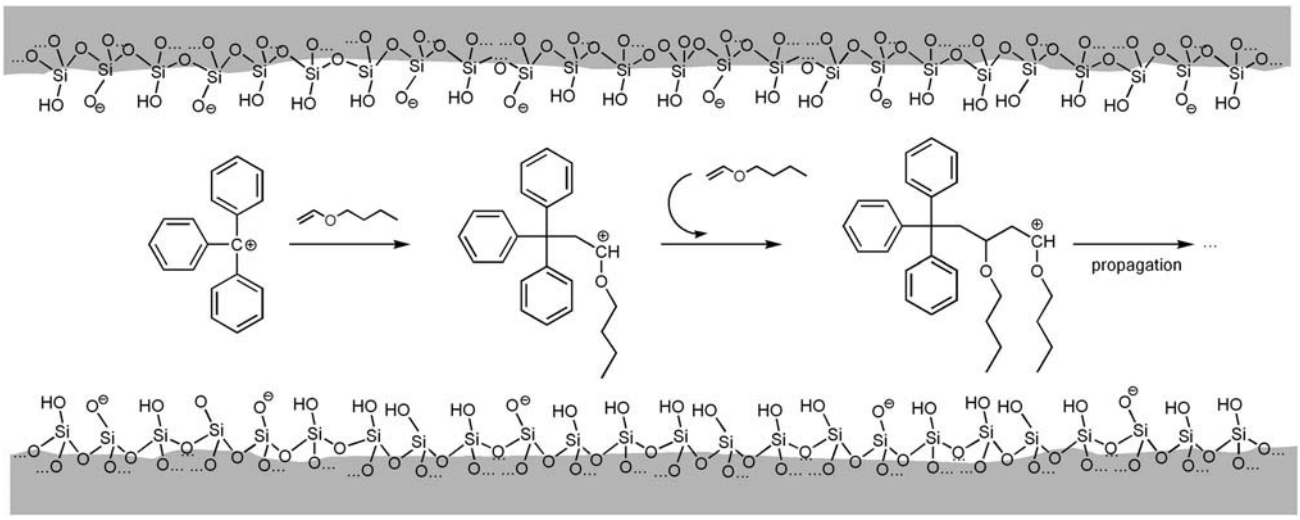


**Fig. 13** Schematic description of the cationic initiation and propagation of substituted vinyl ethers inside mesoporous silica channels.

In a similar way, the intrinsic acid–base properties of silica have been exploited to promote ring-opening polymerization (ROP) reactions. The functionalisation of silica surfaces with (1,1′-ferrocenediyl) dimethylsilane, was first reported by Wrighton and co-workers[154] and utilises the susceptibility of [1]ferrocenophanes to nucleophilic attack by the hydroxy groups on the surface of the silica wall. It has been found previously that reaction of [1]ferrocenophanes with nucleophiles can lead, depending on the reaction conditions, to oligomeric and high molecular mass species as well as stoichiometrically

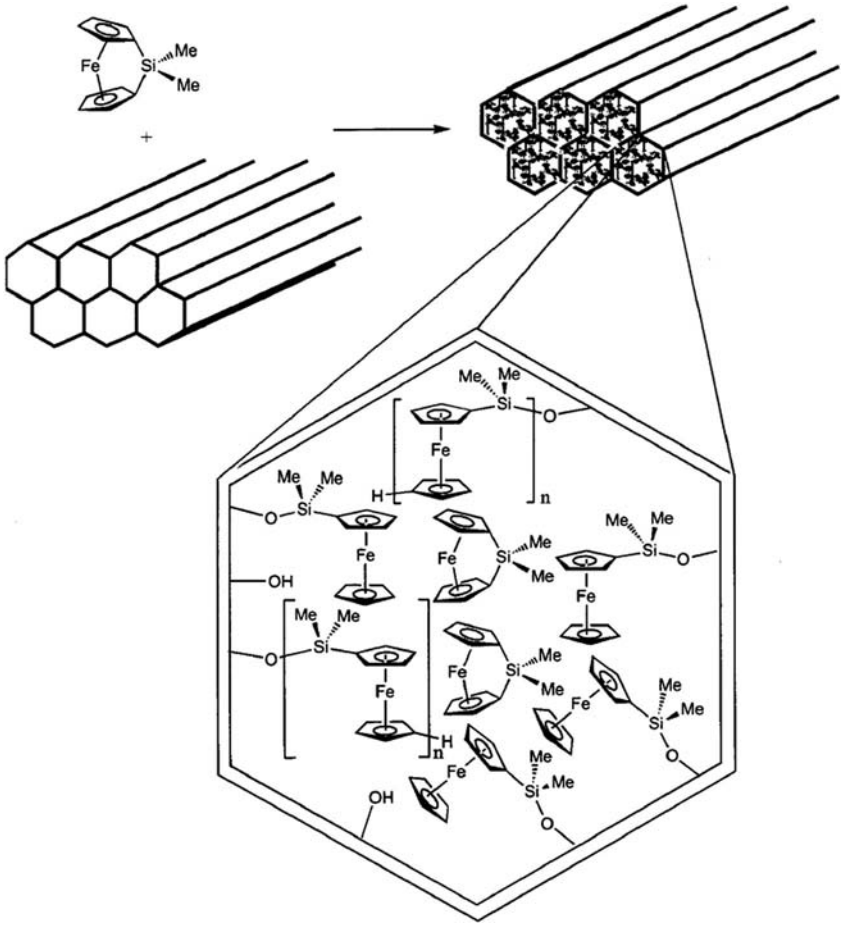

**Fig. 14** Simplified scheme describing the ring-opening polymerization of [1]silaferrocenophanes inside mesoporous silica as a route to generate functional building blocks inside the mesoporous channels. Reproduced with permission from M. J. MacLachlan, M. Ginzburg, N. Coombs, N. P. Raju, J. E. Greedan, G. A. Ozin, I. Manners, *J. Am. Chem. Soc.*, 2000, **122**, 3878–3891. Copyright 2000 American Chemical Society.

 

ring-opened species.[155] This methodology has subsequently been used to modify mesoporous silica, anchoring [1]silaferrocenophanes to the reactive –Si–OH sites present on the surface of the silica. Hence, the formation of grafted polymer chains initiated from the mesopore surface can also take place in the case of the ring-opening polymerization (ROP) of [1]silaferrocenophanes. In this context, Manners and co-workers[156] explored the ROP of [1]silaferrocenophanes inside mesoporous silica as a route to generate highly functional building blocks inside the channels (Fig. 14). Monomers were introduced into MCM-41 by vapor deposition through the combination of dehydrated MCM-41 and monomer in a Schlenk tube under vacuum to allow the monomer to sublime into the channels. NMR data of the composite materials revealed that, at low loadings, ring-opened monomeric species and oligomers are present. Differential scanning calorimetry studies indicated that fully loaded MCM-41 samples displayed a very broad exothermic transition, consistent with ring-opening polymerization in the 75–200 °C temperature range. The broadening of the exothermic transition has been ascribed to the inhomogeneity of the trapping sites for the encapsulated polymer.

The chemical nature of the mesoporous walls can be a versatile tool to tune the reactivity of the confined environment in order to trigger polymerization processes under external stimuli. In this context, Stucky *et al.* have recently developed a route to produce polymer–inorganic mesoporous hybrids based on a semiconductor photopolymerization technique.[157] This method relies on an electric potential generated by the optical absorption by mesoporous semiconductors and the subsequent oxidation of monomer confined within the mesoporous structure. The semiconductor mesoporous scaffold acts as the electrode for electropolymerization, provided that the electrical driving force is supplied by photon energy rather than potentiostatic control. These authors explored the use of mesoporous $TiO_2$ as a photosensitizer and nanostructured template for creating hybrid $TiO_2$–polypyrrole materials. Photon absorption by an inorganic semiconductor can generate oxidative and reductive equivalents to drive chemical reactions such as polymerization. Photopolymerization is initiated wherever photoexcited carriers in the inorganic sensitizer can oxidize or reduce a monomer. In this case, optical excitation of mesoporous $TiO_2$ was used to generate the electric potential necessary for triggering the oxidation and subsequent polymerization of the pyrrole monomer. This was simply achieved by immersing mesoporous $TiO_2$ in an aqueous solution containing pyrrole (0.2 M), sodium sulfate (0.1 M), and methyl viologen dichloride (10 mM) and subjected to UV illumination. The photopolymerization process was monitored by the quartz crystal microbalance, nitrogen sorption, and thermogravimetric techniques revealing that *in situ* generation of polypyrrole was observed to be self-limiting after approximately 20–30% filling of the mesoporous $TiO_2$ network. This strategy introduces two interesting aspects that can have strong implications for the molecular design of functional polymer–inorganic mesoporous hybrids. First, the pore-confined macromolecules formed by this photoinduced polymerization technique should be in good electronic contact with the inorganic semiconductor phase because the polymerization reaction is locally initiated by charge transfer across the inorganic semiconductor–electrolyte interface. Second, the photopolymerization of the monomer can occur at any point on the mesoporous $TiO_2$ surface because monomer-containing solution and UV photons both penetrate the mesoporous network.

### 3.5 Infiltration of polymers into mesoporous frameworks

Incorporation of macromolecular building blocks into mesoporous materials *via* a polymer infiltration approach has received increasing attention. Seminal works from Tolbert and collaborators (see Section 3.7) demonstrated that polymer infiltration from solution could be exploited as a straightforward route to confine polymer chains into nanoscale pores and tailor their topological characteristics. However, polymer infiltration into nanoscale channels depends on the partitioning of the polymer from the solvent, and hence, achieving fine control over the polymer concentration, orientation and uniformity in the corresponding nanocomposite is a nontrivial task. There are two important factors that require special attention. First, when the mesopore size is less that the radius of gyration of the solvated polymer, infiltration proceeds *via* a ''reptation mechanism'' (worm-like motion) that may require long processing times. Second, the polymer chains may suffer a significant loss of conformational entropy when they are confined in a mesopore, as a consequence, spontaneous infiltration will greatly depend on the chemical interactions with the pore walls.[158] The infiltration of polyelectrolytes into mesoporous silica has been investigated in detail by Caruso and collaborators.[159] They studied the infiltration of poly(acrylic acid) (PAA) of different molecular weights (2–250 KDa) in amine-functionalized mesoporous silica particles with different pore sizes (4–40 nm). The surface charge of the nanopores and the charge density and conformation of PAA were tuned by changing the PAA solution conditions (*e.g.*, pH and ionic strength) to which the particles were exposed. Thermogravimetric analysis and dynamic light scattering revealed that the extent of PAA infiltration strongly depends upon the relative sizes of the nanopores and the PAA molecules. Nanopores with diameters larger that 10 nm were capable of infiltrating a broader range of PAA molecular weights. The pH and ionic strength of the PAA solution govern the conformation of the macromolecules and the charge of the nanopores, and hence the ability of the macromolecules to infiltrate the mesoporous media (Fig. 15). It was observed that the adsorption conditions play an important role in PAA infiltration. As the pH increases, the PAA charge density increases, and the polymer chains adopt a more rigid, linear conformation, resulting in a lower loading. When the pH of the PAA solution increased above 3, the amount of PAA loaded in the particles decreased due to the polymer chains adopting a more extended conformation. On the other hand, in the presence of salt, the degree of loading depends upon a balance between screening of the polyelectrolyte charge and screening of the particle surface charge.

PAA loading decreases linearly with increasing salt concentration for PAA molecules below 100 KDa. The decrease in loading upon increasing salt concentration is even more pronounced in the case of low molecular weight PAA.

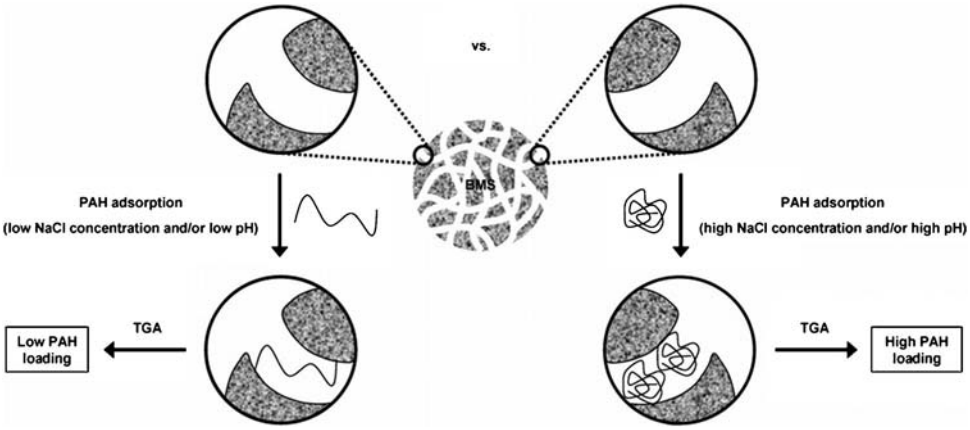


**Fig. 15** Simplified illustration of polyallylamine (PAH) adsorption and infiltration inside mesoporous silica particles under low and high ionic strength conditions. Reproduced with permission from A. S. Angelatos, Y. Wang, F. Caruso, *Langmuir*, 2008, **24**, 4224–4230. Copyright 2008 American Chemical Society.

This reduction in PAA loading with increasing ionic strength has been attributed to increased screening of the particle surface charge by salt ions, which weakens the electrostatic attraction between the PAA molecules and the mesopore walls. This indicates that besides polymer conformation electrostatic interactions between the polyelectrolyte and the pore walls also dominates to a great extent the infiltration process. Nanoconfinement within the mesopore may significantly influence the conformation of the adsorbed polyelectrolyte molecules, leading to the macromolecules exhibiting a more coiled conformation in nanopores than when adsorbed on planar surfaces. The nanoconfinement-driven conformational change may have profound effects on the functional features of the polyelectrolytes. For example, the preparation of diverse functional colloids involves the sequential assembly of interacting polymers within the nanopores of mesoporous particles. For the weak polyelectrolyte pair, PAA and poly(allylamine hydrochloride) (PAH), PAA is first deposited within the nanopores of amine-functionalized mesoporous particles, after which chemical or thermal cross-linking is performed to selectively form amide bonds between the carboxylic acid groups of the PAA and the primary amine groups grafted onto pore surface. Cross-linking is an important requirement in the preparation of these systems, which can be formed when two or more polyelectrolyte layers are deposited within the nanopores. In stark contrast, when the same PAA/PAH polyelectrolyte pair is deposited on nonporous particles, stable systems are produced without the need for cross-linking between the polyelectrolyte layers. The necessity for cross-linking in the construction of mesopore-confined PAA/PAH systems eloquently illustrates the importance of conformational and electrostatic changes taking place within the mesopore environment. Electrostatic interactions between infiltrated polyelectrolytes and the mesoporous walls have been exploited to build up an efficient pH-responsive carrier system. Xiao *et al.* constructed a mesoporous platform in which active molecules such as vancomycin can be stored and released from poly(dimethyldiallylammonium chloride) (PDDA)-loaded pores of SBA-15 by changing pH values at will. The amount of vancomycin stored in the mesopores is up to 36 wt% at pH $\sim$ 7. When the pH is at mild acidity, vancomycin is steadily released from the pores of SBA-15, thus resembling an "active" nanostructured framework that contains drug reservoirs and environment-sensitive pores, and the state of these pores (closed or open) can be controlled by the pH value. Polycations (PDDA) immobilized onto the anionic SBA-15 by electrostatic interactions were acting as "closed gates" for storage of drugs in the mesopores. Upon decreasing pH the ionized carboxylate species ($COO^-$) are transformed into protonated groups (COOH) and polycations are separated from the surface of modified SBA-15, leading to opening of the gates for drug release from the mesopores.[160] On the other hand, alternative approaches involve the incorporation of uncharged hydrophobic semiconducting polymer into nanoporous materials by placing the materials in contact with a liquid solution of the polymer, either by spin-casting or direct immersion. Stucky and co-workers described a technique for incorporating the poly(3-hexyl thiophene) (RR P3HT) into titania mesopores by spin casting a film of the polymer on top of the titania film, and then heating at temperatures in the range of 100–200 °C in order to fill 33% of the total volume with the semiconducting polymer. Conjugated polymer films were spin-cast on top of the mesoporous films, and then the samples were heated for various times and temperatures. Following the thermal treatment, the excess polymer was removed by rinsing the samples with toluene.[161] UV-vis absorption measurements confirmed that the amount of polymer incorporated into the mesoporous sample remained constant after 5–10 min of solvent rinsing. It is worthwhile indicating that control experiments performed on similar polymers deposited on the top of bare ITO or glass dissolved very quickly during toluene rinsing. This observation reveals that polymer penetrates into the pores and remains there even if the film is rinsed in a good solvent. Even though the infiltration process implies a significant conformational entropy loss, the experimental evidence indicates that the polymer is remarkably stable within the titania mesopores. This has been attributed to the fact that the entropy loss is compensated by a strong enthalpic interaction between the highly polarizable main chain of the conjugated polymer and the polar titania,

 

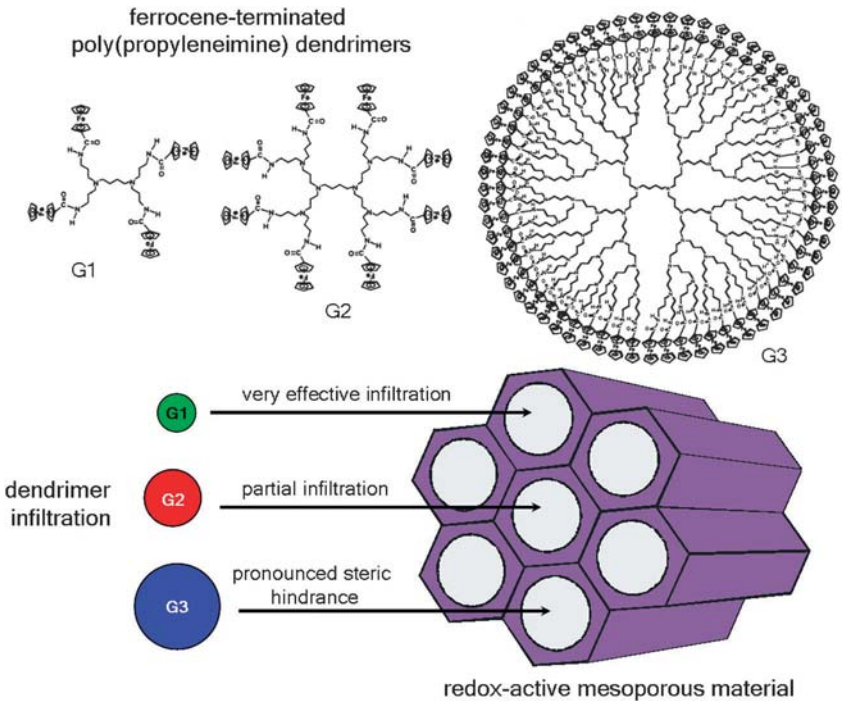


**Fig. 16** Redox-active mesostructured materials constituted of mesoporous silica hosts infiltrated with electroactive poly(propyleneimine) dendrimers containing 4, 8, and 64 amidoferrocenyl moieties. Reproduced with permission from I. Díaz, B. García, B. Alonso, C. M. Casado, M. Morán, J. Losada, J. Pérez-Pariente, *Chem. Mater*., 2003, **15**, 1073–1079. Copyright 2003 American Chemical Society.

and that a chain of polymer will infiltrate only if some segments are able to adsorb on the walls of titania. In the case of this semiconducting polymer upon heating from 100 °C to 200 °C its π-stacked structure evolves into a coiled configuration. Inside the pores coiled chains occupy a smaller titania surface area than rod-like chains and, consequently, a greater number of polymer–wall contacts can be generated upon increasing the temperature. Interestingly, the absorption spectra of the infiltrated polymer chains were blue-shifted, thus suggesting that some chain segments remain locked in a coiled conformation and are unable to crystallize following infiltration at high temperatures. In a similar vein, Xi *et al.* also reported the critical role of polymer–pore wall interactions in defining the conformational state of the confined polymer chains. Studies performed on poly(*p*-phenylenevinylene) derivatives (DDMAPPV) bearing alkoxy side-chains of different lengths also revealed that the polarity of the pore wall has strong effects on the absorption/emission properties of confined conjugated polymers.[162]

Polymer infiltration followed by chemical transformations can be exploited as a route to anchor pre-synthesized macromolecular building blocks into mesopores. Kruk *et al.* applied the ''click chemistry'' concept, *i.e.*: azide-alkyne cycloaddition, to covalently graft polymer chains to the surface of ordered mesoporous silica.[163] The surface of the silica was modified with aminopropyl groups that were converted to propargyl-bearing groups through a reaction with 4-pentynoyl chloride. The ''clickable'' mesopores were then reacted with azide-terminated polymers[164] including poly(methyl methacrylate) (PMMA) and oligo(ethylene glycol). The combined infiltration and ''grafting-to'' strategy enabled the formation of covalently anchored uniform polymer films of thickness up to about 2 nm without any appreciable pore blocking, even for polymer loadings close to 25 wt%. As expected, the infiltration and grafting process was affected by the molecular weight of the polymeric building blocks owing to an increasing steric hindrance in the case of infiltration of larger macromolecules. Similar experiments performed on higher-molecular-weight PMMA resulted in polymer loading of 18 wt% and polymer film thickness of ~0.8 nm. Infiltration of macromolecular building blocks into mesoporous materials not only involves the use of linear polymers, mesopore-infiltrated dendrimers were also used to confer interesting functional properties to hybrid porous frameworks. Morán *et al.* reported a novel type of redox-active materials constituted of mesoporous silica hosts containing electroactive dendrimers within the ordered channels (Fig. 16). The infiltrated redox-active functional units corresponded to poly(propyleneimine) dendrimers containing 4, 8, and 64 amidoferrocenyl moieties in MCM-41 mesoporous matrices (pore size ~ 3 nm).[165] Prior to infiltrating the dendrimer, MCM-41 samples were treated with $Me_2SiCl_2$ in order to decrease the population of free Si–OH in the outer surface of the mesoporous samples provided that the silane anchoring reaction on external Si–OH groups occurs more rapidly than those located in the inner environment of the mesopore.[166] Incorporation of redox dendrimers (generations 1, 2 and 3) into the mesoporous material was achieved by refluxing a $CH_2Cl_2$ solution of the corresponding dendrimer in the presence of a pretreated sample of MCM-41 during 5–12 h. The integrity of the redox dendrimer within the mesopores was confirmed by IR and NMR spectroscopy, thus suggesting the formation of a stable dendrimer–matrix complex in which

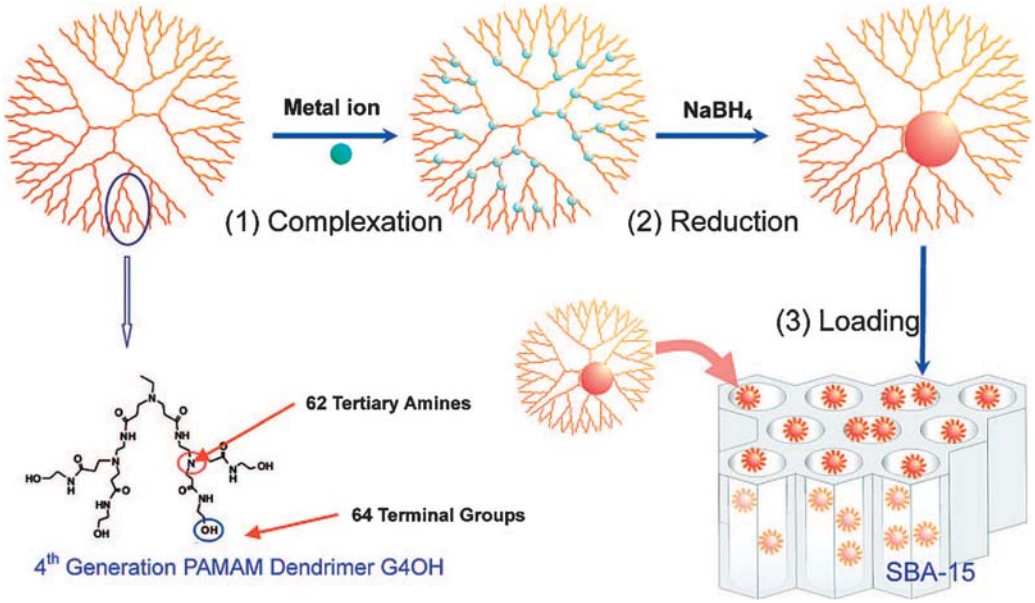


**Fig. 17** Schematic depiction describing the synthesis of dendrimer encapsulated metal nanoparticles and the subsequent loading inside the mesoporous matrix. Reproduced with permission from W. Huang, J. N. Kuhn, C.-K. Tsung, Y. Zhang, S. E. Habas, P. Yang, G. A. Somorjai, *Nano Lett*., 2008, **8**, 2027–2034. Copyright 2008 American Chemical Society.

hydrogen bond interactions, CONH···OH–Si, may play a determinant role. X-Ray diffraction and nitrogen adsorption isotherms confirmed the full occupancy of the channels by the smallest dendrimer, whereas less effective infiltration was observed in the case of bulkier dendrimers due to the emergence of pronounced steric hindrance (dendrimer loading for G1, G2 and G3 corresponded to 34, 15 and 8 wt%, respectively). One remarkable feature of these hybrid materials is that the ferrocenyl units in the guest dendrimers are easily accessible to electrochemical oxidation as observed by cyclic voltammetry and differential pulse voltammetry experiments. Careful analysis of the electrochemical data revealed that the majority of G3 dendrimers were located on the outer part of the mesoporous matrix, whereas G2 dendrimers were located inside the MCM-41 channels as well as out of the mesoporous material. On the other hand, electrochemical data indicated that the whole population of G1 dendrimers was entirely located inside the mesopores. Electrochemical experiments showed that upon infiltrating the electroactive G1 dendrimers inside the mesopores, a more positive redox potential was obtained. This observation can be explained considering the decrease of effective electron density on the redox centers as a result of the binding of the amidoferrocenyl moieties to the silanol groups inside the mesopores, rendering oxidation more difficult. In a similar vein, the infiltration of nanoparticle-loaded dendrimers into mesoporous materials has recently introduced a new strategy to prepare hybrid nanostructured materials displaying tailored catalytic properties.[167]

Dendrimers represent versatile building blocks to synthesize very small metal nanoparticles (diameter $\sim$ 1 nm) in an accurate and reproducible manner.[168] The globular architecture and chemical topology of dendrimers provide not only internal groups for nanoparticle growth upon reduction, but also a shell to prevent aggregation of the as-synthesized nanoparticles. Somorjai and co-workers reported the synthesis of $\sim$1 nm Rh and Pt nanoparticles in aqueous solution using PAMAM dendrimer templates and the subsequent loading onto SBA-15 mesoporous supports.[167] The infiltration of the NP-loaded dendrimers was accomplished by sonicating the slurry formed by mixing the nanoparticle solution and the SBA-15 (Fig. 17). The infiltration process was performed in a solution with pH $\sim$ 5. At this pH, the PAMAM dendrimer is positively charged, while the surface of SBA-15 silica is negatively charged (isoelectric point of silica is $\sim$2). The strong electrostatic interactions between the NP-loaded dendrimers and the mesopore walls act as a driving force to fill the cavities of the macromolecular functional units. Catalytic studies revealed that the hybrid NP-loaded mesostructured substrates were active for ethylene hydrogenation without any pretreatment. This was attributed to the 3D support provided by SBA-15 that may prevent dendrimer collapsing on the nanoparticle surface and blocking of their active sites. Catalytic activity was also demonstrated over the dendrimer encapsulated nanoparticles for the pyrrole hydrogenation reaction.

### 3.6 Nanostructured polymer–inorganic hybrids *via* surface-initiated polymerization in mesoporous hosts

Grafting of polymer chains onto mesoporous materials through the condensation of infiltrated end-functionalized polymers with reactive surface groups on the mesopore walls may lead to low grafting densities because polymer chains have to diffuse against an increasing concentration gradient. In this context, the "grafting from" approach in which the polymer chains are grown from the initiator-modified mesopore wall is expected to achieve high grafting densities provided that monomer diffusion into the reactive chain end is not significantly hindered by the growing polymer chains.[169] Hybrid materials were synthesized by grafting polymer chains from the surface of ordered mesoporous silica (OMS) particles

 

(mesopore diameter 9–14 nm), *via* surface initiated atom transfer radical polymerization (SI-ATRP)[170] of methyl methacrylate or styrene.[171] A systematic study of the molar mass, molar mass distribution and chain-end structure of both the grafted chains grown from the mesoporous silica surface and the free chains produced in solution from an additional free initiator revealed the emergence of confinement effects on the results of the polymerization. The polymerizations of methyl methacrylate and styrene were perfectly controlled in the homogeneous medium *via* the ATRP mechanism. However, on the other hand, SEC and MALDI-TOF analyses of the growing polymer chains cleaved from the mesoporous particles confirmed the presence of dead chains of low molar mass resulting from termination *via* disproportionation.

Furthermore, a systematic study investigating the effect of varying the channel length revealed that the proportion of short dead chain decreased upon decreasing the average length of the cylindrical mesopore. This observation suggests a strong influence of the mass transport processes under nanoconfinement on the polymerization control. Kruk and Matyjaszewski[172] also used SI-ATRP polymerization to graft uniform layers of polyacrylonitrile (PAN), poly(2-(dimethylamino)ethyl methacrylate), and polystyrene on concave surfaces of cylindrical mesopores of diameter ~10 nm and spherical mesopores of diameter ~15 nm (Fig. 18). In this work, the grafting process was optimized through the introduction of appropriate amounts of Cu(II) species that acted as a deactivator, allowing them to achieve better control over the nanoconfined polymerization reaction. Gas adsorption isotherms and gel permeation chromatography indicated that the SI-ATRP process resulted in polymer layers of controlled thickness (from several tenths of a nanometre to at least 2 nm) in which the macromolecular building blocks consisted of monodisperse polymer chains of controlled molecular weight. For example, in the case of PAN displaying grafting densities of 0.28 chains $nm^{-2}$, the degrees of polymerization (DP) ranged from DP 25 to 70, and the polydispersity indexes (PDI = Mw/Mn) were as low as 1.06–1.07. It is worthwhile to note that the addition of Cu(II) in the reaction mixture not only helps to promote a better control over the polymer film thickness but also mitigates pore blocking. If the surface-grafted polymer layer does not fill the pores completely, the tailored pores in the polymer–silica hybrids are accessible to the transport of different species, and the pore size distributions are similarly narrow as those of the corresponding silica supports.[173] The synthetic versatility and simplicity makes ATRP a powerful technique for designing well-ordered mesoporous organic–inorganic hybrid materials using widely available monomers, like *N*-isopropylacrylamide or glycidyl methacrylate, in order to attain highly functional nanostructured materials.[174] Recently, Cao and Kruk demonstrated that atom transfer radical polymerization with activators regenerated by electron transfer (ARGET) can be implemented for grafting of polymer brushes from mesoporous supports. ARGET represents a major improvement in the versatility of ATRP because it can be performed using a closed vial instead of using air-tight glassware (*e.g.*: Schlenk tubes) and a vacuum line, and it involves low concentrations of copper catalyst (10–100 ppm *vs.* 1000–10 000 ppm used in normal ATRP). The ARGET-based approach was illustrated on mesoporous SBA-15 silica (pore diameter 14 and 22 nm) modified with poly(methyl methacrylate) (PMMA) and polystyrene (PS) brushes. Polymer

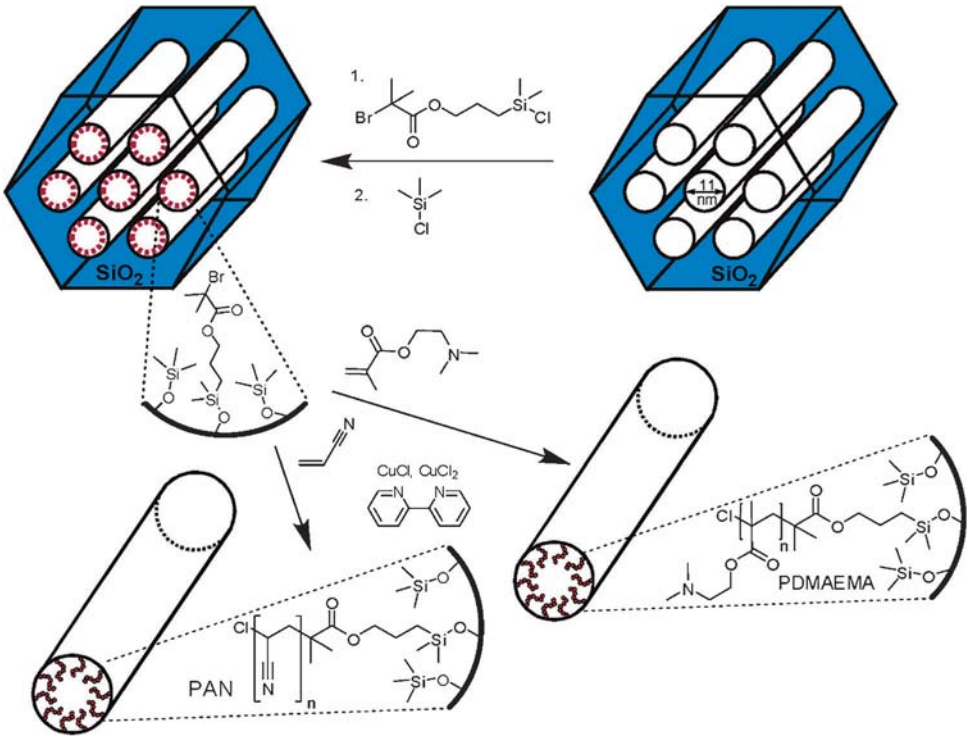


**Fig. 18** Surface-initiated atom transfer polymerization inside mesoporous materials. Reproduced with permission from M. Kruk, B. Dufour, E. B. Celer, T. Kowalewski, M. Jaroniec, K. Matyjaszewski, *Macromolecules*, 2008, **41**, 8584–8591. Copyright 2008 American Chemical Society.

loadings up to 36 wt% and layer thicknesses of up to at least 2 nm were achieved in the polymerization process carried out in small vials without using a vacuum line. The polymer chains exhibited low polydispersity indexes (PDI $\sim$ 1.18–1.32) for polymer loadings up to 29 wt%, while a higher polydispersity (PDI $\sim$ 2.1) was observed for higher loadings (48 wt%).[175]

Surface-initiated polymerization from mesoporous supports was further extended to *N*-carboxyanhydride (NCA) chemistry by Shantz and co-workers in order to create polypeptide–mesoporous hybrids.[176] Organic–inorganic nanocomposites were readily synthesized through the surface-initiated polymerization of *N*-carboxyanhydrides from amine-functionalized ordered mesoporous silica (Fig. 19).

A combination of experimental techniques verified the formation of the peptide brushes, poly-*Z*-L-lysine (PZK) and poly-L-alanine (PA), and indicated that much of the polymer layer is formed within the silica mesopores. L-Lys(*Z*) peptide brushes can be synthesized and deprotected on the solid surface. L-Ala peptide brushes may also be synthesized, but mass spectrometry evidenced the appearance of nanoconfinement effects in polymer growth as the number of alanine units per brush appears dependent on the silica pore size/topology. Similar studies also indicate that the initial amine loading may strongly affect the filling of the mesoporous framework. In the PA–silica nanocomposites the porosity increases with decreasing amine loading. This has been attributed to an increase in spacing of polymers with equal or similar lengths inside the pores. These results show that NCA polymerization chemistry can be used to synthesize well-defined polypeptide-based composite materials in which the properties of the nanostructured hybrid and the grafted polymer can be tuned by altering the surface initiator loading, pore size, pore topology, and monomer identity.

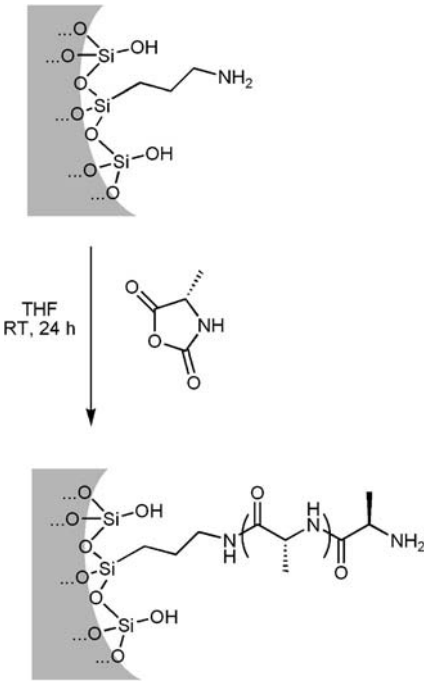


**Fig. 19** Scheme describing the grafting of peptides from the mesoporous silica surface.

The use of well-controlled nitroxide-mediated surface-initiated polymerization was also exploited as a route to build up polymer-mesoporous hybrids. Lenarda *et al.* reported the preparation and use of a TEMPO (2′,2′,6′,6′-tetramethyl-1′-piperidinyloxy)-based derivative, covalently tethered to the internal mesoporous walls of MCM-41 silica, to initiate the controlled radical polymerization of styrene (Fig. 20).[177] The surface derivatization of the pore walls demanded simple sequential post-grafting steps to yield the desired initiator-modified mesoporous material. The most important feature of these TEMPO-based initiators is the presence of a homolytically unstable alkoxyamine (C–ON) bond that permits, during polymerization, reversible homolysis of the covalent species, followed by monomer insertion and reversible recombination. The presence of inactive chain ends results in a dramatic reduction of the concentration of radical chain ends which coupled with the inability of the nitroxide free radicals to initiate new chain growth, leads to a lower number of unwanted side reactions (termination, combination or disproportionation). This experimental route enabled the formation of polystyrene-mesoporous silica nanocomposites in which the styrene polymerization occurred inside the MCM-41 channels and the filling of the pores was tuned according to the polymerization conditions without affecting the structural and morphological features of the starting silica.

Surface-initiated polymerization was exploited as a strategy to build up a delivery system based on stimuli-responsive poly(*N*-isopropylacrylamide) (PNIPAM) brushes synthesized inside a mesostructured matrix *via* atom transfer radical polymerization (ATRP). The control over drug release in response to the environmental temperature was investigated using ibuprofen (IBU) as a probe molecule. At low temperature, ibuprofen drug molecules are confined in the pores owing to the swelling of the PNIPAM brushes and the formation of hydrogen bonding between PNIPAM chains and IBU provided that carboxylic acid groups of IBU could bind to both carbonyl oxygen and nitrogen of *N*-isopropylacrylamide monomer units *via* hydrogen bonding. Upon increasing temperature, the polymer chains become hydrophobic upon collapse of hydrogen bonds which in turn leads to the release of drug molecules from the pores. Consequently, this implies that the temperature-driven actuation of the PNIPAM chains can be used for controlled release of drugs.[178,179]

### 3.7 One-pot synthesis of functional polymer–mesoporous hybrids

Tolbert and co-workers synthesized optically active nanostructured composite materials by using an amphiphilic semiconducting polymer, a poly(phenylene ethynylene) (PPE), and a conventional ammonium surfactant as the structure-directing agents (Fig. 21). These hybrid materials were synthesized in basic aqueous solution by adapting a standard procedure for preparing mesoporous silica using cetyltrimethylammonium bromide (CTAB) as the surfactant and tetraethyl orthosilicate (TEOS) as the silica source. These authors replaced 1–5 wt% of the CTAB in the formulation with PPE. The presence of the

 

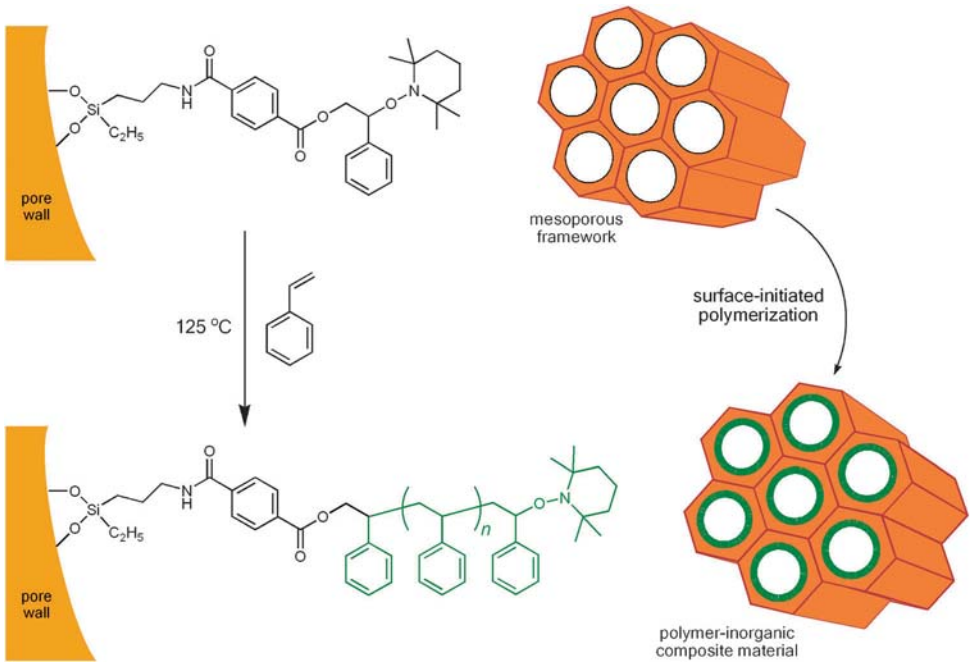


**Fig. 20** Controlled radical polymerization of polystyrene inside mesoporous frameworks by using TEMPO-modified pore walls.

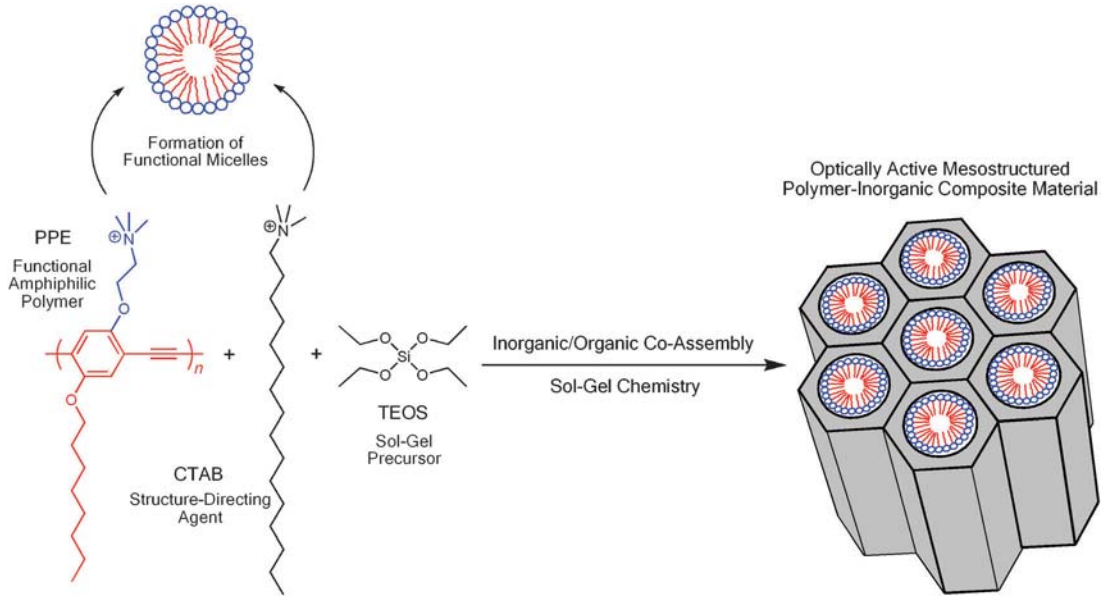


**Fig. 21** Synthesis of optically active nanostructured composite materials by using amphiphilic semiconducting polymers, a conventional surfactant as the structure-directing agents and tetraethyl orthosilicate (TEOS) as the silica source.

CTAB in addition to the PPE was necessary because the solubility of the polymer was insufficient to drive inorganic/organic co-assembly. The ratio of CTAB/PPE is dictated by the solubility of the polymer in the aqueous solution. At the maximum PPE concentration (~5% relative to CTAB) some polymer precipitation out of the solution might take place upon addition of TEOS, thus leading to the formation of composite materials with irreproducible amounts of polymer. However, solutions containing lower PPE concentrations (1%) yielded composite samples with consistent amounts of polymer incorporation (~8%) with essentially no PPE left in solution after composite precipitation. The experimental protocol to prepare the sol–gel mixture indicates that PPE is added after the CTAB in order to facilitate the solubilization of the polymer. Thereafter, this mixture is stirred under mild heating (50 °C) to completely dissolve the polymer. TEOS was then added, and the mixture was allowed to continue stirring for another 3 h at room temperature. The resulting precipitate was then filtered and dried to achieve mesoporous silica incorporating semiconducting polymers into the 2D hexagonal architecture.[180]

Frey *et al.* also reported the one-pot deposition of conjugated polymer-incorporated mesostructured metal oxide

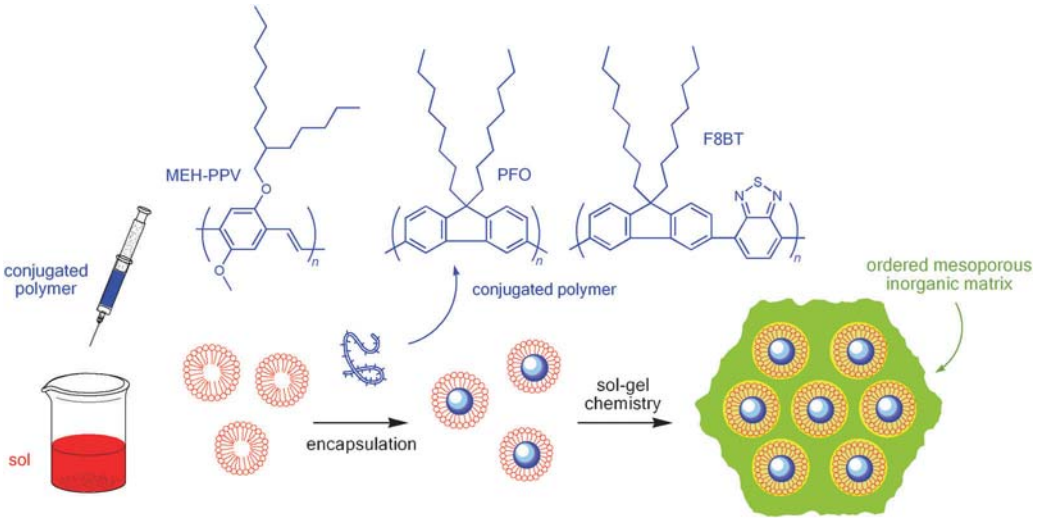


**Fig. 22** Schematic illustration of the one-pot deposition of conjugated polymer-incorporated mesostructured metal oxide films.

films, with control over charge and energy transfer.[181] The conjugated polymer dissolved in xylene is added dropwise into the polar precursor solution including the metal oxide precursor species and the block copolymer acting as structure directing agent (Fig. 22). The hydrophobicity and relatively low volatility of the xylene cosolvent drives the conjugated polymers into the hydrophobic domains of the self-organizing block copolymer mesophases that template the metal oxide scaffold.

This experimental strategy enables the controlled incorporation of conjugated polymers into the organic domains of block copolymer-templated mesostructured metal oxides, thus leading to the deposition of conjugated polymer-incorporated 2D-hexagonal and 3D-cubic silica and titania films from aqueous solutions. Spatially locating the conjugated polymer guests in the organic domains of the hybrid mesostructure suppresses energy transfer between polymer chains in adjacent micelles. Hence, incorporation of red- and blue-emitting polymers in separate micelles resulted in simultaneous red and blue emission, *i.e.*: white light generation. The efficacy of the conjugated polymer-incorporated metal oxide films for optoelectronic devices was demonstrated by integrating the white-emitting 3D-cubic silica film, which supports carrier transport along the continuous through-film conjugated polymer pathways, as the active layer in white light emitting devices. The experimental protocol to prepare these highly functional films is quite straightforward. The conjugated polymers are first dissolved in xylene and then dropwise added into aqueous or aqueous/ethanolic solutions including a block copolymer surfactant and a metal oxide precursor species. Depending on surfactant concentration and type of metal-oxide precursor, conjugated polymer-incorporated 2D-hexagonal and 3D-cubic silica and titania films can be achieved through well-known evaporation-induced self-assembly processes. A similar strategy was also explored to build up mesostructured nanocomposite films by introducing pre-synthesized semiconducting polymers, such as blue-emitting poly(9,9-dioctylfluorenyl-2,7-diyl) (PFO), green-emitting poly(9,9-dioctylfluorenyl-2,7-diyl)-*co*-1,4-benzo-(2,1,3)-thiadiazole) (F8BT), or red-emitting poly[2-methoxy-5-(2-ethyl-hexyloxy)-1,4-phenylenevinylene] (MEHPPV), into a tetrahydrofuran (THF)–water homogeneous sol solution containing silica precursor species and a surface-active agent. Dovgolevsky *et al*. showed that depending on the concentration of the surface active agent, it was possible to prepare polymer–inorganic structured films with three different types of mesostructural order: (i) a 2D hexagonal mesophase silica with conjugated polymer guest species incorporated within the hydrophobic cylinders organized in domains aligned parallel to the substrate surface plane; (ii) a lamellar mesophase silica with the layers oriented parallel to the substrate surface and the conjugated polymer guest species incorporated in the hydrophobic layers; or (iii) an apparent intermediate phase consisting of a mixture of the hexagonal and lamellar phases in addition to worm-like aggregates with no appreciable orientational order. In particular, the continuous through-film conductive pathway provided by the intermediate phase has allowed the integration of ordered semiconducting polymer–silica nanocomposites into optoelectronic device architectures.[182] Along these lines, Zink and co-workers introduced an alternative method to locate macromolecular luminophores into mesostructured films through a one-pot procedure (Fig. 23).[183] This method relies on the use of a water-soluble organic conducting polymer containing sulfonate groups, poly(2,5-methoxypropyloxysulfonate)phenylene vinylene (MPSPPV), that has a chain length of 1900 units. The polymer is dissolved in the initial sol and, as the film is formed, the organic backbone is incorporated in the organic region of the film while the sulfonate groups reside in the ionic interface region together with the positive alkylammonium headgroups of the surfactant.

The orientation of the polymers within the matrix was studied by fluorescence polarization. These studies revealed that polymer chains were preferentially oriented within the mesostructured matrix. This was explained considering that most of the polymer chains are longer than the width of a cylindrical micelle and, consequently, the chains are forced to run parallel to the rods within which they are confined.[183] Sol–gel polymerization of tetraethoxysilane in the presence of amphiphilic phthalocyanine polymer has been reported to

 

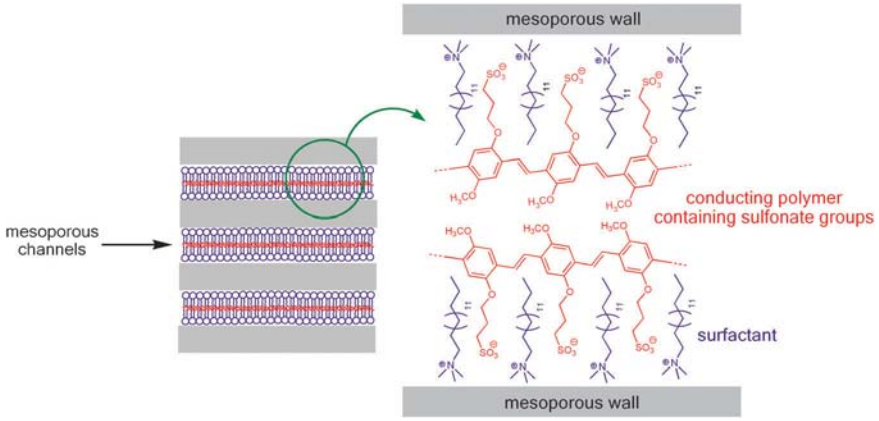


**Fig. 23** Scheme of the sol–gel film incorporating the conducting polymer within the mesoporous matrix. The figure depicts an ionic interfacial region in which the sulfonate groups of the functional polymer reside together with the positive alkylammonium headgroups of the surfactant.

produce organic–inorganic composites with the rod-like phthalocyanine polymers incorporated within ordered hexagonal channels. The amphiphilic rod-like phthalocyanine polymer acted as a structure-directing agent for the sol–gel polymerization of an inorganic source. The inorganic framework served to isolate the rod-like conductive polymers which may lead to directional electronic conductivity through highly conductive phthalocyanine polymers within an ordered nanoscopic channel.[184] Finally, Fujiwara *et al.* reported the preparation of functional hybrid polymer–mesoporous silica composite materials by simply mixing hexadecyltrimethylammonium bromide, sulfonated polymers such as Nafion or poly(sodium 4-styrenesulfonate), and TEOS in alkaline aqueous solution.[185] XRD characterization revealed that the crystallinity of the hexagonal structure of composite materials was not affected by the incorporation of the polymers. However, when an excess amount of Nafion was mixed in the sol, a significant loss of the acid sites of Nafion is observed. This indicates that the sulfonated polymer might be incorporated in the wall framework of mesoporous silica matrix in close resemblance to a "framework polymer composite" of mesoporous silica.

## 4. Spatially-addressing macromolecular functional units on mesoporous supports: tailoring "inner" and "outer" chemistries in hybrid nanostructured assemblies

The bottom-up fabrication of (multi)functional materials requires a thorough control of the chemistry of the building blocks across multiple length scales. In a similar vein, molecular design of hybrid mesoporous materials demands new methodologies for the incorporation of functional units into mesoscale architectures in predetermined arrangements, thus enabling the formation of hierarchical materials in which *chemistry* and *topology* define the functional features of the composite material. Large efforts in contemporary materials science are being aimed at the processing of ordered mesoporous architectures, using low-cost and up-scalable strategies, in which functional macromolecular units are deliberately placed in specifically spatially separated regions of the mesostructure. The very possibility of providing new avenues to site-selectively incorporate functional building blocks into mesostructured platforms marks an important advance in the development of highly functional hybrid materials.[186] Building up mesoporous materials in which shape, order and spatial distribution of chemical groups control function and utility is central for the creation of locally delimited nanoscopic reaction spaces in thin films or the construction of chemo-responsive mesostructured optical waveguides.[187]

Benchmark examples of spatially-controlled functionalization of mesostructured materials with macromolecular building blocks rely on the selective chemical derivatization of the inner and outer environment of the mesoporous framework.[188,189] Hong *et al.*[190] described the functionalization of the exterior surface of mesoporous silica particles *via* reversible addition–fragmentation chain transfer (RAFT) polymerization without affecting the mesoporous structure. Mesoporous silica particles with diameter of $\sim$100 nm and mesopores $\sim$2 nm in diameter were synthesized using cetyltrimethylammonium bromide (CTAB) as surfactant. Then the mesoporous material filled with CTAB was reacted with 5,6-epoxyhexyltriethoxysilane (EHTES) under reflux in toluene, forming EHTES-coated particles. Since the mesopores of the silica nanoparticles were filled with CTAB, EHTES was only grafted on the exterior surface of mesoporous particles. The presence of the surfactant in the mesopores precludes functionalization on the inner mesoporous environment of the particle. After the EHTES-coated particles were refluxed in a methanol solution of hydrochloric acid, the CTAB inside the mesopores was removed and the epoxyhexyl groups on the exterior surface of particle were converted into 5,6-dihydroxyhexyl units. This experimental protocol facilitates the unclogging of the mesopores which in turn leads to a spatially-controlled derivatization of the outer surface with epoxy groups. Thereafter, the RAFT agent (*S*-1-dodecyl-*S*-($\alpha$,$\alpha'$-dimethyl-$\alpha''$-acetic acid)-trithiocarbonate) was attached onto the mesoporous particle *via* esterification with the hydroxyl units on the surface catalyzed by DCC, forming mesoporous silica particles with RAFT agents on the exterior surface. Finally, pH-sensitive poly(acrylic acid) (PAA) chains were grown from the exterior surface of the mesoporous particles *via* surface RAFT polymerization of acrylic acid using AIBN as the

initiator. This strategy enabled the straightforward preparation of core–shell mesoporous particles that can act as "active" nanocontainers for guest molecules provided that the pH-responsive PAA nanoshell can be reversibly opened and closed, triggered by pH change, resembling a nanovalve that regulates the loading and release of guest molecules from the mesoporous core. This strategy exploiting the synthetic versatility of RAFT polymerization and the structural features of mesoporous silica nanoparticles has been extended recently to diverse "responsive" core–shell systems.[191]

In a similar vein, Shantz *et al.* demonstrated that amines and thiols can be selectively grafted to the exterior surface and within the pores of SBA-15 using a post-synthetic approach, in which external surface functionalization was achieved by reacting as-made SBA-15 and the desired organosilane prior to removing the template. The site-selective functionalization of the external mesoporous surface with amine groups was used for the grafting of large amounts of poly-*Z*-L-lysine in order to create novel hybrid materials.[192]

The spatially-controlled functionalization of mesoporous materials *via* preferential growth of hyperbranched poly(ethylene imine) (PEI) on the outer surface of the mesoporous silica was also demonstrated by Linden and co-workers.[193] As described above, the monomer aziridine was polymerized in the presence of mesoporous silica particles in which the surfactant used as structure-directing agent has not yet been extracted from the mesopores. This experimental strategy enables the facile incorporation of carboxylic acid functionalities preferentially to the outer part of the PEI layer by succinylation of the terminal amino groups (Fig. 24). The relative concentration of carboxylic acid to amino groups in the PEI layer can be rationally controlled and, hence, a fine-tuning of the surface charge of the particles for a given application can be achieved. In addition, these authors demonstrated that the inner environment of the mesoporous silica core can be further functionalized with monolayer assemblies, *e.g.*: hexamethyldisilazane, even after growing the polymer shell from the outer surface. PEI-modification of mesoporous silica provides stable, non-toxic particles that can be further functionalized with biomolecules. The folic acid-modified PEI–silica composite can be targeted and selectively endocytosed by cancer cells *via* identification by the folate receptor. This result is promising for cancer detection and eventually treatment.[194]

## 5. Polymer–inorganic mesoporous hybrids as versatile platforms to achieve materials with tailored and enhanced functional properties

One of the most appealing aims of hybrid ordered mesoporous assemblies is to create molecular materials that combine the molecular properties originating from the "host" porous inorganic framework and the "guest" macromolecular entities. The primary purpose is to extend the spectrum of functional properties by controlling the chemical environment of the mesopores "hosts" through the modification with macromolecular building blocks. However, we shall see that the

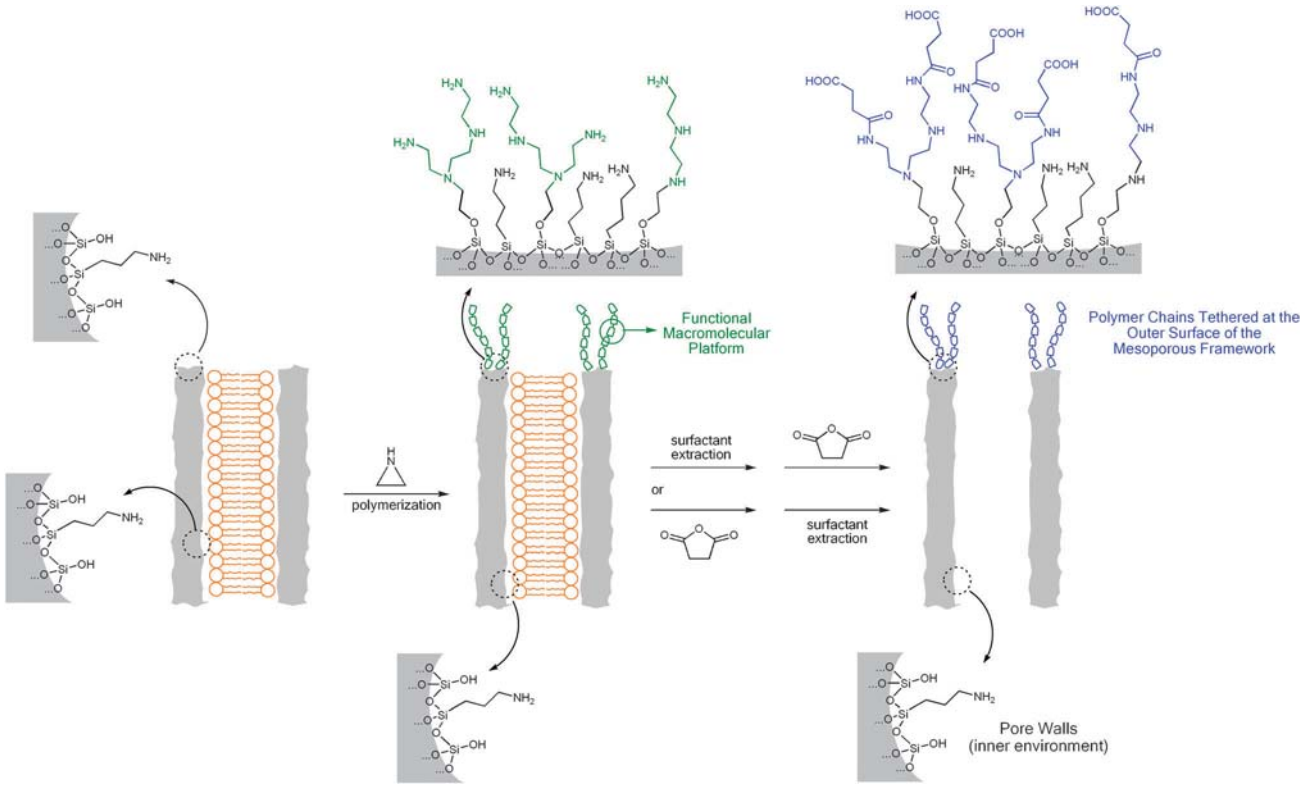


**Fig. 24** Schematic illustration showing the different steps involved in the functionalization of mesoporous silica with amino-terminated hyperbranched polymers preferentially located on the outer surface of the porous matrix and their subsequent conversion to carboxylic acid groups.

 

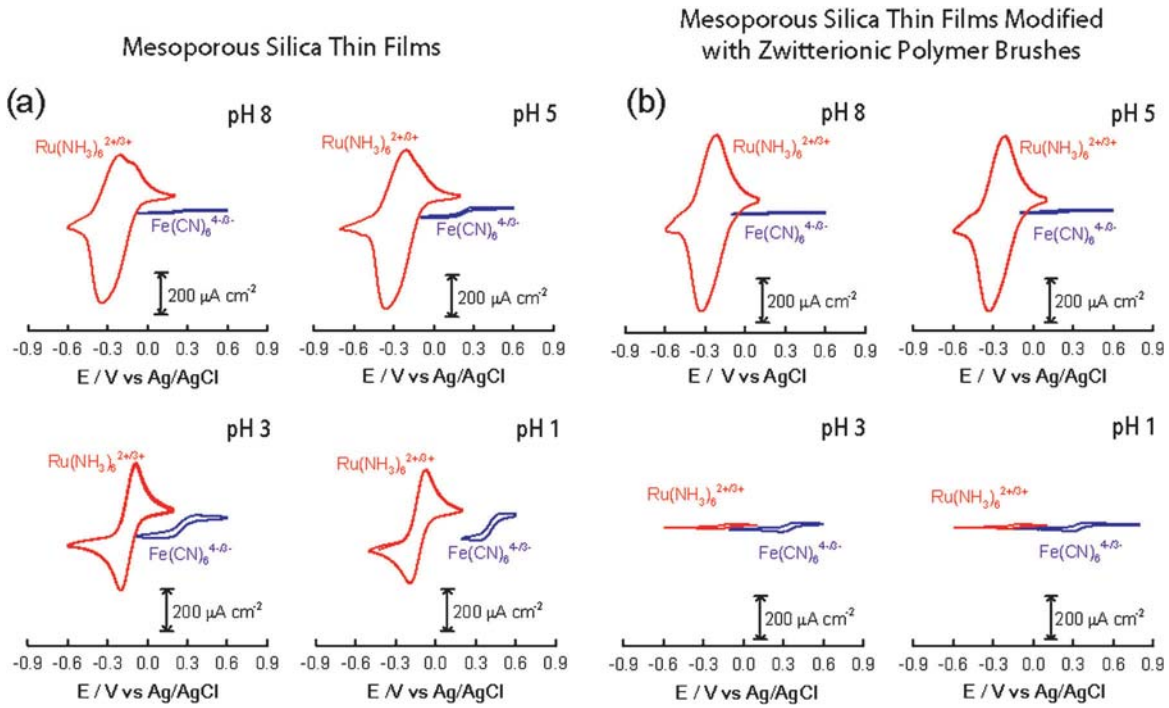


**Fig. 25** Cyclic voltammograms corresponding to a mesoporous silica film (a) and a mesoporous silica film modified with zwitterionic polymer brushes (b) deposited on an ITO electrode in the presence of 1 mM $Ru(NH_3)_6^{3+}$ and 1 mM $Fe(CN)_6^{3-}$, respectively, under different pH conditions. Reproduced with permission from A. Calvo, B. Yameen, F. J. Williams, G. J. A. A. Soler-Illia, O. Azzaroni, *J. Am. Chem. Soc.*, 2009, **131**, 10866–10868. Copyright 2009 American Chemical Society.

incorporation of mesoporous particles into polymeric matrices can also be a valuable alternative for designing functional platforms. The combination of approaches allows the fine-tuning of the properties of the hybrid nanomaterials and offers new perspectives for bridging the gap between molecular materials science and nanotechnology.

### 5.1 Case study 1: building up ionic filters—functional synergism in the permselective properties of mesoporous oxide thin films modified with polyzwitterionic brushes

The assembly of different building blocks allows the generation of materials with new properties or the combination of properties not accessible otherwise. In the case of mesoporous materials a long-standing goal has been to achieve a synergy between the inorganic and macromolecular counterparts. In the recent years, the scientific community has witnessed a remarkable interest in creating new methodologies to achieve active control over molecular transport in highly confined geometries. This interest originates from the many technological processes relying on controlled transport of molecular species in nanoconfined environments, like molecular separation, dosing, or drug delivery. In particular, the generation of interfaces discriminating the transport of ionic species through which the passage of ions can be triggered or inhibited under the influence of an external stimulus has received increasing attention from the materials science community. Along these lines, Calvo *et al.*[195] described the creation of hybrid organic–inorganic assemblies displaying unique pH-dependent ionic transport properties originating from the combination of polyzwitterionic brushes and silica mesoporous matrices. In principle, the presence of pore wall-confined silanolate groups (Si–$O^-$), with $pK_a \sim 2$, conferred permselective properties to the mesoporous silica thin films. The transport of ionic species through the mesoporous silica was electrochemically probed by using charged electroactive species diffusing across the film deposited on conductive ITO substrates. Cyclic voltammetric studies of mesoporous silica films supported on ITO in the presence of 1 mM $Ru(NH_3)_6^{3+}$ and $Fe(CN)_6^{3-}$ revealed that at pH's significantly above the $pK_a$ of silica, *i.e.*, 8 and 5, the detection of electrochemical response of $Ru(NH_3)_6^{3+}$ ions was feasible whereas that corresponding to the $Fe(CN)_6^{3-}$ species was hardly detectable (Fig. 25). The mesopore walls are negatively charged and permselectively repel the transport of $Fe(CN)_6^{3-}$ while at the same time allow the diffusion of $Ru(NH_3)_6^{3+}$ to the underlying ITO electrode. Lowering the pH to 3 or 1 resulted in a minor decrease in the voltammetric signal of $Ru(NH_3)_6^{3+}$ while the corresponding signal for $Fe(CN)_6^{3-}$ was slightly increased (Fig. 25). This electrochemical behaviour was attributed to the loss of surface-confined negative charges due to the close proximity to the $pK_a$ value of silica. However, the electrochemical results indicate that the mesoporous silica films exposing SiO– groups act as permselective barriers precluding the transport of anionic species. On the other hand, similar mesoporous silica films displaying mesopore walls functionalized with zwitterionic poly(methacryloyl-L-lysine) (PML) brushes evidenced a completely different permselective behaviour.

Fig. 25 describes the voltammograms of PML brush-modified mesoporous silica film in contact with electrolyte

solutions containing $Fe(CN)_6^{3-}$ and $Ru(NH_3)_6^{3+}$, respectively. It is evident that the presence of the polyzwitterionic brush introduces dramatic changes in the transport properties of the mesoporous film. At pH's 8 and 5 the brush-modified mesoporous film still hindered the transport of anions while enabling the diffusion of cations into the film. Then, in stark contrast to that observed in bare mesoporous silica films, at pH's 3 and 1 the transport of both cationic and anionic species was completely inhibited (Fig. 25). The isoelectric point (pI) of the zwitterionic brush is ~5, and as such, it should be expected that at pH > 5 the nanopore was negatively charged, *i.e.*, cation-permselective, and at pH < 5 the same pore walls were positively charged, *i.e.*, anion-permselective. Intriguingly, PML brush-modified mesoporous film acted as an ionic barrier at pH < 5 instead of behaving as an anion permselective membrane. The explanation for this particular behaviour relies on the actual understanding of the physicochemical changes taking in the pore environment rather than merely analyzing the pH-induced changes occurring in the monomer units of the zwitterionic brush (Fig. 26). In the pore walls the grafted polyzwitterionic chains coexist with silanol sites, which are negatively charged at pH > 2. At pH's > 5 both the zwitterionic moieties and the $SiO^-$ groups bear negative charges. As a result, the hybrid mesoporous film shows a remarkable cation-permselective behavior. Then, at pH < 5 the zwitterionic monomers bear positive charges while the silanol groups are still negatively charged. This experimental scenario leads to the emergence of a zwitterionic, "bipolarly charged" mesopore in the $pI^{brush} > pH > pK_a^{silica}$ range. In contrast to the typical Donnan exclusion phenomenon which refers to confined negative charges repelling anions and confined positive charges repelling cations, the confinement of both negative and positive charges leads to a very particular exclusion condition. Initially the anions are attracted to the pore by the positive charges in the "bipolar" wall. However, the negative charges in the "bipolar" wall are very close to the positive ones, and as a result, repulsion of the anions occurs simultaneously. In a similar way, the diffusing cations will have the same electrostatic behavior due to their interaction with the "bipolar" environment. As a result, the *synergy* between the electrostatic characteristics of the brush layer and the silica scaffold is responsible for building up, in a reversible manner, a chemically actuated ionic barrier at pH < 5. The unique barrier properties of the film could be only observed in the presence of the cooperative interaction between the brush and the mesoporous silica provided that the behavior of the whole system significantly differs from the behavior of their parts taken separately.

### 5.2 Case study 2: hybrid Nafion–mesostructured silica assemblies for advanced design of proton exchange membranes

Proton exchange membranes (PEMs) are key constituent elements in different industrial applications and particularly in energy conversion technologies. To date, the PEMs are typically constituted of perfluorinated polyelectrolytes, like Nafion. This material, considered "the golden standard", is characterized by forming nanoscopic hydrophilic channels suitable for the conduction of protons across the membrane. However, Nafion membranes exhibit dramatic alteration in their conductivity performances upon water evaporation. In a low-humidity environment, dehydration of the Nafion occurs and the collapse of the physical architecture of the membrane leads to a significant loss of conductivity. In this context, sol–gel processing opened up new possibilities to manipulate the water content of proton conducting membranes. Along these lines, diverse research groups reported the modification of Nafion membranes *via* sol–gel chemistry in order to prevent the loss of water from the membrane. However, the condensation of the sol–gel precursors yielded poorly ordered solids with amorphous structures and low specific surface areas. Recently, Sanchez and his collaborators described a novel approach for the synthesis of hybrid proton conducting membranes using self-assembly silica phase growth in a host Nafion matrix.[196] This approach is contrary to the traditional scenario in which the inorganic counterpart acts as the "host" and the macromolecular building blocks play their part as the "guest" entities. The experimental protocol for the construction of Nafion–mesoporous silica hybrid membranes involves initially the preparation of a sol containing absolute ethanol, Pluronic P123, and TEOS. Alternatively, TEOS can be substituted by (2-(4-chlorosulfonylphenyl)ethylsilane) to tune the acidity of the mesoporous framework. The organosilane solution was added dropwise to a stirred Nafion alcoholic solution. Then the hybrid membranes were obtained by

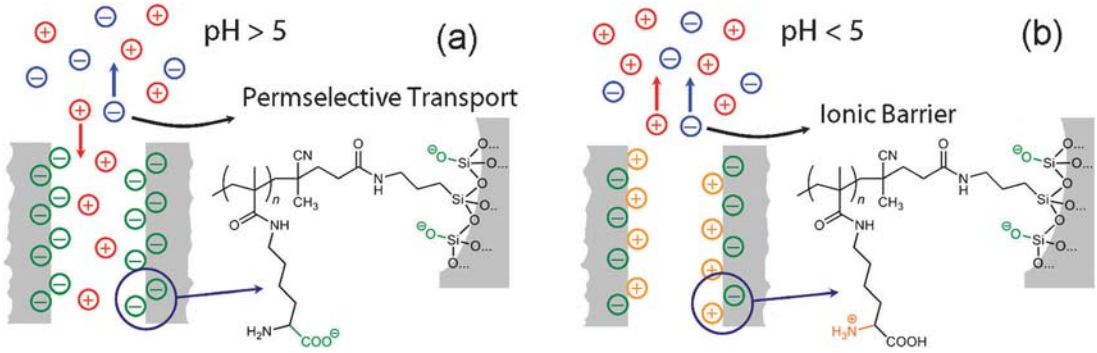


**Fig. 26** Schematic illustration of the ionic transport processes taking place in the mesoporous silica film modified with the zwitterionic polymer brushes at different pH values: (a) pH > 5, permselective transport of cations and (b) pH < 5, ionic barrier (exclusion of ionic species). Reproduced with permission from A. Calvo, B. Yameen, F. J. Williams, G. J. A. A. Soler-Illia, O. Azzaroni, *J. Am. Chem. Soc.*, 2009, **131**, 10866–10868. Copyright 2009 American Chemical Society.

 

pouring the solution onto a glass support followed by drying at 30 °C for 10 h. In parallel with the slow solvent evaporation, the growth of a polymeric mesoporous silica-based phase occurs within the hydrophilic domains of Nafion *via* hydrolysis and condensation of inorganic precursors. Depending on the working conditions this experimental protocol enables the formation of hybrid Nafion membranes with different mesoporous silica content in which the nanosized particles are homogeneously dispersed within the polymer matrix. The highly hydrophilic character of the SiOH groups exposed on the mesoporous silica surface plays a key role in increasing the water content in the membrane matrix. For instance, modification of the silica mesopore walls with sulfonic groups could further improve the water uptake due to the combined presence of hydrophilic sulfonic and silanol groups inside the mesopores. Experimental estimations of water uptake in hybrid membranes containing 13% by weight mesoporous silicon oxide bearing only silanol groups (*i.e.*: NMS13—water uptake 48%) and sulfonic and silanol groups (*i.e.*: NSMS13—water uptake 56%) corroborated that the presence of sulfonic groups in the mesoporous particles certainly improves the water uptake of the hybrid membrane. From the standpoint of "rational design" of hybrid proton conducting membranes, it might be worth mentioning here that an increase in silicon oxide content into the hybrid membrane leads to a substantial decrease in the ionic exchange capacity while water uptake is enhanced. Hence, there is a trade-off between ion exchange capacity and water uptake upon varying the silica content within the polymer matrix. As a result, high silicon oxide content involves an elevated number of water molecules in the membrane but a reduced efficiency for proton conduction. According to Sanchez *et al.* the optimal percentage of silicon oxide for the hybrid membranes was close to 13% by weight. Further characterization of the hybrid membranes under different relative humidity (RH) conditions measured at 95 °C revealed that the hybrid platforms possess higher proton conductivity values than Nafion membranes over the whole RH range and, furthermore, this improvement of proton conductivity is more significant at higher RH. This was ascribed to the inclusion of hygroscopic mesoporous silica within the Nafion membrane resulting in beneficial effects for water management. In addition, the hybrid membranes containing sulfonated mesoporous silica (NSMS13) evidenced much higher conductivity values than Nafion 112. This can be interpreted by considering that the functionalized hybrid membrane has a higher ion exchange capacity due to the *in situ* growth of sulfonated organosilica. This modification promotes an increase in proton conduction even though the membrane hydration is only slightly higher than that of Nafion. This experimental evidence eloquently illustrates the versatility of hybrid polymer–inorganic membranes to create proton conduction platforms and how alternative approaches may lead to clever design of functional platforms using readily available building blocks and fairly simple experimental protocols.

### 5.3 Case study 3: controlled-release systems and gate-like ensembles based on hybrid mesoporous architectures

Mesoporous silica nanoparticles (MSNs) are increasingly recognized as potential scaffoldings for designing controlled-release systems in which the combination of unique features such as biocompatibility, tunable pore structure and broad diversity in pore surface modification play a determinant role. Along these lines, seminal work from Lin and co-workers introduced the use of dendrimer–mesoporous hybrids as a novel gene transfection system. The hybrid architecture consisted of a second generation (G2) PAMAM dendrimer covalently attached to the surface of a MCM-41-type mesoporous silica nanoparticles. The mesoporous structure of the MSN allowed membrane-impermeable molecules, such as pharmaceutical drugs and fluorescent dyes, to be encapsulated inside the MSN channels whilst the amine terminated G2-PAMAMs were used as caps to encapsulate the guest (Texas Red) molecules inside the porous framework.[197] In recent years, the creativity of chemists and materials scientists provided a means for developing a series of MSN-based controlled-release systems that are responsive to different external stimuli, including light, pH or even "supramolecular" triggers.[198] Sun *et al.*[199] showed that pH responsive poly-(2-(diethylamino)ethyl methacrylate) (PDEAEMA) brushes anchored on MSNs could serve as a switch to control the opening and closing of the mesopores. Experimental results revealed that release of guest molecules (rhodamine B) can be controlled through pH variations in the environmental solution leading to a rapid release in acidic aqueous solution but very little leakage in alkaline solution. These authors also demonstrated that the pH-controlled "nanovalves" can perform reversible opening and closing of the mesopores. Martínez-Mañez and co-workers[200] recently reported an in-depth study of the behavior of a pH-driven and anion-controlled MCM-41-based mesoporous platforms obtained by anchoring polyamines on the pore entrance of the inorganic framework. The gating effect was studied by monitoring the release of entrapped probe molecules ($Ru(bpy)_3^{2+}$) from the porous matrix. Interestingly, these authors observed that hydrogen-bonding interactions between the amines at neutral pH (open gate) and electrostatic repulsions at low pH between ammonium groups at the entrance of the pore were responsible for the pH-driven open/close mechanism. Furthermore, the opening/closing of the gate-like mesoporous platform could also be modulated through an anion-controlled mechanism. In the presence of a range of anions with different structural dimensions and charges, including chloride, sulfate, phosphate or ATP, the choice of a certain anionic guest resulted in a different gate-like ensemble behavior, ranging from basically no action (chloride) to complete (ATP) or partial pore blockage, depending on the pH (sulfate and phosphate). These authors suggest that the synergic anion-controlled outcome might result from the formation of complexes between the protonated amines and a certain anion. The same group also described a gate-like pH-controlled functional hybrid platform consisting of MCM-41-based mesoporous architectures functionalized on the pore entrance with a saccharide derivative. This building block is capable of interacting with boronic acid functionalized gold nanoparticles (AuNPs) that subsequently act as "nanoscopic caps". The gating mechanism involves the reversible reaction between polyalcohols and boronic acids to form boronate esters. In this way it was possible to obtain a very effective guest release control using polyalcohol entities anchored onto mesoporous materials and

boronic acid functionalized gold nanoparticles as effective caps. The pH-controlled release is fully reversible, and the entrapped guests can be delivered by simple changes in the solution pH. The pH-controlled "gating" mechanism has been ascribed to the reversible formation of boroesters between the hydroxy groups on the pore entrance and the boronic acid functionalized nanoparticles ("closed" state) and their fast hydrolysis ("open" gate). The versatile use of gold NPs also opened up the possibility of exploiting the interaction of light and metal NPs as a stimulus for triggering the release of the entrapped molecules. It is well-known that Au NPs display the ability to raise their temperature locally by "plasmonic heating". As a result, the absorption of light resulted in the cleavage of the boronic ester linkage that anchored the nanoparticles to the surface of the mesoporous silica-based material, thus enabling the release of the entrapped guests.[201]

The combination of mesoporous materials and polymeric building blocks displaying active response to multiple stimuli has been also exploited to create nanoscopic hybrid gate-like ensembles. The formation of copolymer brushes on the outer surface of mesoporous nanoparticles led to the construction of light-responsive hybrid nanogates which allowed the encapsulation and release of drug and biological molecules upon light irradiation. Copolymer poly(*N*-isopropylacrylamide-*co*-2-nitrobenzyl acrylate) (poly(NIPAMNBAE)) brushes, bearing photocleavable hydrophobic 2-nitrobenzyl (NBAE) groups, display lower critical solubility temperature (LCST) below environmental temperature. As a consequence, at room temperature the polymer is in a collapsed (insoluble) state and the gate is "closed" so that the loaded molecules are locked in the pores. Upon UV light irradiation, the hydrophobic 2-nitrobenzyl acrylate moiety is photocleaved leading to the formation of a hydrophilic acrylate which, in turn, leads to an increase in the LCST of the resultant copolymers (Fig. 27). The outcome of this light-triggered process is the conformational/physicochemical change of the tethered polymers chains from a collapsed state to a swollen hydrophilic state, so that the gate is "opened" thereby allowing the entrapped molecules to escape.[202]

The incoming development of novel hybrid organic–inorganic mesoporous ensembles taking profit from the characteristics of

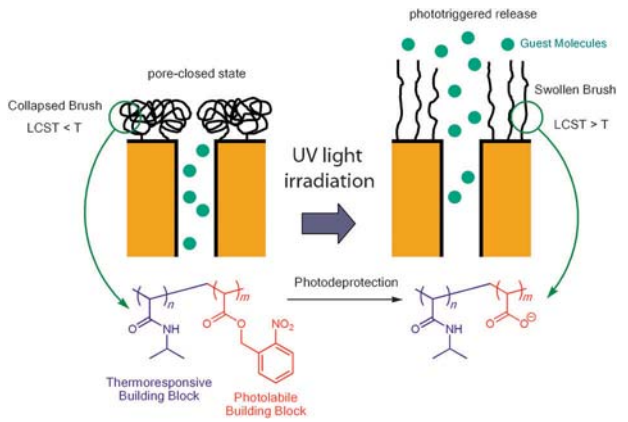


**Fig. 27** Light-responsive mesostructured assembly generated by grafting thermoresponsive/photolabile polymeric building blocks on the outer surface of the porous matrix.

*supramolecular building blocks* has also gained increasing interest in the materials science community in recent years. Much of this interest arises from the synergistic assembling of supramolecular entities with inorganic mesostructured solids leading to an exquisite control over the functional features of the hybrid architecture. Zink and co-workers recently described the use phosphonate-clothed mesoporous silica nanoparticles in which supramolecular machineries covering the surface of the nanoparticle acted as "nanopistons" enabling the release of guest molecules in a controlled fashion under acidic conditions.[203] The supramolecular "actuating" building blocks consist of a monolayer of β-cyclodextrin (β-CD) rings positioned selectively around the orifices of the pores of the mesoporous nanoparticles. These β-CD rings on the surface served as gates for the storage of large cargo molecules (*e.g.*, rhodamine B) inside the mesopores under neutral conditions. Since imine bonds can be hydrolyzed under acidic conditions, the β-CD rings could be removed from the surface of the mesostructured particles when the pH was decreased to 6, thus releasing the "guest" molecules in an accurate manner. By a combination of different spectroscopic techniques these authors demonstrated that the "supramolecular nanopistons" are able to incorporate "guest" molecules inside the mesopores of the particles under neutral pH conditions but release them under subtle pH variations.[203] In a similar vein, Park *et al.*[204] reported on the pH-controlled release of guest molecules entrapped in the pores of mesoporous silica particles that are blocked by the surface-grafted pH-responsive polyethyleneimine (PEI)/cyclodextrin (CD) polypseudorotaxane. Low-molecular-weight linear PEI, which is known as a biocompatible polycationic polymer, was used as the guest polymer for CD hosts. The incorporation of this type of reversible pseudorotaxane onto the surface of mesoporous materials enabled the creation of pH-responsive nanocarrier systems in which CDs play the role of a pH-responsive valve for pores of mesoporous materials. Experimental results eloquently illustrated the pH-responsive release properties of the hybrid supramolecular system. Upon decreasing the environmental pH value of calcein-loaded CD/PEI mesoporous hybrids from 11 to 5.5 fluorescence measurements confirmed the release of calcein guest molecules from the mesopores owing to dethreading of CDs from the surface-confined PEI chains. The different experimental scenarios discussed in this case study section clearly reveal that the incorporation of surface functional groups or supramolecular building blocks able to open or close at will or including capping molecules provides advanced control release applications. For instance, the unique architecture of mesoporous solids, containing well-defined and controllable pore architecture, opens up a broad range of opportunities to design "on/off" systems able to achieve "zero" release, which can be fully opened using external physical or chemical stimuli.

### 5.4 Case study 4: solid state dye-sensitized solar cells (ss-DSSC) made up from mesoporous nanocrystalline titania and electroactive polymers

Solar energy harvesting is one of the major challenges in the current quest for renewable and sustainable energy sources.

 

Silicon-based photovoltaic (PV) cells find widespread use in several devices, but their cost per watt of solar energy is still not competitive with traditional sources, mainly because of the high cost of manufacturing silicon. Dye-Sensitized Solar Cells (DSSC), introduced in the mid-eighties, are one sound alternative to crystalline silicon PV cells, because they can in principle be produced from inexpensive precursors and wet-processing techniques on large area transparent electrodes. These cells could provide electricity at reasonable costs provided that efficiency and lifetime are increased to *ca.* 10% and 10 years, respectively, and mass production can be achieved. DSSC are composed of an n–p junction consisting in a large band-gap semiconductor oxide (typically $TiO_2$, ZnO or $SnO_2$) that acts as an electron conductor (n), and a hole conducting material or electrolyte, which acts as the p region. The electron and hole conductors are in intimate contact through a large area interface. Sensitizer molecules located at this interface act as light harvesters in the visible region and facilitate electron transfer between the n and p regions, by injecting the photo-generated electrons into the conduction band of the oxide. The sensitizer is regenerated by hole injection from the p region. State-of-the art cells can yield current density values ($J_{sc}$) ranging from 16 to 22 mA $cm^{-2}$, while open circuit potentials ($V_{oc}$) attain 0.7–0.86 V and efficiencies are reaching 10–11%.[205] Current challenges in this area are to attain significant light harvesting in the red region, and enhanced lifetime. In addition, the liquid containing cells need careful sealing, handling and maintenance, for they are prone to suffer corrosion, which severely limits its application in real devices that require outdoor exposure or deposition on flexible substrates. Therefore, the development of all-solid state DSSC in which the liquid electrolyte is replaced by a polymeric hole carrier is a promising area.

A typical solid-state-DSSC is composed of a bicontinuous composite of $TiO_2$ and an interpenetrating polymer that forms a bulk heterojunction, as schematized in Fig. 28. A transparent substrate such as ITO or FTO (F-doped $SnO_2$) is used as the light-collecting electrode. A porous $TiO_2$ film is the electron collector, in contact with the polymer, which forms an overlayer of 30–50 nm on top of the film, in order to avoid short circuits. A metallic layer (silver, aluminium) is sputtered onto this polymer overlayer, constituting the hole acceptor electrode. Ideally, the titania phase should be nanocrystalline and continuous, in order to permit an efficient electron flow, and to ensure intimate contact between the titania and the polymer phase, and present mesopores (*i.e.* pore diameter $< 50$ nm) in order to avoid loss by light scattering. In traditional cells, thick films (1–10 μm thickness) are produced by screen-printing or doctor-blade processing colloidal pastes formed by nanosized titania particles and additives. The resulting film is thermally treated, and the polymer is normally infiltrated in the textural pores that remain after calcining. This procedure is simple, but it lacks reproducibility and control over important parameters such as pore size and homogeneity. Mesoporous titania films (MPTF) constitute potentially interesting electron carriers that provide a continuous nanocrystalline framework, monodisperse pores, and a large framework–polymer contact area. Early works by Zukalovà *et al.* demonstrated that MPTF were useful to produce Grätzel cells with liquid electrolytes,

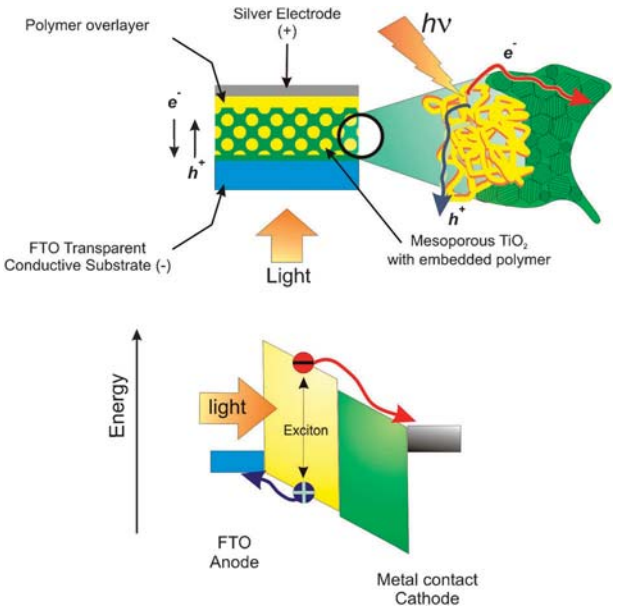


**Fig. 28** Scheme of a solid state DSSC composed of a polymer infiltrated into mesoporous titania, and the processes leading to charge separation.

reaching conversion efficiencies in the order of 4–5%.[206] The combination of highly ordered MPTF and conjugated polymers along a large interfacial area should form an ideal bulk heterojunction, in which every exciton formed upon irradiation in the electron donor (polymer) will readily diffuse to the interface, followed by an efficient electron transfer to the acceptor. The donor and acceptor materials should also present "straight pathways to the electrode to minimize the carrier transport time and reduce the probability of back electron transfer".[207] In principle, control of the mesoscale architecture of ordered mesoporous thin films would permit to achieve controlled energy flux. The requirements for such an ideal device are: tunable porosity in the 5–20 nm scale, accessibility to polymers, large fraction of the pores filled by the polymer (*i.e.*, pore filling), nanocrystalline walls, good adhesion to the substrate, micrometre thickness and lack of cracks or flaws. In addition, the ideal framework would present vertical pores, in order to minimize the electron and hole collection at the electrodes.

The first reported MPTF-conjugated polymer nanocomposite for solar cell applications was reported by Coakley *et al.*[161] MPTF with accessible pore systems were produced according to an EISA-based technique using Ti alkoxides and acidic conditions, which led to cubic mesopore systems with interconnected ellipsoidal pores of 7 nm estimated major diameter, as assessed by SEM and low-angle XRD. A layer of regioregular poly(3-hexyl thiophene) RR P3HT, a semiconductor polymer with small bandgap and high hole mobility (0.1 $cm^2\ V^{-1}\ s^{-1}$ in Field Effect Transistors), was spin-cast on the MPTF. The resulting system was heated at temperatures of 125–200 °C, above the polymer glass transition (25 °C), for varying periods, after which the excess polymer was removed by washing. The presence of polymer infiltrated within the mesopores was assessed by UV-visible spectroscopy and

quantified by analyzing XPS depth profiles. According to XPS profiling, the polymer is evenly distributed along the film thickness. A maximum pore filling of about 50–60% is obtained after heating at 200 °C in less than an hour. Lower pore loadings are reached at longer times for lower temperatures. Absorption and luminescence spectra of confined polymers present blue shifts, demonstrating that π–π conjugation is almost lost upon infiltration and that confined chains are mostly in the coiled conformation. It is likely that an entropy loss occurs, due to the confinement of polymer chains into pores smaller than their gyration radius. An important enthalpic contribution due to strong polymer–titania interactions that overcomes this entropy loss was proposed as the driving force of the polymer infiltration process. Photoluminescence spectra also showed that the polymers are not aggregated in the pores, and revealed some hindered electron transfer to the titania walls. In further development, Coakley and McGehee showed that an all-ss-DSSC can be produced from MPTF infiltrated with RR 3PHT, obtaining an External Quantum Efficiency (EQE) of 10% and a 1.5% power conversion efficiency under 514 nm illumination.[208] Detailed studies of the conduction mechanisms permitted to assess the charge-carrier mobility in titania systems with different geometry, obtained by different routes such as nanoimprinting (macropores) or block copolymer lithography (nanopillars). Even if the systems are complex, valuable information was extracted in order to aim at exciton harvesting without substantial recombination.[209]

Following a systematic approach, Lancelle-Beltran *et al.* made a comparison between titania–polymer films with different thicknesses, crystalline structure and preparation method (*i.e.*, mesostructured *versus* colloidal aggregation), using regioregular poly(3-octylthiophene), P3OT. A maximum conversion efficiency of *ca.* 1.5% was found for films with optimal thickness of 1.5 μm derived from anatase colloids.[210] Another method recently developed implies the direct construction of a hybrid titania–block copolymer gyroid mesophase with large pores. 400 nm-thick films with homogeneous thickness, highly organized and open pore structure, and nanocrystalline walls can be obtained by electrochemical deposition in a pre-formed liquid crystalline phase (TLCT approach, see above) made up of a designed block copolymer (polyfluorostyrene-*b*-polylactic acid, PFS-*b*-PLA). The inorganic matrix was infiltrated with spiro-OMeTAD, which acted as a hole carrier. Power conversion efficiencies of 0.7–1.7% were obtained in first trials. These relatively high values were attributed to the ease of polymer impregnation in the mesopores, due to the open structure characteristic of the gyroid mesophase.[211] Further studies carried out using PI-*b*-PEO templated titania and spiro-OMeTAD polymer showed higher efficiency (2.4–3.2%). It seems that this kind of template can play a central role in the crystallization process of the titania framework, tuning the sub-band gap levels, and thus enhancing photocurrent generation.[212]

In summary, the production of photovoltaic devices based on MPTF and conjugate polymers is a promising and active area of research. Although the systems are yet far from presenting competitive features for commercial applications, much has been learnt from the basic point of view. It is clear that the precise geometrical arrangement of the mesopores and the organic functions (carrier, sensitizers) are crucial for making an all-solid state PV cell. The synthetic tools developed so far have permitted to test the systems, and to identify the relevant variables (crystallinity of the inorganic framework, confinement-dependent conjugation of the polymer, interactions leading to quenching...), and to advance in the enhancement of conversion efficiency. However, several challenges remain, mostly derived from lack of precise characterization in two central aspects: the quantitative determination of pore filling, and an adequate knowledge of the molecular geometry of the polymer–titania interface, including the role of the sensitizer. Thorough characterization techniques such as X-Ray Reflectometry, X-Ray Spectroscopy or NMR should be applied systematically in order to understand precisely these issues. Yet, ss-DSSC constitute an excellent example of the needs for precise tailoring of molecular and mesoscopic position and geometries in space, in order to achieve the relevant properties for a desired application.

## 6. Summary and outlook

Our ability to engineer materials with molecular precision has brought unprecedented opportunities in materials design.[213] Today, there is a general consensus within the scientific community that the introduction of mesoporous materials over two decades ago has led to a paradigm shift in materials science. The ease of design of the mesoporous materials requiring simple and inexpensive experimental protocols makes them suitable building blocks not only for fundamental research but also for the technological world. Their unique properties such as control of pore structure and morphology, the tailoring of pore surface chemistry, and the variety of framework composition represent key features that certainly have a strong impact on a wide variety of technological applications, like catalysis or adsorption processes.

Chemists have learnt ways to merge concepts and tools from self-assembly and "soft chemistry" in order to construct multi-functional materials[214] and hierarchical structures[215] in close resemblance to biological examples (Fig. 29). However, a higher degree of sophistication and functionality probably cannot yet be obtained by sole reliance on the combination of self-assembly and sol–gel process. Incorporation of macromolecular building blocks into inorganic frameworks can yield unique materials that have neither inorganic nor organic analogues. Whilst the inorganic mesostructure constitutes a topologically well-defined but rigid structure, polymeric components have a flexible nature. The incorporation of polymeric units within the mesoporous inner environment represents a unique tool for designing hybrid organic–inorganic mesoporous assemblies. Considering the chemical diversity of polymers, the macromolecular building blocks can endow the mesoporous scaffold with a myriad of functional properties that cannot be readily obtained through the modification of the pore walls with monolayer assemblies. For this reason, the design and realization of polymer architectures into mesoporous materials has become an important goal in contemporary macromolecular science.

 

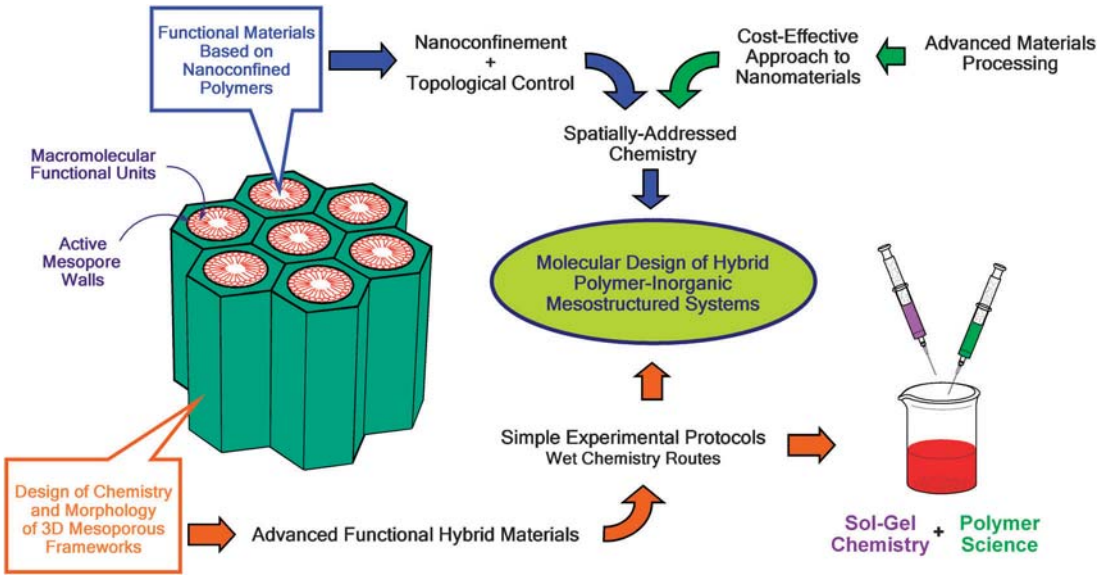


**Fig. 29** Conceptual illustration of the chemical strategy based on the combination of tools from sol–gel chemistry and polymer science in order to design polymer–inorganic mesoporous materials displaying spatially-addressed chemistries.

Over the past several years, we have witnessed the appearance of different synthetic schemes enabling the formation of polymeric assemblies inside mesopores, and this trend is still continuing. At present, more and more monomers become eligible for incorporation into the inorganic matrix, thus adding more possible functions into the hybrid polymer–inorganic mesostructured materials.

An essential aspect of mesoporous and mesostructured materials is that "function" can be located in well-structured confined geometries. Control of the local and medium-range interactions that take place at the mesoscale has opened the door to a better understanding of the self-assembly and self-positioning processes that lead to materials with complex morphology and chemical function positioning.[216] The nanoscale dimensions of mesoporous materials bring the possibility of a versatile toolbox for designing functional hetero-assemblies in which pore size and geometry may control or enhance functional features.[217] Because mesopore size can regulate orientation and arrangement of confined functional units mesostructured materials provide attractive environments for exploring a new kind of chemistry in which functional properties might be entirely governed by nanoconfinement effects. We should bear in mind that in a physically constrained environment,[218] interfacial interactions and confinement-induced entropy loss can play dominant roles in determining molecular organization or chemical reactivity. Hence, confinement inside a mesopore can definitively change the interaction between pre-programmed functional units and their surroundings.[219,220] For instance, in confined spaces of nearly molecular dimensions, all the adsorbed molecules are in close interaction with the surface, leading to remarkable consequences in their physical and chemical properties. As a result, materials confined in nanoscale geometries show structures and dynamics different from those exhibited in bulk. Or, in other words, the richness of chemical phenomena in confined environments opens the path to advanced applications that rely on designed substrate–surface interactions. We have shown that part of the appeal of blending mesostructured inorganic frameworks and macromolecular functional units relies on the combination of their complementary properties which in turn leads to topological control of highly functional polymeric materials by inorganic nanostructures that exhibit wide chemical flexibility, good stability and excellent processability. However, it is worth highlighting that as in many cases of supramolecular materials comprising many components, the functions and structures of hybrid polymer–inorganic mesostructures are in general not the sum of each component but can provide quite different, novel functional features. This critical review has provided a broad description of the current synthetic strategies as well as a discussion of the experimental tools that are required to fully characterize polymer–inorganic mesoporous materials. The primary aim was to suggest and describe the multiple approaches to functional hybrids by combining ordered mesoporous materials and macromolecular building blocks. Hopefully, this work will engender interest in acquiring a basic understanding and stimulate further explorations in the topological control of hybrid mesostructured materials as a route towards spatially-addressed chemistry. In this context, the new horizons provided by hybrid polymer–inorganic mesoporous materials appear very wide and the future offers the prospect of many developments as chemists show an increased mastery in construction of functional macromolecules in mesoporous environments. The development of mesoporous materials around the turn of last century was accompanied by applications of these discoveries and insights in understanding chemical processes taking place in nanoconstrained environments. Yet, there is a need to keep exploring new avenues to attain hybrid mesostructured materials exhibiting strictly controlled *structure*, *topology* and *function*.[221] This is the cornerstone to convert macromolecular functions, built-in within the inorganic framework, into

macroscopic properties expressed at the level of the confined assemblies and thus leading to the production of addressable molecular materials and interfacial architectures. In the long-term perspective, we envision that "macromolecular chemistry in confined environments" will evolve as a main subject in chemistry and materials science during the 21st century as it offers a broad repertoire of approaches to molecularly design complex hybrid systems. With this in mind, we hope that this review can trigger a cascade of new, refreshing ideas in hybrid mesoporous materials as well as assist in the rational design of functional materials based on nanoconfined polymers.

## Acknowledgements

The authors gratefully acknowledge financial support from Agencia Nacional de Promoción Científica y Tecnológica (ANPCyT) (PICT 34518, PAE 2004 22711, PICT-PRH 163/08)), Centro Interdisciplinario de Nanociencia y Nanotecnología (CINN, PAE 2006 37063, projects: PRH 2007-74-PIDRI No. 74, and PME 00038), Universidad de Buenos Aires (UBACyT X003), Fundación Petruzza, Gabbos (DG-017), Max-Planck-Gesellschaft (MPG), Consejo Nacional de Investigaciones Científicas y Técnicas (CONICET), Alexander von Humbolt Stiftung and Laboratório Nacional de Luz Síncrotron (LNLS). G.J.A.A.S.-I. and O.A are staff members of CONICET.

## References

1 *Chem. Mater.*, 2008, **20**, Special Issue: Templated Materials, ed. M. Jaroniec and F. Schüth, pp. 599, and articles included therein.
2 (*a*) C. T. Kresge, M. E. Leonowicz, W. J. Roth, J. C. Vartuli and J. S. Beck, *Nature*, 1992, **359**, 710; (*b*) J. S. Beck, J. C. Vartuli, W. J. Roth, M. E. Leonowicz, C. T. Kresge, K. D. Schmitt, C. T. W. Chu, D. H. Olson, E. W. Sheppard, S. B. McCullen, J. B. Higgins and J. L. Schlenker, *J. Am. Chem. Soc.*, 1992, **114**, 10834; (*c*) I. Ichinose and T. Kunitake, *Chem. Rec.*, 2002, **2**, 339–351.
3 T. Yanagisawa, T. Shimizu, K. Kuroda and C. Kato, *Bull. Chem. Soc. Jpn.*, 1990, **63**, 1535.
4 K. J. C. van Bommel and S. Shinkai, *Langmuir*, 2002, **18**(12), 4544.
5 E. D. Sone, E. R. Zubarev and S. I. Stupp, *Angew. Chem., Int. Ed.*, 2002, **41**, 1705–1709.
6 F. Kleitz, in *Nanoscale Materials in Chemistry*, ed. K. J. Klabunde and R. M. Richards, John Wiley & Sons, New York, 2nd edn, 2009, ch. 9, pp. 243–349.
7 N. Hüsing, in *Hybrid Materials. Synthesis, Characterization, and Applications*, ed. G. Kickelbick, Wiley-VCH, Weinheim, 2007, ch. 5, pp. 175–223.
8 J.-M. Lehn, *Proc. Natl. Acad. Sci. U. S. A.*, 2002, **99**, 4763–4768.
9 G. A. Ozin, *Adv. Mater.*, 1992, **4**, 612–649.
10 K. Ariga, J. P. Hill, M. V. Lee, A. Vinu, R. Charvet and S. Acharya, *Sci. Technol. Adv. Mater.*, 2008, **9**, 014109.
11 K. Ariga, A. Vinu, J. P. Hill and T. Mori, *Coord. Chem. Rev.*, 2007, **251**, 2562–2591.
12 S. Mann and G. A. Ozin, *Nature*, 1996, **382**, 313.
13 C. Sanchez, H. Arribart and M. M. Giraud Guille, *Nat. Mater.*, 2005, **4**, 277–288.
14 R. J. P. Corriu, *Eur. J. Inorg. Chem.*, 2001, 1109–1121.
15 S. Mann, S. L. Burkett, S. A. Davis, C. E. Fowler, N. H. Mendelson, S. D. Sims, D. Walsh and N. T. Whilton, *Chem. Mater.*, 1997, **9**, 2300–2310.
16 G. J. A. A. Soler-Illia, C. Sanchez, B. Lebeau and J. Patarin, *Chem. Rev.*, 2002, **102**, 4093–4138.
17 R. Backov, *Soft Matter*, 2006, **2**, 452–464.
18 X. Feng, G. E. Fryxell, L.-Q. Wang, A. Y. Kim, J. Liu and K. M. Kemner, *Science*, 1997, **276**, 923–926.
19 Z. Yang, Y. Lu and Z. Yang, *Chem. Commun.*, 2009, 2270–2277.
20 J.-l. Shi, Z.-l. Hua and L.-x. Zhang, *J. Mater. Chem.*, 2004, **14**, 795–806.
21 M. Pagliaro, R. Cirimina and G. Palmisano, *Chem. Rec.*, 2010, **10**, 17–28.
22 (*a*) A. Calvo, M. C. Fuertes, B. Yameen, F. J. Williams, O. Azzaroni and G. J. A. A. Soler-Illia, *Langmuir*, 2010, **26**, 5559–5567; (*b*) A. Calvo, B. Yameen, F. J. Williams, O. Azzaroni and G. J. A. A. Soler-Illia, *Chem. Commun.*, 2009, 2553–2555.
23 (*a*) F. Goettmann and C. Sanchez, *J. Mater. Chem.*, 2007, **17**, 24–30; (*b*) R. A. Schoonheydt and B. M. Weckhuysen, *Phys. Chem. Chem. Phys.*, 2009, **11**, 2794–2798; (*c*) Y. Wu, G. Cheng, K. Katsov, S. W. Sides, J. Wang, J. Tang, G. H. Frederickson, M. Moskovits and G. D. Stucky, *Nat. Mater.*, 2004, **3**, 816–822; (*d*) O. Azzaroni, B. Trappmann, P. van Rijn, F. Zhou, B. Kong and W.T.S. Huck, *Angew. Chem., Int. Ed.*, 2006, **45**, 7440–7443.
24 (*a*) P. Lambooy, T. P. Russell, G. J. Kellogg, A. M. Mayes, P. D. Gallagher and S. K. Satija, *Phys. Rev. Lett.*, 1994, **72**, 2899–2902; (*b*) S. Zhu, Y. Liu, M. H. Rafailovich, I. Sokolov, D. Gersappe, D. A. Winesett and H. Ade, *Nature*, 1999, **400**, 49–51.
25 (*a*) M. Tagliazucchi, O. Azzaroni and I. Szleifer, *J. Am. Chem. Soc.*, 2010, **132**, 12404–12411; (*b*) M. Ali, B. Yameen, J. Cervera, P. Ramírez, R. Neumann, W. Ensinger, W. Knoll and O. Azzaroni, *J. Am. Chem. Soc.*, 2010, **132**, 8338–8348.
26 (*a*) T. S. Koblenz, J. Wassenaar and J. N. H. Reek, *Chem. Soc. Rev.*, 2008, **37**, 247–262.
27 (*a*) B. Yameen, M. Ali, R. Neumann, W. Ensinger, W. Knoll and O. Azzaroni, *Chem. Commun.*, 2010, **46**, 1908–1910; (*b*) B. Yameen, A. Kaltbeitzel, G. Glasser, A. Langner, F. Müller, U. Gösele, W. Knoll and O. Azzaroni, *ACS Appl. Mater. Interfaces*, 2010, **2**, 279–287; (*c*) B. Yameen, M. Ali, R. Neumann, W. Ensinger, W. Knoll and O. Azzaroni, *Nano Lett.*, 2009, **9**, 2788–2793; (*d*) B. Yameen, A. Kaltbeitzel, A. Langner, F. Müller, U. Gösele, W. Knoll and O. Azzaroni, *Angew. Chem., Int. Ed.*, 2009, **48**, 3124–3228.
28 C. J. Brinker and G. W. Scherrer, *Sol–Gel Science, The Physics and Chemistry of Sol–Gel Processing*, Academic Press, San-Diego, CA, 1990.
29 Q. Huo, D. I. Margolese, U. Ciesla, D. G. Demuth, P. Feng, T. E. Gier, P. Sieger, A. Firouzi, B. F. Chmelka, F. Schüth and G. D. Stucky, *Chem. Mater.*, 1994, **6**, 1176–1191.
30 G. J. A. A. Soler-Illia and P. Innocenzi, *Chem.–Eur. J.*, 2006, **12**, 4478–4494.
31 G. S. Attard, J. C. Glyde and C. G. Göltner, *Nature*, 1995, **378**, 366–368.
32 C. J. Brinker, Y. Lu, A. Sellinger and H. Fan, *Adv. Mater.*, 1999, **11**, 579–585.
33 D. Grosso, F. Cagnol, G. J. A. A. Soler-Illia, E. L. Crepaldi, H. Amenitsch, A. Brunet-Bruneau, A. Bourgeois and C. Sanchez, *Adv. Funct. Mater.*, 2004, **14**, 309–322.
34 (*a*) F. Schüth, *Angew. Chem., Int. Ed.*, 2003, **42**, 3604–3622; (*b*) M. Tiemann, *Chem. Mater.*, 2008, **20**, 961–971.
35 A. Monnier, F. Schüth, Q. Huo, D. Kumar, D. Margolese, R. S. Maxwell, G. D. Stucky, M. Krishnamurty, P. Petroff, A. Firouzi, M. Janicke and B. F. Chmelka, *Science*, 1993, **261**, 1299–1303.
36 A. Firouzi, D. Kumar, L. M. Bull, T. Besier, P. Sieger, Q. Huo, S. A. Walker, J. A. Zasadzinski, C. Glinka, J. Nicol, D. Margolese, G. D. Stucky and B. F. Chmelka, *Science*, 1995, **267**, 1138.
37 (*a*) J. Frasch, B. Lebeau, M. Soulard and J. Patarin, *Langmuir*, 2000, **16**, 9049–9057; (*b*) J. Patarin, B. Lebeau and R. Zana, *Curr. Opin. Colloid Interface Sci.*, 2002, **7**, 107–115.
38 (*a*) J. Morell, C. V. Teixeira, M. Cornelius, V. Rebbin, M. Tiemann, H. Amenitsch, M. Fröba and M. Lindén,

 

*Chem. Mater.*, 2004, **16**, 5564–5566; (*b*) K. Flodström, H. Wennerström, C. V. Teixeira, H. Amenitsch, M. Lindén and V. Alfredsson, *Langmuir*, 2004, **20**, 10311–10316.
39 Q. Huo, D. I. Margolese and G. D. Stucky, *Chem. Mater.*, 2006, **8**, 1147–1160.
40 C. Boissiere, A. Larbot and E. Prouzet, *Chem. Mater.*, 2000, **12**, 1937–1940.
41 D. M. Antonelli and J. Y. Ying, *Angew. Chem., Int. Ed. Engl.*, 1995, **34**, 2014–2017.
42 S. Cabrera, J. El-Haskouri, J. Alamo, A. Beltrán, S. Mendioroz, M. D. Marcos and P. Amorós, *Adv. Mater.*, 1999, **11**, 379–382.
43 M. Fröba, O. Muth and A. Reller, *Solid State Ionics*, 1997, **101–103**, 249–253.
44 D. Trong-On, *Langmuir*, 1999, **15**, 8561–8564.
45 G. S. Attard, P. N. Bartlett, N. R. B. Coleman, J. M. Elliott, J. R. Owen and J. H. Wang, *Science*, 1997, **278**, 838–840.
46 (*a*) E. L. Crepaldi, G. J. A. A. de Soler-Illia, D. Grosso and C. Sanchez, *New J. Chem.*, 2003, **27**, 9–13; (*b*) U.-H. Lee, H. Lee, S. Wen, S.-I. Mho and Y.-U. Kwon, *Microporous Mesoporous Mater.*, 2006, **88**, 48–55; (*c*) V. N. Urade and H. W. Hillhouse, *J. Phys. Chem. B*, 2005, **109**, 10538–10541.
47 (*a*) Y. Lu, H. Y. Fan, A. Stump, T. L. Ward, T. Rieker and C. J. Brinker, *Nature*, 1999, **398**, 223–226; (*b*) C. Boissiere, D. Grosso, A. Chaumonnot, L. Nicole and C. Sanchez, *Adv. Mater.*, 2011, DOI: 10.1002/adma.201001410, in press.
48 C. Sanchez, C. Boissiere, D. Grosso, C. Laberty and L. Nicole, *Chem. Mater.*, 2008, **20**, 682–737.
49 (*a*) P. C. Angelomé, M. C. Fuertes and G. J. A. A. Soler-Illia, *Adv. Mater.*, 2006, **18**, 2397–2402; (*b*) S. Y. Choi, M. Mamak, G. von Freymann, N. Chopra and G. A. Ozin, *Nano Lett.*, 2006, **6**, 2456; (*c*) M. C. Fuertes, F. J. López-Alcaraz, M. C. Marchi, H. Troiani, V. Luca, H. Míguez and G. J. A. A. Soler-Illia, *Adv. Funct. Mater.*, 2007, **17**, 1247–1254.
50 (*a*) R. Ryoo, S. H. Joo and S. Jun, *J. Phys. Chem. B*, 1999, **103**, 7743; (*b*) R. Ryoo, S. H. Joo, M. Kruk and M. Jaroniec, *Adv. Mater.*, 2001, **13**, 677–681.
51 (*a*) J. Roggenbuck and M. Tiemann, *J. Am. Chem. Soc.*, 2005, **127**, 1096–1097; (*b*) H. Tüysüz, M. Comotti and F. Schüth, *Chem. Commun.*, 2008, 4022–4024.
52 J. C. Vartuli, K. D. Schmitt, C. T. Kresge, W. J. Roth, M. E. Leonowicz, S. B. McCullen, S. D. Hellring, J. S. Beck, J. L. Schlenker, D. H. Olson and E. W. Sheppard, *Chem. Mater.*, 1994, **6**, 2317–2326.
53 D. Y. Zhao, Q. Huo, J. Feng, B. F. Chmelka and G. D. Stucky, *J. Am. Chem. Soc.*, 1998, **120**, 6024–6036.
54 (*a*) S. A. Bagshaw and T. J. Pinnavaia, *Angew. Chem., Int. Ed. Engl.*, 1996, **35**, 1102–1105; (*b*) E. Prouzet and T. J. Pinnavaia, *Angew. Chem., Int. Ed. Engl.*, 1997, **36**, 516–518; (*c*) T. R. Pauly and T. J. Pinnavaia, *Chem. Mater.*, 2001, **13**, 987–993.
55 (*a*) R. Ryoo, S. Hoon and S. Jun, *J. Phys. Chem. B*, 1999, **103**, 7743–7746; (*b*) S. H. Joo, S. Jun and R. Ryoo, *Microporous Mesoporous Mater.*, 2001, **44–45**, 153–158; (*c*) United States Patent US6585948.
56 Y. Huang, H. Cai, T. Yu, F. Zhang, F. Zhang, Y. Meng, D. Gu, Y. Wan, X. Sun, B. Tu and D. Zhao, *Angew. Chem., Int. Ed.*, 2007, **46**, 1089–1093.
57 P. Yang, D. Zhao, D. I. Margolese, B. F. Chmelka and G. D. Stucky, *Chem. Mater.*, 1999, **11**, 2813–2826.
58 D. Zhao, P. Yang, N. Melosh, J. Feng, B. F. Chmelka and G. D. Stucky, *Adv. Mater.*, 1998, **10**, 1380–1385.
59 E. L. Crepaldi, G. J. A. A. Soler-Illia, D. Grosso, F. Cagnol, F. Ribot and C. Sanchez, *J. Am. Chem. Soc.*, 2003, **125**, 9770–9786.
60 Y. Wan and D. Y. Zhao, *Chem. Rev.*, 2007, **107**, 2821.
61 J. N. Israelachvili, *Intermolecular and Surface Forces*, Elsevier, Amsterdam, 2nd edn, 1992.
62 Q. Huo, R. Leon, P. M. Petroff and G. D. Stucky, *Science*, 1995, **268**, 1324–1327.
63 (*a*) D. Grosso, F. Babonneau, P.-A. Albouy, H. Amenitsch, A. R. Balkenende, A. Brunet-Bruneau and J. Rivory, *Chem. Mater.*, 2002, **14**, 931–939; (*b*) X. Zhang, W. Wu, J. Wang and C. Liu, *Thin Solid Films*, 2007, **515**, 8376–8380.
64 P. Innocenzi, L. Malfatti, T. Kidchob and P. Falcaro, *Chem. Mater.*, 2009, **21**, 2555–2564.
65 M. H. Lim and A. Stein, *Chem. Mater.*, 1999, **11**, 3285–3295.
66 R. Ryoo, C. H. Ko, M. Kruk, V. Antochshuk and M. Jaroniec, *J. Phys. Chem. B*, 2000, **104**, 11465–11471.
67 M. Impéror-Clerc, P. Davidson and A. Davidson, *J. Am. Chem. Soc.*, 2000, **122**, 11925–1933.
68 D. Zhao, P. Yang, D. I. Margolese, B. F. Chmelka and G. D. Stucky, *Chem. Commun.*, 1998, 2499–2500.
69 G. J. A. A. Soler-Illia, E. L. Crepaldi, D. Grosso and C. Sanchez, *Curr. Opin. Colloid Interface Sci.*, 2003, **8**, 109–126.
70 T.-W. Kim, R. Ryoo, M. Kruk, K. P. Gierszal, M. Jaroniec, S. Kamiya and O. Terasaki, *J. Phys. Chem. B*, 2004, **108**, 11480–11489.
71 K. Yu, B. Smarsly and C. J. Brinker, *Adv. Funct. Mater.*, 2003, **13**, 47–52.
72 M. Templin, A. Franck, A. Du Chesne, H. Leist, Y. Zhang, R. Ulrich, V. Schädler and U. Wiesner, *Science*, 1997, **278**, 1795–17988.
73 D. Zhao, J. Feng, Q. Huo, N. Melosh, G. H. Fredrickson, B. F. Chmelka and G. D. Stucky, *Science*, 1998, **279**, 548–552.
74 R. Corriu and N. Trong Anh, *Molecular Chemistry of Sol–Gel Derived Nanomaterials*, John Wiley and Sons, 2009, ch. 3, pp. 27–71.
75 K. Egeblad, C. H. Christensen, M. Kustova and C. H. Christensen, *Chem. Mater.*, 2008, **20**, 946–960.
76 G. J. A. A. Soler-Illia, A. Louis and C. Sanchez, *Chem. Mater.*, 2002, **14**, 750–759.
77 (*a*) S. T. Hyde, *Pure Appl. Chem.*, 1992, **64**, 1617–1622; (*b*) S. T. Hyde, *Progr. Colloid Polym. Sci.*, 1990, **82**, 236–242.
78 F. Schüth, *Chem. Mater.*, 2001, **13**, 3184–3194.
79 (*a*) P. V. Braun, P. Osenar and S. Stupp, *Nature*, 1996, **380**, 325; (*b*) A. Wolosiuk, O. Armagan and P. V. Braun, *J. Am. Chem. Soc.*, 2005, **127**, 16356–16357.
80 B. Tian, X. Liu, B. Tu, C. Yu, J. Fan, L. Wang, S. Xie, G. D. Stucky and D. Y. Zhao, *Nat. Mater.*, 2003, **2**, 159–163.
81 C. Liang, Z. Li and S. Dai, *Angew. Chem., Int. Ed.*, 2008, **47**, 3696–3717.
82 N. A. Melosh, P. Lipic, F. S. Bates, G. D. Stucky, F. Wudl, G. H. Fredrickson and B. F. Chmelka, *Macromolecules*, 1999, **32**, 4332–4342.
83 (*a*) B. L. Kirsch, E. K. Richman, A. E. Riley and S. H. Tolbert, *J. Phys. Chem. B*, 2004, **108**, 12698–12706; (*b*) S. Y. Choi, M. Mamak, S. Speakman, N. Chopra and G. A. Ozin, *Small*, 2005, **1**, 226–232.
84 Y. Sakatani, D. Grosso, L. Nicole, C. Boissiere, G. J. A. A. Soler-Illia and C. Sanchez, *J. Mater. Chem.*, 2006, **16**, 77–82.
85 J. N. Kondo and K. Domen, *Chem. Mater.*, 2008, **20**, 835–847.
86 D. Grosso, C. Boissiere, B. Smarsly, T. Brezesinski, N. Pinna, P. A. Albouy, H. Amenitsch, M. Antonietti and C. Sanchez, *Nat. Mater.*, 2004, **3**, 787–792.
87 A. Stein, B. J. Melde and R. C. Schroden, *Adv. Mater.*, 2000, **12**, 1403–1419.
88 R. Anwander, *Chem. Mater.*, 2001, **13**, 4419–4438.
89 P. C. Angelomé and G. J. A. A. Soler-Illia, *Chem. Mater.*, 2005, **17**, 322–331.
90 P. C. Angelomé, M. C. Fuertes and G. J. A. A. Soler-Illia, *Adv. Mater.*, 2006, **17**, 2397–2402.
91 A. Fisher, M. Kuemmel, M. Järn, M. Linden, C. Boissiere, L. Nicole, C. Sanchez and D. Grosso, *Small*, 2006, **2**, 569–574.
92 J.-L. Shi, Z.-L. Hua and L.-X. Zhang, *J. Mater. Chem.*, 2004, **14**, 795–806.
93 F. Hoffmann, M. Cornelius, J. Morell and M. Fröba, *Angew. Chem., Int. Ed.*, 2006, **45**, 3216–3251.
94 A. Mehdi, C. Reye and R. Corriu, *Chem. Soc. Rev.*, 2011, DOI: 10.1039/b920516k, in press.
95 M. Kruk and M. Jaroniec, *Langmuir*, 1997, **13**, 6267–6273.
96 T. Azaïs, C. Tourné-Péteilh, F. Aussenac, N. Baccile, C. Coelho, J.-M. Devoisselle and F. Babonneau, *Chem. Mater.*, 2006, **18**, 6382–6390.
97 L. M. Bronstein, *Top. Curr. Chem.*, 2003, **226**, 55–89.

98 A. Taguchi and F. Schüth, *Microporous Mesoporous Mater.*, 2005, **77**, 1–45.
99 H. Yoshitake, *J. Mater. Chem.*, 2010, **20**, 4537–4550.
100 F. Hoffmann and M. Fröba, in *The Supramolecular Chemistry of Organic-Inorganic Hybrid Materials*, ed. K. Rurack and R. Martínez-Máñez, John Wiley and Sons, Inc, 2010, ch. 3, pp. 39–111.
101 (*a*) T. Asefa, M. J. MacLachlan, N. Coombs and G. A. Ozin, *Nature*, 1999, **402**, 867–871; (*b*) S. Inagaki, S. Guan, Y. Fukushima, T. Ohsuna and O. Terasaki, *J. Am. Chem. Soc.*, 1999, **121**, 9611–9614; (*c*) B. J. Melde, B. T. Holland, C. F. Blanford and A. Stein, *Chem. Mater.*, 1999, **11**, 3302–3308.
102 F. Schüth, *Annu. Rev. Mater. Res.*, 2005, **35**, 209–238.
103 D. Brunel, A. Cauvel, F. Di Renzo, F. Fajula, B. Fubini, B. Onida and E. Garrone, *New J. Chem.*, 2000, **24**, 807–813.
104 F. Cagnol, D. Grosso and C. Sanchez, *Chem. Commun.*, 2004, 1742–1744.
105 A. Calvo, M. Joselevich, G. J. A. A. Soler-Illia and F. J. Williams, *Microporous Mesoporous Mater.*, 2009, **121**, 67–72.
106 S. Inagaki, S. Guan, T. Ohsuna and O. Terasaki, *Nature*, 2002, **416**, 304–307.
107 Q. Yang, J. Liu, L. Zhang and C. Li, *J. Mater. Chem.*, 2009, **19**, 1945–1955.
108 P. C. Angelomé and G. J. A. A. Soler-Illia, *J. Mater. Chem.*, 2005, **15**, 3903–3912.
109 G. E. Fryxell, S. V. Mattigod, Y. Lin, H. Wu, S. Fiskum, K. Parker, F. Zheng, W. Yantasee, T. S. Zemanian, R. S. Addleman, J. Liu, K. Kemner, S. Kelly and X. Feng, *J. Mater. Chem.*, 2007, **17**, 2863–2874.
110 D. Brühwiler, *Nanoscale*, 2010, **2**, 887.
111 T. Bein and P. Enzel, *Angew. Chem., Int. Ed. Engl.*, 1989, **28**, 1692–1694.
112 P. Enzel and T. Bein, *J. Phys. Chem.*, 1989, **93**, 6270–6272.
113 C.-G. Wu and T. Bein, *Science*, 1994, **264**, 1757–1759.
114 F. F. Fang, H. Jin Choi and W. S. Ahn, *Compos. Sci. Technol.*, 2009, **69**, 2088–2092.
115 K. Moller, T. Bein and R. X. Fischer, *Chem. Mater.*, 1998, **10**, 1841–1852.
116 J. Jang, B. Lim, J. Lee and T. Hyeon, *Chem. Commun.*, 2001, 83–84.
117 T. L. Kelly, K. Yano and M. O. Wolf, *Langmuir*, 2010, **26**, 421–431.
118 B. Zhang, X. Chen, S. Ma, Y. Chen, J. Yang and M. Zhang, *Nanotechnology*, 2010, **21**, 065304.
119 J. Dong, Y. Hu, J. Xu, X. Qu and C. Zhao, *Electroanalysis*, 2009, **21**, 1792–1798.
120 S. A. Johnson, D. Khushalani, N. Coombs, T. E. Mallouk and G. A. Ozin, *J. Mater. Chem.*, 1998, **8**, 13–14.
121 (*a*) A. G. Pattantyus-Abraham and M. O. Wolf, *Chem. Mater.*, 2004, **16**, 2180–2186; (*b*) M. A. Álvaro, A. Corma, B. Ferrer, M. S. Galletero, H. García and E. Peris, *Chem. Mater.*, 2004, **16**, 2142–2147.
122 (*a*) T. L. Kelly, S. P. Y. Che, Y. Yamada, K. Yano and M. O. Wolf, *Langmuir*, 2008, **24**, 9809–9815; (*b*) T. L. Kelly, Y. Yamada, S. P. Y. Che, K. Yano and M. O. Wolf, *Adv. Mater.*, 2008, **20**, 2616–2621.
123 M. Choi, F. Kleitz, D. Liu, H. Y. Lee, W.-S. Ahn and R. Ryoo, *J. Am. Chem. Soc.*, 2005, **127**, 1924–1932.
124 S. M. Ng, S.-i. Ogino, T. Aida, K. A. Koyano and T. Tatsumi, *Macromol. Rapid Commun.*, 1997, **18**, 991–996.
125 (*a*) D.-H. Choi and R. Ryoo, *J. Mater. Chem.*, 2010, **20**, 5544–5550; (*b*) M. T. Run, S. Z. Wu, D. Y. Zhang and G. Wu, *Mater. Chem. Phys.*, 2007, **105**, 341–347; (*c*) M. Wainer, L. Marcoux and F. Kleitz, *J. Mater. Sci.*, 2009, **44**, 6538–6545.
126 R. Guillet-Nicolas, L. Marcoux and F. Kleitz, *New J. Chem.*, 2010, **34**, 355–366.
127 B.-S. Tian and C. Yang, *J. Phys. Chem. C*, 2009, **113**, 4925–4931.
128 (*a*) S. Yoo, J. D. Lunn, S. González, J. A. Ristich, E. E. Simanek and D. F. Shantz, *Chem. Mater.*, 2006, **18**, 2935–2942; (*b*) D. M. Ford, E. E. Simanek and D. F. Shantz, *Nanotechnology*, 2000, **16**, S458–S475.
129 (*a*) P. Li and S. Kawi, *J. Catal.*, 2008, **257**, 23–31; (*b*) P. Li and S. Kawi, *Catal. Today*, 2008, **131**, 61–69.
130 S. Yoo, S. Yeu, R. L. Sherman, E. E. Simanek, D. F. Shantz and D. M. Ford, *J. Membr. Sci.*, 2009, **334**, 16–22.
131 (*a*) J. P. K. Reynhardt, Y. Yang, A. Sayari and H. Alper, *Chem. Mater.*, 2004, **16**, 4095–4102; (*b*) J. P. K. Reynhardt, Y. Yang, A. Sayari and H. Alper, *Adv. Funct. Mater.*, 2005, **15**, 1641–1646.
132 M. P. Kapoor, H. Kuroda, M. Yanagi, H. Nanbu and L. R. Juneja, *Top. Catal.*, 2009, **52**, 634–642.
133 S. Yoo, J. D. Lunn, S. González, J. A. Ristich, E. E. Simanek and D. F. Shantz, *Chem. Mater.*, 2006, **18**, 2935–2942.
134 Y. Jiang, Q. Gao, H. Yu, Y. Chen and F. Deng, *Microporous Mesoporous Mater.*, 2007, **103**, 316–324.
135 E. J. Acosta, C. S. Carr, E. E. Simanek and D. F. Schantz, *Adv. Mater.*, 2004, **16**, 985–989.
136 Z. Liang, B. Fadhel, C. J. Schneider and A. L. Chaffee, *Microporous Mesoporous Mater.*, 2008, **111**, 536–543.
137 Q. Wang, V. Varela Guerrero, A. Ghosh, S. Yeu, J. D. Lunn and D. F. Shantz, *J. Catal.*, 2010, **269**, 15–25.
138 B. González, M. Colilla, C. López de Laorden and M. Vallet-Regí, *J. Mater. Chem.*, 2009, **19**, 9012–9024.
139 J. M. Rosenholm, A. Penninkangas and M. Lindén, *Chem. Commun.*, 2006, 3909–3911.
140 (*a*) J. C. Hicks, J. H. Drese, D. J. Fauth, M. L. Gray, G. Qi and C. W. Jones, *J. Am. Chem. Soc.*, 2008, **130**, 2902–2903; (*b*) J. H. Drese, S. Choi, R. P. Lively, W. J. Koros, D. J. Fauth, M. L. Gray and C. W. Jones, *Adv. Funct. Mater.*, 2009, **19**, 3821–3832.
141 E. Martinez-Ferrero, G. Franc, S. Mazeres, C. O. Turrin, C. Boissiere, A. M. Caminade, J. P. Majoral and C. Sanchez, *Chem.–Eur. J.*, 2008, **14**, 7658.
142 (*a*) C. J. Bhongale, C.-H. Yang and C.-S. Hsu, *Chem. Commun.*, 2006, 2274–2276; (*b*) R. Guo, G. Li, W. Zhang, G. Shen and D. Shen, *ChemPhysChem*, 2005, **6**, 2025–2028.
143 (*a*) Y. Lu, Y. Yang, A. Sellinger, M. Lu, J. Huang, H. Fan, R. Haddad, G. Lopez, A. R. Burns, D. Y. Sasaki, J. Shelnutt and C. J. Brinker, *Nature*, 2001, **410**, 913–917; (*b*) Y. Yang, Y. Lu, M. Lu, J. Huang, R. Haddad, G. Xomeritakis, N. Liu, A. P. Malanoski, D. Sturmayr, H. Fan, D. Y. Sasaki, R. A. Assink, J. A. Shelnutt, F. van Swol, G. P. Lopez, A. R. Burns and C. J. Brinker, *J. Am. Chem. Soc.*, 2003, **125**, 1269–1277.
144 H. Peng, J. Tang, L. Yang, J. Pang, H. S. Ashbaugh, C. J. Brinker, Z. Yang and Y. Lu, *J. Am. Chem. Soc.*, 2006, **128**, 5304–5305.
145 M. Ikegame, K. Tajima and T. Aida, *Angew. Chem., Int. Ed.*, 2003, **42**, 2154–2157.
146 (*a*) G. Li, S. Bhosale, F. Li, Y. Zhang, R. Guo, H. Zhu and J.-H. Fuhrhop, *Chem. Commun.*, 2004, 1760–1761; (*b*) G. Li, S. Bhosale, T. Wang, Y. Zhang, H. Zhu and J.-H. Fuhrhop, *Angew. Chem., Int. Ed.*, 2003, **42**, 3818–3821; (*c*) W. Zhang, J. Cui, C. Lin, Y. Wu, L. Ma, Y. Wen and G. Li, *J. Mater. Chem.*, 2009, **19**, 3962–3970; (*d*) Z. Yang, X. Kou, W. Ni, Z. Sun, L. Li and J. Wang, *Chem. Mater.*, 2007, **19**, 6222–6229.
147 (*a*) K. Kageyama, J.-i. Tamazawa and T. Aida, *Science*, 1999, **285**, 2113–2115; (*b*) P. Lehmus and B. Rieger, *Science*, 1999, **285**, 2081–2082.
148 R. R. Rao, B. M. Weckhuysen and R. A. Schoonheydt, *Chem. Commun.*, 1999, 445–446.
149 S.-H. Chan, Y.-Y. Lin and C. Ting, *Macromolecules*, 2003, **36**, 8910–8912.
150 R. Anwander, I. Nagl, C. Zapilko and M. Widenmeyer, *Tetrahedron*, 2003, **59**, 10567–10574.
151 D. J. Cardin, S. P. Constantine, A. Gilbert, A. K. Lay, M. Alvaro, M. S. Galletero, H. García and F. Márquez, *J. Am. Chem. Soc.*, 2001, **123**, 3141–3142.
152 V. S.-Y. Lin, D. R. Radu, M.-K. Han, W. Deng, S. Kuroki, B. H. Shanks and M. Pruski, *J. Am. Chem. Soc.*, 2002, **124**, 9040–9041.
153 (*a*) S. Spange, A. Graser, H. Muller, Y. Zimmermann, P. Rehak, C. Jager, H. Fuess and C. Baehtz, *Chem. Mater.*, 2001, **13**, 3698–3708; (*b*) S. Spange, A. Gräser, A. Huwe, F. Kremer, C. Tintemann and P. Behrens, *Chem.–Eur. J.*, 2001, **7**, 3722–3728.
154 A. B. Fischer, J. B. Kinney, R. H. Staley and M. S. Wrighton, *J. Am. Chem. Soc.*, 1979, **101**, 6501–6506.

 

155 S. O'Brien, J. Tudor, S. Barlow, M. J. Drewitt, S. J. Heyes and D. O'Hare, *Chem. Commun*., 1997, 641–642.
156 (*a*) M. J. MacLachlan, M. Ginzburg, N. Coombs, N. P. Raju, J. E. Greedan, G. A. Ozin and I. Manners, *J. Am. Chem. Soc*., 2000, **122**, 3878–3891; (*b*) M. J. MacLachlan, P. Aroca, N. Coombs, I. Manners and G. A. Ozin, *Adv. Mater*., 1998, **10**, 144–149.
157 N. C. Strandwitz, Y. Nonoguchi, S. W. Boettcher and G. D. Stucky, *Langmuir*, 2010, **26**, 5319–5322.
158 G. D. Stucky, *Nature*, 2001, **410**, 885–886.
159 (*a*) A. S. Angelatos, Y. Wang and F. Caruso, *Langmuir*, 2008, **24**, 4224–4230; (*b*) Y. Wang, A. S. Angelatos, D. E. Dunstan and F. Caruso, *Macromolecules*, 2007, **40**, 7594–7600.
160 Q. Yang, S. Wang, P. Fan, L. Wang, Y. Di, K. Lin and F.-S. Xiao, *Chem. Mater*., 2005, **17**, 5999–6003.
161 K. M. Coakley, Y. Liu, M. D. McGehee, K. L. Frindell and G. D. Stucky, *Adv. Funct. Mater*., 2003, **13**, 301–306.
162 H. Xi, B. Wang, Y. Zhang, X. Qian, J. Yin and Z. Zhu, *J. Phys. Chem. Solids*, 2003, **64**, 2451–2455.
163 L. Huang, S. Dolai, K. Raja and M. Kruk, *Langmuir*, 2010, **26**, 2688–2693.
164 B. Yameen, M. Ali, M. Alvarez, R. Neumann, W. Ensinger, W. Knoll and O. Azzaroni, *Polym. Chem*., 2010, **1**, 183–192.
165 I. Díaz, B. García, B. Alonso, C. M. Casado, M. Morán, J. Losada and J. Pérez-Pariente, *Chem. Mater*., 2003, **15**, 1073–1079.
166 (*a*) D. S. Shephard, W. Zhou, T. Maschmeyer, J. M. Matters, C. L. Roper, S. Parsons, B. F. G. Johnson and M. J. Duer, *Angew. Chem., Int. Ed*., 1998, **37**, 2719–2723; (*b*) T. Maschmeyer, R. D. Oldroy, G. Sankar, J. M. Thomas, I. J. Shannon, J. A. Klepetko, A. F. Masters, J. K. Beattie and C. R. A. Catlow, *Angew. Chem., Int. Ed. Engl*., 1997, **36**, 1639–1642.
167 W. Huang, J. N. Kuhn, C.-K. Tsung, Y. Zhang, S. E. Habas, P. Yang and G. A. Somorjai, *Nano Lett*., 2008, **8**, 2027–2034.
168 R. M. Crooks, M. Zhao, L. Sun, V. Chechik and L. K. Yeung, *Acc. Chem. Res*., 2001, **34**, 181–190.
169 (*a*) M. Save, G. Granvorka, J. Bernard, B. Charleux, C. Boissiére, D. Grosso and C. Sanchez, *Macromol. Rapid Commun*., 2006, **27**, 393–398; (*b*) F. Audouin, H. Blas, P. Pasetto, P. Beaunier, C. Boissiere, C. Sánchez, M. Save and B. Charleux, *Macromol. Rapid Commun*., 2008, **29**, 914–921; (*c*) C. Li, J. Yang, P. Wang, J. Liu and Q. Yang, *Microporous Mesoporous Mater*., 2009, **123**, 228–233; K. Ikeda, M. Kida and K. Endo, *Polym. J*., 2009, **41**, 672–678; (*d*) A. Martín, G. Morales, F. Martínez, R. van Grieken, L. Cao and M. Kruk, *J. Mater. Chem*., 2010, **20**, 8026–8035.
170 J. Pyun and K. Matyjaszewski, *Chem. Mater*., 2001, **13**, 3436–3448.
171 P. Pasetto, H. Blas, F. Audouin, C. Boissiere, C. Sanchez, M. Save and B. Charleux, *Macromolecules*, 2009, **42**, 5983–5995.
172 M. Kruk, B. Dufour, E. B. Celer, T. Kowalewski, M. Jaroniec and K. Matyjaszewski, *J. Phys. Chem. B*, 2005, **109**, 9216–9225.
173 M. Kruk, B. Dufour, E. B. Celer, T. Kowalewski, M. Jaroniec and K. Matyjaszewski, *Macromolecules*, 2008, **41**, 8584–8591.
174 (*a*) J. Moreno and D. C. Sherrington, *Chem. Mater*., 2008, **20**, 4468–4474; (*b*) Q. Fu, G. V. R. Rao, L. K. Ista, Y. Wu, B. P. Andrewzjeski, L. A. Sklar, T. L. Ward and G. P. López, *Adv. Mater*., 2003, **15**, 1262–1266.
175 L. Cao and M. Kruk, *Polym. Chem*., 2010, **1**, 97–101.
176 J. D. Lunn and D. F. Shantz, *Chem. Mater*., 2009, **21**, 3638–3648.
177 M. Lenarda, G. Chessa, E. Moretti, S. Polizzi, L. Storaro and A. Talon, *J. Mater. Sci*., 2006, **41**, 6305–6312.
178 Z. Zhou, S. Zhu and D. Zhang, *J. Mater. Chem*., 2007, **17**, 2428–2433.
179 Q. Fu, G. V. Rama Rao, T. L. Ward, Y. Lu and G. P. Lopez, *Langmuir*, 2007, **23**, 170–174.
180 A. P.-Z. Clark, K.-F. Shen, Y. F. Rubin and S. H. Tolbert, *Nano Lett*., 2005, **5**, 1647–1652.
181 S. Kirmayer, S. Neyshtadt, A. Keller, D. Okopnik and G. L. Frey, *Chem. Mater*., 2009, **21**, 4387–4396.
182 E. Dovgolevsky, S. Kirmayer, E. Lakin, Y. Yang, C. J. Brinker and G. L. Frey, *J. Mater. Chem*., 2008, **18**, 423–436.
183 R. Hernández, A.-Ch. Franville, P. Minoofar, B. Dunn and J. I. Zink, *J. Am. Chem. Soc*., 2001, **123**, 1248–1249.
184 M. Kimura, K. Wada, Y. Iwashima, K. Ohta, K. Hanabusa, H. Shirai and N. Kobayashi, *Chem. Commun*., 2003, 2504–2505.
185 M. Fujiwara, K. Shiokawa and Y. Zhu, *J. Mol. Catal. A: Chem*., 2007, **264**, 153–161.
186 K. Vallé, P. Belleville, F. Pereira and C. Sanchez, *Nat. Mater*., 2006, **5**, 107–111.
187 R. Casasús, M. D. Marcos, R. Martínez-Máñez, J. V. Ros-Lis, J. Soto, L. A. Villaescusa, P. Amorós, D. Beltrán, C. Guillem and J. Latorre, *J. Am. Chem. Soc*., 2004, **126**, 8612–8613.
188 F. De Juan and E. Ruiz-Hitzky, *Adv. Mater*., 2000, **6**, 430–432.
189 (*a*) J. Kecht, A. Schlossbauer and T. Bein, *Chem. Mater*., 2008, **20**, 7207–7214; (*b*) C.-Y. Hong, X. Li and C. Y. Pan, *Eur. Polym. J*., 2007, **43**, 4114–4122; (*c*) X. Li, C.-Y. Hong and C.-Y. Pan, *Polymer*, 2010, **51**, 92–99; (*d*) P.-W. Chung, R. Kumar, M. Pruski and V. S.-Y. Lin, *Adv. Funct. Mater*., 2008, **18**, 1390–1398.
190 C.-Y. Hong, X. Li and C.-Y. Pan, *J. Mater. Chem*., 2009, **19**, 5155–5160.
191 (*a*) F. Roohi and M. M. Titirici, *New J. Chem*., 2008, **32**, 1409–1414; (*b*) C.-Y. Hong, X. Li and C.-Y. Pan, *J. Phys. Chem. C*, 2008, **112**, 15320–15324.
192 J. D. Lunn and D. F. Shantz, *Chem. Commun*., 2010, **46**, 2926–2928.
193 J. M. Rosenholm, A. Duchanoy and M. Lindén, *Chem. Mater*., 2008, **20**, 1126–1133.
194 (*a*) J. M. Rosenholm, A. Meinander, E. Peuhu, R. Niemi, J. E. Eriksson, C. Sahlgren and M. Lindén, *ACS Nano*, 2009, **3**, 197–206; (*b*) J. M. Rosenholm, E. Peuhu, L. Tabe Bate-Eya, J. E. Eriksson, C. Sahlgren and M. Lindén, *Small*, 2010, **6**, 1234–1241.
195 A. Calvo, B. Yameen, F. J. Williams, G. J. A. A. Soler-Illia and O. Azzaroni, *J. Am. Chem. Soc*., 2009, **131**, 10866–10868.
196 F. Pereira, K. Vallé, P. Belleville, A. Morin, S. Lambert and C. Sanchez, *Chem. Mater*., 2008, **20**, 1710–1718.
197 D. R. Radu, C.-Y. Lai, K. Jeftinija, E. W. Rowe, S. Jeftinija and V. S.-Y. Lin, *J. Am. Chem. Soc*., 2004, **126**, 13216–13217.
198 C. Wu, C. Chen, J. Lai, J. Chen, X. Mu, J. Zheng and Y. Zhao, *Chem. Commun*., 2008, 2662–2664.
199 J.-T. Sun, C.-Y. Hong and C.-Y. Pan, *J. Phys. Chem. C*, 2010, **114**, 12481–12486.
200 R. Casasús, E. Climent, M. D. Marcos, R. Martínez-Máñez, F. Sancenón, J. Soto, P. Amorós, J. Cano and E. Ruiz, *J. Am. Chem. Soc*., 2008, **130**, 1903–1917.
201 E. Aznar, M. D. Marcos, R. Martínez-Máñez, F. Sancenón, J. Soto, P. Amorós and C. Guillem, *J. Am. Chem. Soc*., 2009, **131**, 6833–6843.
202 J. Lai, X. Mu, Y. Xu, X. Wu, C. Wu, C. Li, J. Chen and Y. Zhao, *Chem. Commun*., 2010, **46**, 7370–7372.
203 Y.-L. Zhao, Z. Li, S. Kabehie, Y. Y. Botros, J. F. Stoddart and J. I. Zink, *J. Am. Chem. Soc*., 2010, **132**, 13016–13025.
204 C. Park, K. Oh, C. S. Lee and C. Kim, *Angew. Chem., Int. Ed*., 2007, **46**, 1455–1457.
205 M. Grätzel, *Acc. Chem. Res*., 2009, **42**, 1788–1798, and references therein.
206 M. Zukalovà, A. Zukal, L. Kavan, M. K. Nazeeruddin, P. Liska and M. Grätzel, *Nano Lett*., 2005, **5**, 1789–1792.
207 K. M. Coakley and M. D. McGehee, *Chem. Mater*., 2004, **16**, 4533–4542.
208 K. M. Coakley and M. D. McGehee, *Appl. Phys. Lett*., 2003, **83**, 3380–3382.
209 M. D. McGehee, *MRS Bull*., 2009, **34**, 95–100.
210 E. Lancelle-Beltran, P. Prené, C. Boscher, P. Belleville, P. Buvat and C. Sanchez, *Adv. Mater*., 2006, **18**, 2579–2582.
211 E. J. W. Crossland, M. Kamperman, M. Nedelcu, C. Ducati, U. Wiesner, D.-M. Smilgies, G. E. S. Toombes, M. A. Hillmyer, S. Ludwigs, U. Steiner and H. J. Snaith, *Nano Lett*., 2009, **9**, 2807–2812.
212 P. Docampo, S. Guldin, M. Stefik, P. Tiwana, M. C. Orilall, S. Hüttner, H. Sai, U. Wiesner, U. Steiner and H. J. Snaith, *Adv. Funct. Mater*., 2010, **20**, 1787–1796.
213 M. Wark, in *Host–Guest-Systems Based on Nanoporous Crystals*, ed. F. Laeri, F. Schüth, U. Simon and M. Wark, Wiley-VCH, Weinheim, 2003, pp. 2–6.
214 M. Tirrell, *AIChE J*., 2005, **51**, 2385–2390.

215 P. Yang, T. Deng, D. Zhao, P. Feng, D. Pine, B. F. Chmelka, G. M. Whitesides and G. D. Stucky, *Nature*, 1998, **282**, 2244–2246.
216 M. Antonietti and G. A. Ozin, *Chem.–Eur. J.*, 2004, **10**, 28–41.
217 A. B. Descalzo, R. Martínez-Máñez, F. Sancenón, K. Hoffmann and K. Rurack, *Angew. Chem., Int. Ed.*, 2006, **45**, 5924–5948.
218 P.-G. de Gennes, *Adv. Polym. Sci.*, 1999, **138**, 91–105.
219 A. Thomas, M. Schierhorn, Y. Wu and G. Stucky, *J. Mater. Chem.*, 2007, **17**, 4558–4562.
220 A. Serghei, D. Chen, D. H. Lee and T. P. Russell, *Soft Matter*, 2010, **6**, 1111–1113.
221 A. B. Descalzo, R. Martínez-Mañez, F. Sancenón, K. Hoffmann and K. Rurack, *Angew. Chem., Int. Ed.*, 2006, **45**, 5924–5948.



 